Summer 2016

Shale instability of deviated wellbores in southern Iraqi fields

Ahmed Ali Shanshool Alsubaih

Department:

SHALE INSTABILITY OF DEVIATED WELLBORES IN SOUTHERN IRAQI FIELDS

by

AHMED ALI SHANSHOOL ALSUBAIH

A THESIS

Presented to the Faculty of the Graduate School of the

MISSOURI UNIVERSITY OF SCIENCE AND TECHNOLOGY

In Partial Fulfillment of the Requirements for the Degree

MASTER OF SCIENCE IN PETROLEUM ENGINEERING

2016

Approved by

Dr. Runar Nygaard (Advisor)

Dr. Ralph Flori

Dr. Andreas Eckert

ABSTRACT

Wellbore instability problems are the cause for the majority of nonproductive time in the southern Iraqi fields' developments. The most severe problem in terms of effort and disbursement which is referred to a pipe sticking in Tanuma shale formation. Examining the drilling data revealed that this phenomenon was mostly related to the shear failure of the wellbore. Thus, a geomechanical analysis and drilling parameters/ practice optimization analysis were performed on a field in southern Iraq based on data from 45 deviated wells. The geomechanics analysis predicted the suitable drilling fluid density to prevent onset shear failure by using the Mogi-Coulomb failure criterion, including thermally and chemically induced stresses and the bedding related failure of the wellbore. While the drilling parameters optimization was conducted by DROPS simulator and multi-regression analysis and resulted in a significant reduction in the shale exposure time to the drilling fluid. The drilling practice analysis was derived based on drilling data from stuck-free well also facilitated in preventing the drilling fluid density reduction by tripping processes. These analyses identified the following areas of improvement. First, the mud weight being used was not changed properly with respect to variation in wells azimuth and inclination. Secondly, anisotropic effects of the stress and strength parameters for this shale formation should be considered in wells trajectory design. Thirdly, the time depended-failure of wellbore was observed in even though the drilling fluid density was appropriately selected. Fourthly, the swabbing effect while tripping was negatively contributed to wellbore stability. Due to limited of published studies regarding wellbore problems in southern Iraqi fields; this research could serve as a significant case history for similar fields.

ACKNOWLEDGMENTS

I would like to express my very profound gratitude to my advisor Dr. Runar Nygaard for his expert guidance, immense knowledge, encouragement, motivation, and the fruitful support of my academic study and research. In addition, I would like to appreciation to Dr. Ralph Flori, Dr. Andeas Eckert for having them on my committee. Their insightful comments and questions were valued greatly.

Deepest thanks to my sponor the The Higher Committee of Education Development in Iraq (HCED) for their support during my acadmic study.

I would like to appreciate South oil company managements for their permission to used data.

Last but not the least, I must express my sincere gratitude like to thank my family: my parents, my brothers, sisters and my wife (Doaa) for providing me with unfailing support and continuous encouragement throughout my years of study and through the process of researching and writing this thesis. This accomplishment would not have been possible without them. Thank you.

TABLE OF CONTENTS

LIST OF ILLUSTRATIONS

Page

LIST OF TABLES

Page

NOMENCLATURE

Symbol	Description
S_i	Stress
ϵ	Strain
τ	Shear Stress
Pp	Pore Pressure
Z	Depth
ρ_g	Pore pressure gradient
S_t	Total Stress
g	Gravity Acceleration
E_D	Dynamic Young Modulus
E_s	Static Young Modulus
v	Poisson ratio
V_s	Shear Velocity
V_p	Compressional Velocity
ρ_b	Bulk Density
Δt	Compressional Travel Time
ρ_{ma}	Matrix Density
ρ_f	Fluid Density
Sv	Overburden Stress
Φ	Rock Porosity
Sh	Minimum Horizontal Stress
SH	Maximum Horizontal Stress
μ	Coefficient of the Internal Friction angle
δp	Differential Pressure between Borehole and Pore Pressures
W_{bo}	Breakout Width
m	Constant Depended On the Type of Faulting Regime
$S_x, S_y, S_z, \tau_{xz}, \tau_{xy}, \tau_{yz}$	Stress Components of Original Wellbore Coordinate System
$S_{\theta\theta}, S_{rr}, S_{zz}, \tau_{r\theta}, \tau_{\theta z}, \tau_{rz}$	Stress Components of Wellbore Coordinate System
Symbol	Description

Symbol	Description
γ	Well Inclination
φ	Well geographic azimuth
θ	Well azimuth from maximum horizontal stress
S_1, S_1	Principle Stresses at the Wellbore Wall
T_o	Tensile Stress
aw	Water Activity
as	Shale Activity
I_m	Reflection Coefficient
P_π	Osmotic Potential
R	Universal Gas Constant
V_M	Water Molar Volume
ψ	The Angle Between The Bedding Plane Maximum Principle Stress
C_o	Cohesion
C_1, C_2	The Maximum and Minimum Cohesion, respectively
ψm	The minimum angle of the ψ corresponding to minimum cohesion
τ_{oct}	Octahedral Shear Stress
S_m	Mean Normal Stress
a, b	Material Parameters for Mogi-Coulomb Criterion
TT	Slip To Slip Time

ABBREVIATIONS

Abbreviations	Definition
NPT	Non-productive time
AFE	Authority for Expenditure
ROP	Rate of Penetration
WOB	Weight on Bit
RPM	Revolution per Minute
FL	Flow Rate
BHA	Bottom Hole Assembly
ECD	Equivelnt Circulation Density
WBM	Water Base Mud
FPWD	Formation Pressure While Drilling
RFT	Repeated Formation Test
UCS	Unconfined Compressive Strength
LOT	Leak-Off Test
FPP	Fracture Propagation Pressure
ISIP	Instantaneous Shut in Pressure
FCP	Fracture Closure Pressure
DROPS	Drilling Optimization Simulators
MSE	Mechanic Specific Energy
PDC	Polycrystalline Diamond Compact
TFA	Total Flow Area
MD	Measured Depth
ARSL	Apparent Rock Strength Log

1. INTRODUCTION

1.1. INTRODUCTION TO GEOMECHANICS

Petroleum-related geomechanics plays a vital role in different petroleum applications, especially in hydrocarbon exploration through drilling operations when it is related to extend out to the production zone safely and cost-effectively. Additionally, it's an intrinsic contribution in terms of completion and production design throughout the mitigation of sand production using an optimum perforation direction and production strategy by selecting appropriate hydraulic fracturing designs. Furthermore, it assists in enhancing the oil recovery process by inducing tensile stress that is high enough to initiate new micro fractures or open old fractures in case of stress alteration due to the cooling effect and pore pressure, which leads to the best swept efficiency in terms of water injection (Fakcharoenphol et al., 2012; Teklu et al., 2012). Last but not least, the reduction in porosity and permeability associated with reservoir depletions as well as the initiation of seismicity as a consequence of reactivated pre-existing fault have been studied diligently from the geomechanics point of view to avoid these problems (Chan et al., 2001; Strei et al., 2002).

1.2. THE NON–PRODUCTIVE TIME IN DRILLING CAUSED BY GEOMECHANICS

Non-productive time (NPT) is described as any halt in the operations during subsurface activities related to drilling and well construction (Meng et al., 2013). It is also measured from the time when the problems occurred, continuing until the operations recommence (Rabia, 2010). There are different causes of non-productive time. Commonly, the problems related to geomechanical-induced wellbore failure are among the most time-consuming. These difficulties could be; loss of circulation when the borehole pressure overcomes the tensile strength of the rock, pipe sticking and/or when the borehole pressure is not high enough to support the borehole well, or the inability to run equipment downhole such as casing or logging tools due to the hole collapsing. In shales, the inappropriate

cleaning of the hole leads to aggregation of the rock fragment in the hole causing NPT due to the drill string packing off or losing the entire well.

Around 10-25% of the Authority for Expenditure (AFE) has been allocated to cover the unanticipated potential operation problems (York et al., 2009). Generally, the knowledge transferred from offset wells to new well plans is done to improve the well design and drilling practices and reduce NPT (Pritchard, 2011; Gala et al., 2010). Use of new drilling technologies and real-time monitoring of drilling parameters has shown to be helpful to reduce NPT. One example is the widening the operation mud window by applying wellbore strengthening techniques in depleted reservoirs or when the mud pressure exceeds the fracture gradient (Alberty & Mclean, 2004; Duffadar et al., 2013; Fuh et al., 1992; Salehi & Nygaard, 2012). Other technologies that has reduced NPT are; drilling with casing or liner, managed pressure drilling, constant bottom hole pressure, pressurized mud cap drilling and dual gradient drilling (Pritchard, 2011; Rosenberg & Gala, 2011; York et al., 2009).

1.3. SHALE INSTABILITY

Shale composes about two-thirds of the rock being drilled, and almost 90% of drilling problems are related to shale failures (Azar & Samuel, 2007; Chen, 2003a; Nygård, 2002; Yan, 2013). Shale consists of fine grained, laminated sediment with different types of clay minerals and mica. Shale is loosely defined as sedimentary rocks that contain a majority of clay minerals and/or clay-sized and laminated (Shaw & Weaver, 1989).

Wellbore instability in shale formations is related to the shear failure at the wellbore walls; (i.e. the stresses around well bore exceeds the rock strength due to lack of pressure support from the drilling fluid), or the opposite when the drilling fluid pressure exceeds the wellbore wall strength and creates tensile fracture (Chen et al., 2002). Different parameters, such as high-stress contrast, shale mechanical properties, shale mineral composition, shale anisotropy, improper wellbore fluid pressure, drilling fluid properties, well trajectory design, and heat transfer, have a direct impact on these two failure mechanisms (Fjaer et al., 2008).

Shale instabilities can be related to non-mechanical-induced wellbore failures (i.e. chemical effects). Clay minerals in shales may pose a negative influence on wellbore instability during or after drilling (Creeping) because the mud fluid could interact with the shale mineral leading to the weakening of rock cementation and strength (John & Cook, 2007). The concentration of certain kinds of minerals is significant and interrelated to the treatment that should be used to ensure a stable well. For example, smectites, the clay mineral that is mainly responsible for shale swelling and hole tightening as a result. On the other hand, the high percentage of illite might lead to hole washout while the kaolinite and chlorite could produce a slight effect on hole collapse and time-dependent failures. Therefore, the drilling fluid should be compatible with shale components to reduce the probability of chemical rock degradation. (Asef & Farrokhrouz, 2013).

1.4. NONPRODUCTIVE TIME IN SOUTHERN IRAQ

Drilling experience in South Iraq have given several problems; varying from drilling fluid losses, stuck pipe, hole tightening, caving, poor cementing, and logging tool sticking. Tight hole problems were infrequently encountered in surface sections of the middle Miocene formation while they occurred extensively in the intermediate part of the Paleocene age (Dominantly Limestone) interval. In the intermediate hole, fewer moderate mud losses were reported in the Paleocene age formation (Dominantly Limestone), but they escalated in the middle and late Eocene (interbedded limestone and dolomite) zones. Minor caving problems were detected in the upper Cretaceous limestone production interval that could have occurred because of the formation heterogeneity in the analyzed wells or inadequate drilling circumstances. Moreover, a considerable number of stuck pipe problems, which led to the loss of expensive steering tools or could possibly change the original drilling plan and, subsequently, side-tracking to other trajectories, were surveyed in the upper Cretaceous shale formation. Also, the non-productive time, which surpassed the drilling expenditure immensely, increased enormously.

Intrinsically, in production interval, several procedures have been conducted during the drilling of the shale formation, particularly in deviated wells. However, some of these treatments provoked other problems in different zones. For instance, some of these

practices that resulted in mechanical wellbore failure in this shale formation can be resolved by increasing the mud weight (which is significantly higher than the pore pressure), but it induces differential sticking in the limestone reservoir section and causes formation damage. In brief, finding a solution for the particular formation might provoke other drilling problems. Therefore, examining all problems for each section may increase the likelihood of obtaining the optimum well design with the lowest NPT.

1.5. THESIS OBJECTIVE

The main objective of this thesis was to optimize the controllable parameters in drilling design to mitigate the stuck pipe problems in the upper Cretaceous (Tanuma shale) formation as well as enhance the drilling performance in production cost-effectively. The main objective can be broken down into the following tasks:

1. Construct a geomechanical model of the Tanuma formation including the rock strength and stress field (magnitude and orientation) and take into consideration thermally- and chemically-induced stresses.
2. Perform a wellbore stability history matching with offset wells and, hence, compute the suitable mud weight to prevent onset shear failure and avoid onset tensile failure.
3. Analyze the well trajectory design and determine which directions are less stable and more stable
4. Optimize the drilling parameters to reduce the shale exposure time
5. Evaluate the swabbing effect to enhance the drilling practice.

2. GEOLOGICAL FIELD DESCRIPTIONS AND DRILLING PRACTICES

2.1. TECTONIC EVOLUTION OF SOUTHERN IRAQ

Iraq is located in the northeastern corner of the Arabian Peninsula, more specifically on the boundary of the Arabian plate with Eurasian plate from the Iranian-Turkish side. Tectonically, an extensional movement of this plate was induced in the subduction zone along the Iraq-Iran border. This subduction zone provokes a line of seismic activity due to the rifting of the Arabian plate that was caused by the mid-ocean ridge in both the Red Sea and the Gulf of Aden, as illustrated in Figure 2.1.

Generally, during the Late–Permian/ Early-Triassic period, the Iranian and Turkish plates were separated from the Arabian plate by extensional movement and formed the Neo-Tethys Ocean (Al-Qahtani et al., 2005). The extensional movement continued during the Jurassic period and widened the Neo-Tethys Ocean (Numan, 1997). In the Cretaceous period, geodynamic inversion caused tectonic compression and subduction of the ocean crest of the Iranian and Turkish plates. Thus, the tectonic set up in this time plays an essential role in forming passive margins in the Arabian plate side and active margins in the Iranian-Turkish plate side (Numan, 2000). Since then, a passive margin developed and was divided into the continental shelf and continental slope zones. In the southern Iraq, basins deposited in the lower Cretaceous period, in the area of the ocean crest with the continental crust. The majority of these depostion were continental shelf and contained a half-graben basins formed by a listric fault, as illustrated in Figure 2.2. Four compressional tectonic events occurred in the late and early Cretaceous period had a large influence on the stratigraphy (Numan, 2000). Finally, the Neo-Tethyan Ocean was closed by the convergence of the Arabian and Eurasian plate in the Eocene period. As a result of the compressional movements culminating by closing the Neo-Tethyan Ocean during Eocene on the passive margin, the rock deformed and formed tremendous oil traps that play a significant role in the present petroleum system in the southern Iraq basins, as shown in Figure 2.3.

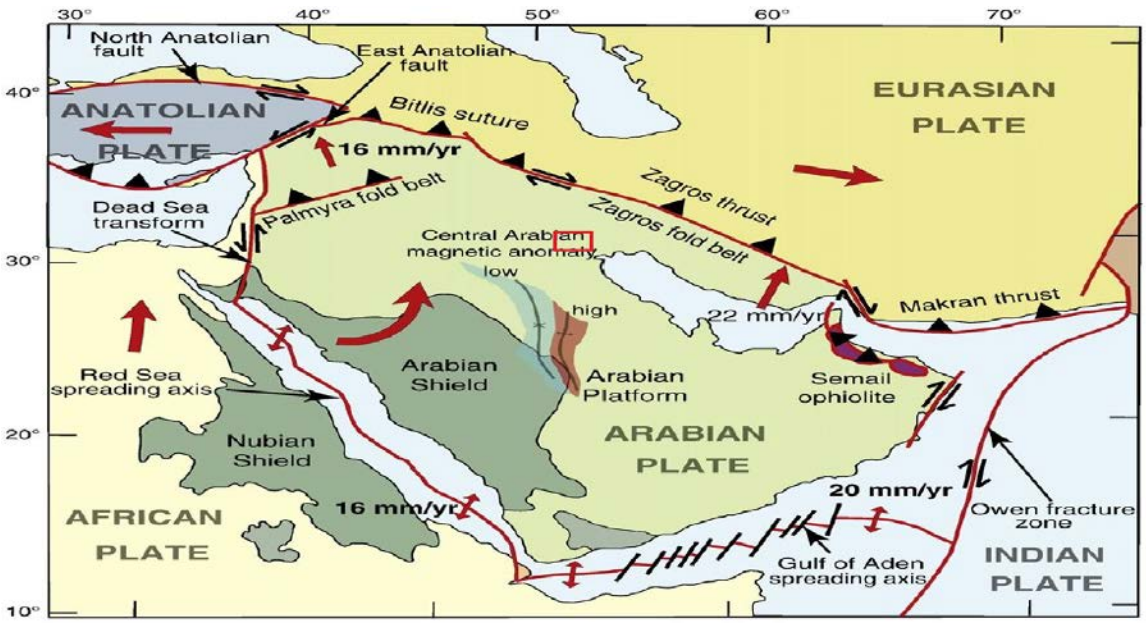

Figure 2.1. Present location of Arabian plate, the red rectangular represent the area of study (Stern & Johnson, 2010).

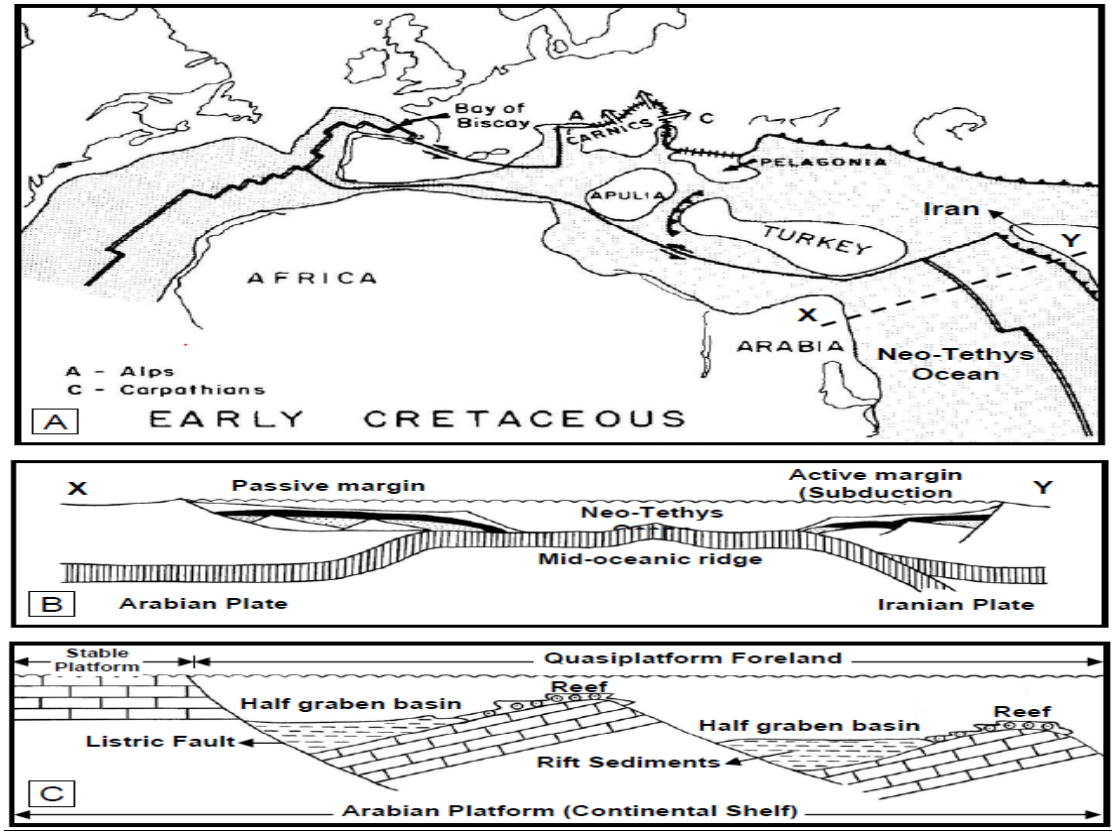

Figure 2.2. The Arabian plate during lower Cretaceous (Al-Bayatee et al., 2010).

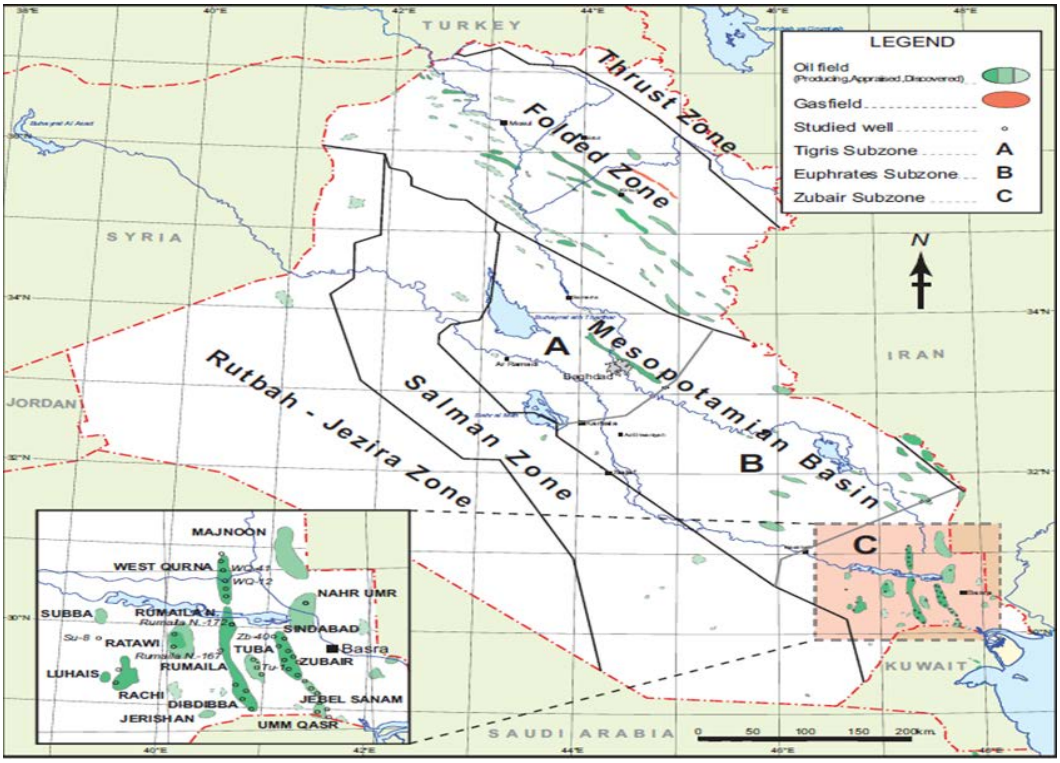

Figure 2.3. Southern Iraq oil fields (Abeed et al., 2011)

2.2. GEOLOGICAL DESCRIPTION

The lithological succession in southern Iraq is basically formed due to five separate tectonic periods named Megasquences (Sharland et al., 2001). Figure 2.4 shows the stratigraphy column for the southern Iraq region and the formations. The lithological column is comprised mainly of carbonate rock with a few shale and sandstone formations.

The analysis was focused on the Khasib and Tanuma formations. The Khasib formation consists of two parts. The upper part contains shale and limestone while the lower part is comprised of limestone that deposited in Lagoon environment. In the same cycle, the Tanuma formation was deposited near the shore basin, in partly euxinic conditions in the Santonian stage. It is also composed mainly of shale with minor streaks of limestone in addition to Marl in some wells (Alsharhan et al., 1997).

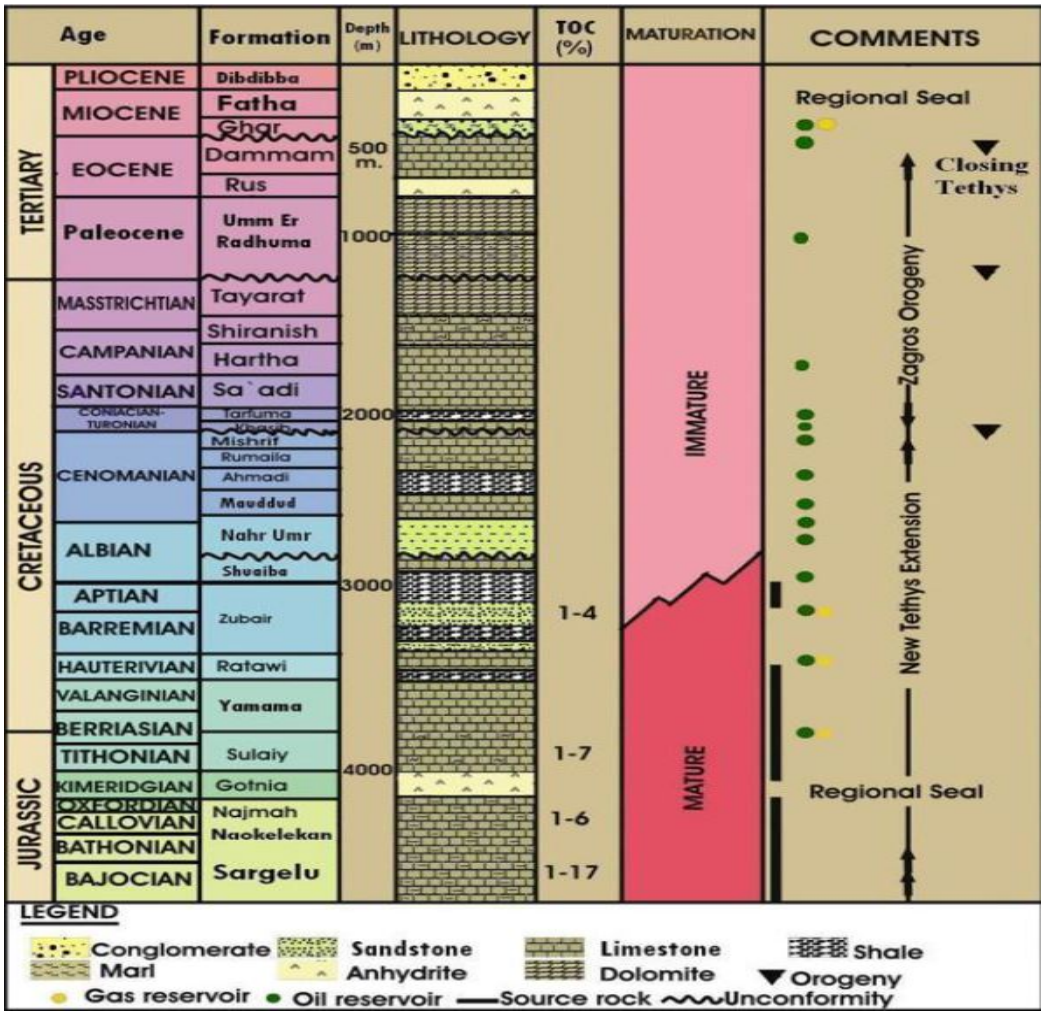

Figure 2.4. The stratigraphy column in southern Iraq (Al-Ameri et al., 2011)

2.3. STRUCTURAL GEOLOGY OF SOUTHERN IRAQ

The area in southern Iraq is gently sloped in the direction of the Persian Gulf and with a limited relief (Jassim and Goff, 2006). Subsurface geological structures such as folds, faults, and salt domes are the primary contributor in forming most of the traps for the petroleum reservoir in southern Iraq (Almutury et al., 2008). In the research area, the seismic studies indicated a plunging asymmetric anticline, which was formed during the compressional movement of the listric fault in the passive margin trending NW-SE (Al-Marsoumi et al., 2005). Particularly, the normal faulting regime is dominant in most of the oil fields in the Tigris subzone (Almutury et al., 2008). In addition, the magnetic and gravity measurements analysis conducted in the part of Mesopotamia located between

Qurna City and Amara province demonstrated a normal faulting regime in most of the area of study, as shown in Figure 2.5 (Amin et al., 2014). Admittedly, there are a limited number of stations that detect the seismic activity in southern Iraq, but a number of authors have investigated the seismicity information in terms of focal mechanism analysis. Ghalib (1974) studied 77 fault plain solutions in Iraq and surrounding countries and concluded that a normal faulting regime resulted from earthquakes events. Recently, a focal mechanism was investigated by Jasim (2010) based on previous seismic measurements and some newly updated readings, and it also suggested a normal faulting regime in the study area.

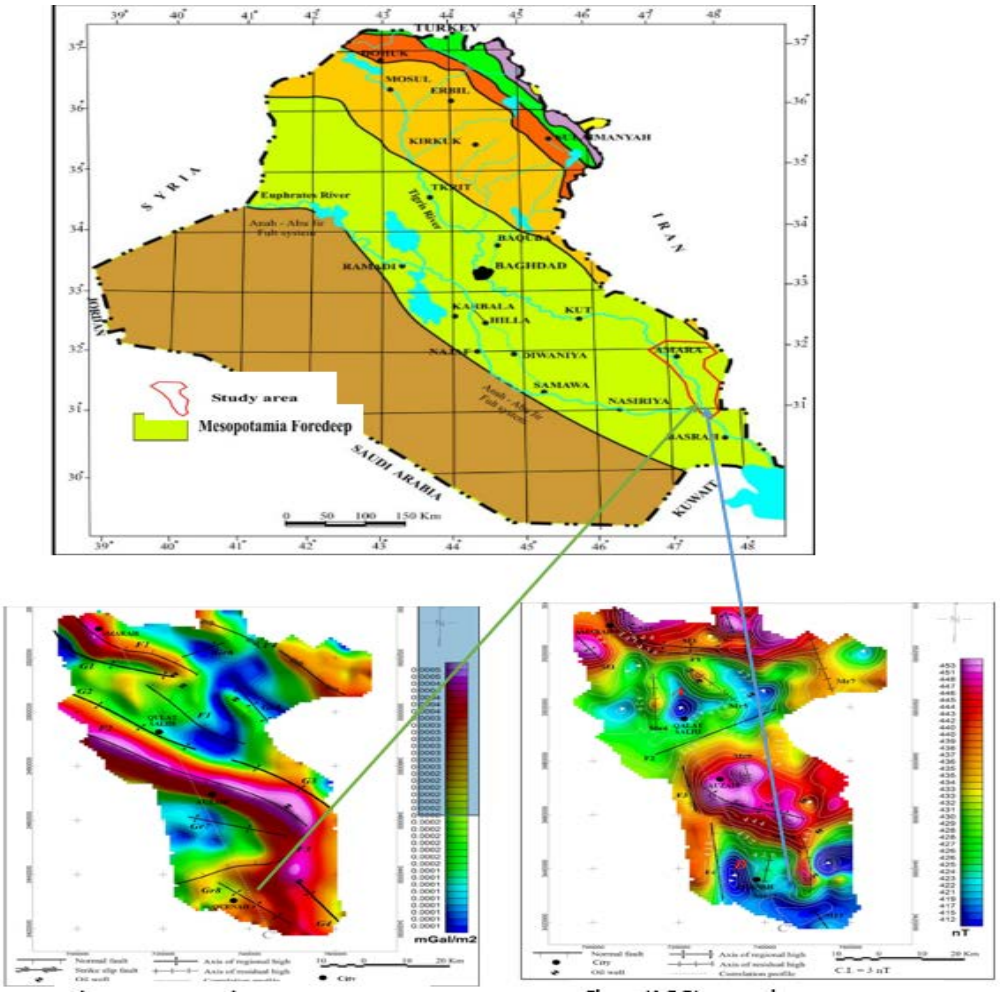

Figure 2.5. Gravity and magnetic measurements (Amin et al., 2014).

2.4. DRILLING OPERATIONS IN SOUTHERN IRAQ

Oil is produced from vertical and highly-deviated wells in southern Iraq fields. The depths of these wells vary between the upper Jurassic and Tertiary ages, but the majority of wells have been drilled to the Cretaceous age. The wells were designed to have four successive sections when the Mishrif limestone is the target interval. Currently, wells are drilled from pads dividing the well location into several clusters, each containing several well slots to saves the rig time by rig moving (Ogoke at al., 2014).

The well head distance between the wells is designed to be 7m on the cluster with numerous wells in each cluster. (Karsakov et al., 2014). Nonetheless, pad drilling has led to more drilling problems that are associated with devaition such as pipe sticking and severe to complete losses. Deviated wells also require accurate well path monitoring to prevent collusion with the other wells. Therefore, as the well number in each pad increases, the complexity of the well design and the affiliated problems intensifies. As a result, proper well design is crucial when dealing with pad type drilling constructions.

2.5. WELL DESIGN

Data from 50 wells in the southern Iraq field was examined to determine the formation and drilling in each section. These wells were selected randomly to describe the drilling design and event in each hole. Figure 2.6 illustrates the typical well design in this region.

The daily drilling and final well reports were used to quantify all necessary drilling parameters and the problems in each interval. The geological reports along with the drill pipe tally sheets were also investigated to obtain; the formation tops, casing size and setting points. The quality control for this data was conducted by comparing it with other data such as mud logging data and real-time monitoring information. A typical well profile in the southern Iraq field was summarized and is presented in the following sections.

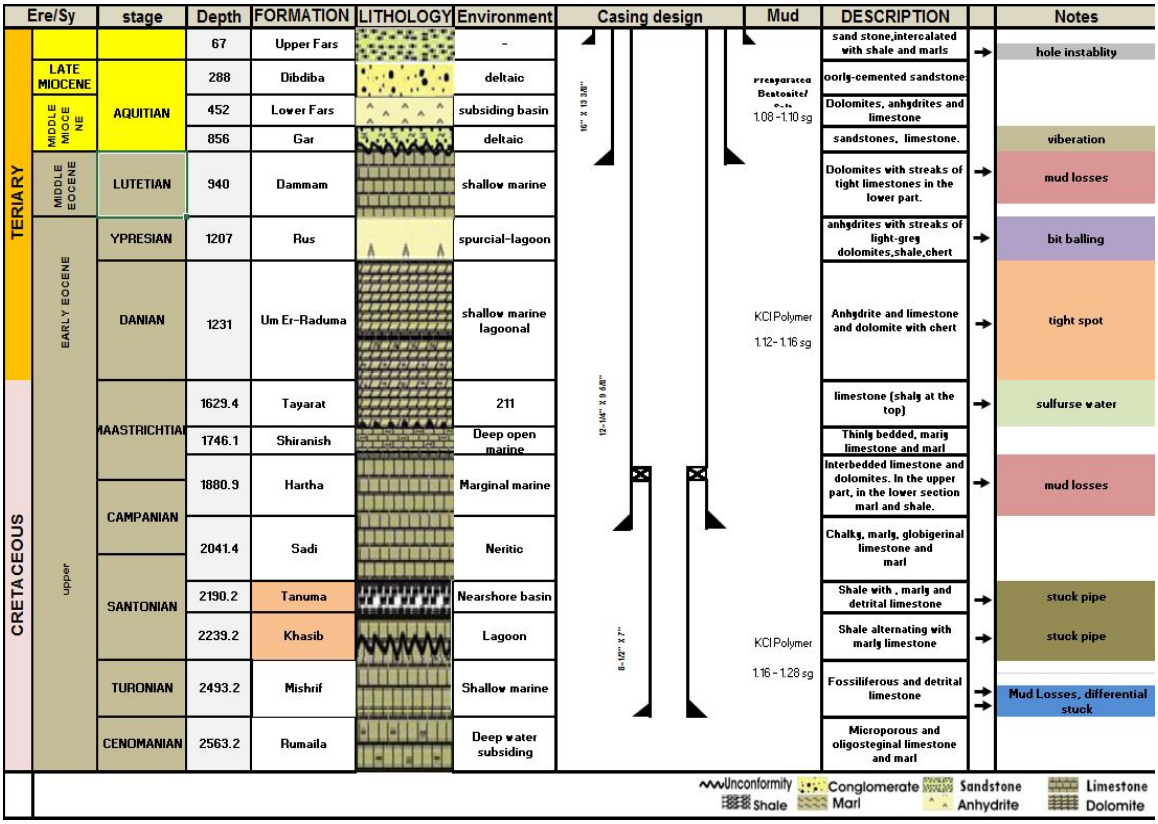

Figure 2.6. Typical well design in area of study

2.5.1.Conductor Section. Commonly, a 24 in. conductor hole is drilled and then cased by an 18 5/8 in. casing to the top of the upper Fars formation. The main function of the conductor is to seal off the fresh water table in the surface hole formations (Armenta et al., 2013). In addition, it prevents washout in the unconsolidated Hammar and Upper Fars formations. The drilling practice in the field is to start with low Rate of Penetration (ROP) and Weight on Bit (WOB) to prevent vibration-related hole stability. The drilling fluid used in this section is pre-hydrated bentonite weighted between 1.05 and 1.08 sg.

2.5.2.Surface Section. The surface section is usually drilled with 16 in. or 17.5 in. bits and cased with a 13 3/8 in. casing to the top of the Dammam formation. The surface section protects the poorly-cemented sandstone in the Dibdibah and Ghar formations as well as the aquifer zone in this interval. Operationally, bit balling has been noticed in the Lower Fars formation and mitigated by adjusting the flow rate or reducing the weight on the bit. A stabilized Bottom Hole Assembly (BHA) is used to mitigate tool vibration in this

interval. The drilling fluid used in this section is Pre-Hydrated Bentonite / salt water Polymer weighted (1.10 -1.14) sg. Similarly, the fluid losses in this drilling fluid were uncontrolled to help in forming mud cake, which improves the stability of the poorly-cemented zones. The formations drilled through this section are Dibdibah, Lower Fars, Ghar, and part of the upper Dammam.

2.5.3.Intermediate Section. The intermediate section is drilled via 12 ¼ in. bit and cased by 9 5/8 in. casing to the top of the Sadi zone. The formations in this section are part of the Dammam, Rus, Um-al-Radhuma, Tayarat, Shiranish, Hartha, and upper Sadi formations. Severe drilling fluid losses are experienced in the Dammam formation due to shaly limestone with high porosity. Some wells in the Rus formation have partial drilling fluid losses, while other wells experience bit damage. Thus, it is necessary to control the drilling parameters such as manipulating low RPM and high WOB. In Um-al-Radhuma, many wells have tight spots. Therefore, hole reaming may be required. The Shiranish formation shows moderate to highly-reactive clay content, which elevates the tendency of bit balling. Hence, an inhibitor might be added to the drilling fluid. Although high-pressure sulfur water in the Tayarat formation is observed, the drilling fluid weight is normally used to control it in most cases. On the other hand, the Hartha formation causes multiple problems like tight spots, partial to severe losses, and stuck pipes in various depths across this formation. The drilling fluid losses do not occur because of a drilling fluid weight larger than the fracture gradient but are caused by the fractured nature of Hartha limestone, so the chemical composition of the drilling fluid should be compatible with this rock, and the rheological properties should be designed to avoid any unwanted ECD that causes a dynamic drilling fluid loss in many wells. In this hole, the drilling fluid type used is KCL polymer with a weight of 1.08-1.16 sg. Ultimately, an intractable cement loss occurs while running the cement job, which has been reported predominantly in this section so that the well integrity is a colossal concern, especially in a sulfurase water zone.

2.5.4.Production Section. The final section in the casing sequences is the liner casing, which has been hangered inside the intermediate section in most cases. Normally, the hole is drilled with an 8 ½ in. bit and cased by 7 in. casing to the target zone (Mishrif formation).. Thus, it isolates the production zones, and it provides appropriate control to the reservoir. Almost always, stuck pipe occurs while drilling the Tanuma shale formation,

especially in deviated wells. However, it is not noticeable in drilling vertical wells. The upper part for Tanuma is shale and tight limestone, but the lower part is unconsolidated and fractured shale with marl in some locations. Furthermore, differential stuck occurs in some wells in the Mishrif formation as well as drilling fluid losses in rare cases. Recently, KCL polymer -Water Base Mud (WBM) with a weight ranging between 1.25-1.35 sg was used.

To sum up, the wellbore instability problems are the major concern during drilling operations in southern Iraq. Therefore, the precise estimation of the rigorous well construction can be helpful in mitigating these difficulties that are commonly derived from geomechanical /drilling factors. However, the interested area doesn’t have such an analysis in spite of the severity of the wellbore problem. Thus, this research addresses as a significant case study for a field in southern Iraq.

3. LITERATURE REVIEW ON WELLBORE STABILITY

3.1. BACKGROUND

Wellbore failure in shale formations has been studied extensively because the majority of drilling problems relates to wellbore failure in shaly intervals (Aadnoy & Chenevert, 1987; Asuelimen & Adetona, 2014; Bradley, 1979; Fjaer, 2008; Cheatham, 1984; Mkpoikana et al., 2015; Yan et al., 2013; Zoback, 2007). The mechanisms beyond the shale instabilities are complicated and unique to each wellbore instability analysis in terms of problem alleviation. Some authors have revealed that these problems are related to mechanically-induced wellbore failure when the stresses around the wellbore exceed the rock strength in specific failure criteria. Others have included chemical sources of wellbore failure when the physio-chemical interaction occurs between the fluids in a wellbore. In addition, the heat transfer between the drilling fluid and underground rock has been shown to contribute to well destabilization by several authors. The anisotropic effect on the shale mechanical properties has also been addressed to determine the more likely failure directions with respect to the well path.

Bradley (1979) introduced the mechanically-induced wellbore failure factors by performing a comprehensive wellbore instability analysis of deviated wells. The study developed the stress cloud concept that was inherently based on the weighted contribution of each wellbore instability variable on the well integrity. It suggested that borehole failure could be avioded when an emphasis is directed to the following factors: the far field stresses, the influence of borehole design on an intact rock, and the impact of wellbore pressure and the drilling fluid properties on the rock strength. He also discussed the variations within the required drilling fluid weights to ensure borehole stability when the well inclinations have been changed

Aadnoy (1988) studied the influence of the shale mechanical and elastic parameter anisotropy on randomly deviated wellbore failure. He developed a mathematical model to account for the cohesion, angle of internal friction, shear, and tensile strengths along and perpendicular to the bedding plane. Mohr-coulomb failure criterion was used to demonstrate the effect of pore pressure on the collapse failure in laminated rock. Moreover, in this type of effect, the shale deformation was sensitive to the orientation of the well with

respect to the bedding planes. It applied the transversely isotropic method in which the elastic parameters are equal in all directions in a horizontal plane.

Hale & Mody (1993) inferred that the wellbore instability analysis in the shale based only on the mechanical effect is not sufficient to ensure well integrity, and the chemical effect should be considered. Therefore, they studied the chemical effect induced stress alteration during the interaction of the drilling fluid properties with such a formation. They concluded the differences between the shale and hole fluid chemical potentials/hydraulics were the main driver for the fluid/ ion exchange between these media. The fluid movement also altered the shale pore pressure and the effective stress magnitude in the vicinity of the wellbore. Indeed, his study involved the impact of salt concentration and drilling fluid density on wellbore failure.

Maury and Guenot (1995) concluded the thermal effect should be included in the borehole instability investigation. They came up with the concept that the heat transferred between the drilling fluid and formation might possibly disturb the wellbore integrity status and drilling fluid properties. The drilling fluid cooling effect was equated to increase the density of the drilling fluid weight. However, the drilling fluid heating effect was deemed similar in reducing drilling fluid density. These two aspects might potentially result in tensile and shear failures, respectively. In addition, they summarized parameters, such as the geothermal gradient, flow rate, drilling fluid thermophysical properties, bit diameter, and well depth that influenced this phenomenon

Kadyrov (2012) investigated the wellbore instability of horizontal wells in the West Kazakhstan field that suffer from serious wellbore problems. The wellbore failure was imputed from inappropriate selections of the following factors: well trajectory, drilling fluid weight, and types. Hence, an extensive geomechanical model has been implemented to minimize the drilling difficulties via maximizing the drilling margin in future planning wells. This study coupled important factors in rock mechanics related to wellbore failures such as the mechanical stresses, temperature effect, shale physicochemical interactions, and fluid flow-induced stress. Then, the Mogi-Coulomb failure criterion was used to obtain the optimal drilling fluid weight

McLellan and Cormier (2013) analyzed the shale stability in the Ferine formation located in NE British Columbia. He observed that the majority of these problems arose due

to the combination of different components such as well trajectory design, shale properties, stress anisotropies, and drilling fluid properties. Moreover, increasing the drilling fluid weight to prevent the onset of the wellbore collapse failure could deteriorate the wellbore failure status. The failure was mostly triggered when the wellbore attack angle increased, especially in rock that had anisotropic strength. Therefore, an extended analysis of geomechanical and drilling hydraulic parameters should be conducted to mitigate wellbore failures.

It has been demonstrated that superimposing all potential wellbore instability perturbations could possibly be facilitated in stabilizing the wellbore (Araujo et al., 2006; Chen & Chenevert, 2001; Chen et al., 2001; Zhai & Corp, 2011,Nes et al, 2015). Therefore, extensive wellbore investigations have been carried out by combining all previously addressed effects in a geomechanical model.

3.2. GEOMECHANICAL MODEL FOR WELLBORE STABILITY ANALYSIS.

An important step in wellbore stability analysis is understanding the fundamental factors that governs rock failure. The crucial factors include the resistance of the rock's internal friction relevant to the applied force per unit area, (i.e. stress (S_i)). Strain (ϵ) deformation is associated with an applied load level, particularly if the material components are displacing to a new position with respect to original location. If the force is oriented in a way other than normal to the cross-section area, it decomposes to normal stresses that are responsible for the tensile or compressive failure and shear stress (τ) that causes slipping or shear failure. The following sections address the geomechanical model components in a wellbore stability analysis.

There are different behaviors of a rock when it undergoes certain load levels and conditions, which can potentially serve as a beneficial tool in failure predictions. Assming linear elasticity, the stress and strain behave linearly, and the slope of the line represents the stiffness of the rock (Jaeger & Cook, 2007). Nonetheless, if the straight line is extended to a point when the rock strength is exceeded, then the plastic deformation starts to evolve. Put differently, in a stress-strain curve, the rock returns to its original state after the stress is unloaded if the applied force ranges in the elastic region limit while it does not if it is in

the plastic region (Fjar et al., 2008). Poro- elasticity and viscoelasticity theories describe other types of rock behaviors that are present when the rocks are saturated with fluid. These methods rely on the fact that some exerting stress can be absorbed by the fluid in the rock‘s void space. Therefore, the rock behavior in a stress-strain chart depends on the rate of applied force as well as the rate of the fluid oust from the rock with respect to the applied force (Zoback, 2007).

3.3. PORE PRESSURE AND EFFECTIVE STRESS.

The pore pressure (Pp) is essential in the safe operational drilling fluid window that is constrained to the lower limit of drilling fluid density in overbalanced drilling. Equation 1 is typically gives the pore pressure of the zone of interest if the depth (z) and pore pressure gradients (ρ_g) for each interval are available. The effective stress concept (Terzaghi, 1943), is defined as the result of subtracting the total stress (S_t) from the pore pressure (Equation 2).

Commonly, there are several methods to predict the pore pressure, and they can be divided into three types of measurements: pre-drill pore pressure, pressure during drilling, and post drill pressure (Li et al., 2012). These methods are validated by the direct measurement of the pore pressure in a permeable zone using Formation Pressure While Drilling (FPWD), to obtain an instant measurement of pore pressure, or packing off the interesting zone and then performing a Repeated Formation Test (RFT) (Azian et al., 2013).

$$Pp = \int_0^z \rho_g * g * dz \tag{1}$$

$$s_{ev} = S_t - P_p \tag{2}$$

Where (g) is the gravity acceleration 9.8 m/s ^{2}.

3.4. ROCK MECHANICAL PROPERTIES.

Elastic parameters describe the behavior of rock in loading and unloading states that can be measured in the lab by using triaxial compressive test. The Young modulus (E_D) is considered to be a reckonable indicator of the rock's stiffness that acquires from lab analysis. The Poisson ratio (v) represents the ratio of lateral strain to longitudinal strain can also be determinate from the tri-axial test.

Other continuous methods for estimate the elastic properties have been innovated by using geophysics logs. Since it is costly and time-consuming to perform coring in the entire well interval, in addition to, the rock sample only represents a small segment of the wellbore wall (Horsrud, 2001). Therefore, the dynamic technique has been employed throughout using the sonic (shear velocity (V_s) and compressional velocity (V_p)) and the density logs (bulk density (ρ_p)) measurements to estimate elastic parameters. However, in some circumstances, the compressional velocity is not recorded therefore an empirical equation might be use to derived it depended on the available shear velocity (Equation 3) (Castagna, 1985). The Poisson ratio can be calculated by using the acoustic log parameters by Equation 4 (Zoback, 2007). The Young moduli also compute mathematically from Equation 5. Then the dynamic Young's modules should be converted to static (E_s) by using Equation 6 (Lacy, 1997).

Similarly, the plastic or inelastic properties of the rock can be calculated by using static and dynamic approaches. In the static method, the Unconfined Compressive Strength (UCS) can be obtained from the core test, in which an unconfined pressure is applied to the rock sample (only axial load). However, in the tri-axial test several confining pressure are conducted associated with axial stress, then the intercept of the tri-axial chart represents the UCS. Concerning dynamic approaches, empirical equations for different lithology and geological time have been derived in many regions base on practical observations of static methods such as Equations 7 and 8 by Horsrud (2001) and Lal (1999) (applicable to high porosity shale in the North Sea), respectively. Also, Equation 9 estimates the UCS values for Pliocene and younger shale in the Gulf of Mexico region. Equation 10 is used to anticipate the compressive strength globally (Chang et al., 2006).

The angle of internal fracture (Φ), can be measured by using the triaxial-test as a static measurement, but there are also several well logging-derived equation such as Equation 11 (Lal, 1999).

$$V_p = 1.16 \times V_s - 1.36 \quad (3)$$

$$E_D = 2 \times G \times (1 + v) \quad (5)$$

$$v = \frac{Vp^2 - 2 \times Vs^2}{2 \times (Vp^2 - Vs^2)} \quad (4)$$

$$E_s = 0.018 \times E_D^2 + 0.422 \times E_D \quad (6)$$

$$\text{UCS} = 0.77 \times \left(\frac{304.8}{\Delta \text{t}}\right)^{2.93} \quad (7)$$

$$UCS = 10 \times \left(\frac{304.8}{\Delta t} - 1\right) \quad (8)$$

$$UCS = 0.43 \times \left(\frac{304.8}{\Delta t}\right)^{3.2} \quad (9)$$

$$UCS = 1.35 \times \left(\frac{304.8}{\Delta t}\right)^{2.6} \quad (10)$$

$$\Phi = \sin^{-1}\left(\frac{\text{vb}-1000}{\text{vb}+1000}\right) \quad (11)$$

Where (Δt) is compressional travel time of the acoustic log usec/ft.

3.5. ANDERSONIAN STATE OF STRESS

The in-situ stresses of the intact rocks are assumed to expose into three principles Andersonian stresses (Anderson, 1951). It assumes that the Earth surface is a free surface, and there are three mutually perpendicular principle stresses in the subsurface: one of them vertical and the other two horizontals. Several methods and approaches have been studied and developed to obtain the directions and magnitudes of each stress (Bell, 2003).

3.5.1.Vertical Stress. Vertical stress (Sv) is the stress representing the bulk density of the overlying rock. The bulk density consists of the weight of the solid particles (matrix density ($\boldsymbol{\rho_{ma}}$) and the fluid (fluid density ($\boldsymbol{\rho_f}$) of the pore fluids expressed in Equation 12. Therefore, There are several approaches to estimate the bulk density such as; core sample analysis, porosity log and use of typical rocks density value, or deploying a wireline density log tool) (Peng, 2007). Because it is not common to core the entire well depth, calibrated dynamic density sources are used in overburden stress calculations (Burnett et al., 1993).

When the bulk density is determined, the total vertical stress is estimated by integrating the bulk density gradient in each formation over the depth of interest using Equation 13 (Rabia, 2010).

$$\rho_b = (1 - \phi) \times \rho_{ma} + \phi \times \rho_f \tag{12}$$

$$Sv = \int_0^z \rho_b \times g \times dz \tag{13}$$

Where (ϕ) is the rock porosity unitless.

3.5.2.Minimum Horizontal Stress Estimation. The magnitude of the minimum horizontal stress (Sh) is fundamental to understanding the rock response during the exploration and development stages to obtain a problem-free wellbore (Plumb, 1994; Woodland & Bell, 1989).

Number of imperially derived equations have been developed for different regions to calculate Sh. Equation 14 was proposed by Hubbert and Willis (1957) to obtain the least

principle stress in the normal faulting regime (Gulf of Mexico) according to vertical stress and pore pressure values (Zoback, 2007). A similar concept was adopted by Matthews and Kelly (1967) to relate the S_h with the formation pressure in Equation 15. This equation was derived for the area in the Gulf coast of and southern Texas through the manipulated ($k_i(z)$) variable that is a function of the depth, and it is the ratio of Sh from fluid injection test to Sv. After that (Eaton, 1969) used the principle of bilateral constraint to drive the ($k_i(z)$) variable to estimate Sh in the Gulf of Mexico by combining: vertical stress, pore pressure and Poisson ratio in Equation 16. (Breckels & van Eekelen, 1982) came up with other empirically-derived equations, that related the depth to the formation pressure and hydrostatic pressure, then data of hydraulic fracturing tests were compiled from various regions to drive Equations 17 and 18. Afterward, the analysis from Zoback and Healy (1984) relied on the frictional strength equilibrium concept; meaning this theory controlled the steady state of a pre-existing complex geological structure such as fractures and fault. These geological structures tend to slip if they undergo to stress level exceeding the coefficient of friction in an area, along with insufficient normal stress. Contradictorily, it is at equilibrium when both the friction coefficient and normal stress are resisted to the slipping action; therefore equation 19 was formulated for Sh estimation. Lately, (Holbrook et al., 1993) found other mathematical relationship to affiliate the Sh with rock porosity in Equation 20. It worth to state, these imperially-derived equations should be calibrated with the available hydraulic fracturing tests to get a robust stress log values. Appendix A contains other types of empirical derived correlations.

For integrity purposes, the Leak-Off Test (LOT) is frequently conducted during the drilling operation to ensure the designed drilling fluid pressure does not fracture the rocks in the next hole as well as the Sh estimations (Lee et al., 2004). Practically, LOT is carried out after (10 to 20 ft.) being drilled below the last casing shoe then the Rate Hole rocks are isolated and pressurized, until the deviation point from a straight line in the pressure vs. time chart is reached, which represents the LOT point shown in Figure 3.2. This point is approximately close to the least principal stress if the pumping continues beyond the formation breakdown pressure when both low flow rate and fluid viscosity are utilized (Zoback, 2007). An excessive pumping procedure is primarily required to extend the induced fracture deep in the formation which is diminished both the wellbore stresses

and rock tensile strength effects. After that, the pumping pressure goes down to a stable level, where the fracture propagates away from the wellbore, which is called Fracture Propagation Pressure (FPP). Then, instantaneous shut-off pump is processed, and the pressure being recorded, named Instantaneous Shut in Pressure (ISIP). This point represents a good estimation of the upper limit of the lease principal stress because the pressure escalation due to high fluid viscosity is disappeared (Woodland & Bell, 1989). In the case of the viscous treatment fluid, the Fracture Closure Pressure (FCP) can be deemed as best representative of the lease principle stress (Zoback, 2010).

.

$$\mathrm{Sh} = 0.3 \times (\mathrm{Sv} - \mathrm{Pp}) + \mathrm{Pp} \tag{14}$$

$$\mathrm{Sh} = \mathrm{k_i}(\mathrm{z}) \times (\mathrm{Sv} - \mathrm{Pp}) + \mathrm{Pp} \tag{15}$$

$$\mathrm{Sh} = \left(\frac{\mathrm{v}}{1 - \mathrm{v}}\right) \times (\mathrm{Sv} - \mathrm{Pp}) + \mathrm{Pp} \tag{16}$$

$$\mathrm{Sh} = 0.197 \times \mathrm{z}^{1.145} + 0.46 \times (\mathrm{Pp} - \mathrm{Ph}) \quad \text{For z} > 11{,}000 \text{ ft} \tag{17}$$

$$\mathrm{Sh} = 0.197 \times \mathrm{z}^{1.145} + 0.46 \times (\mathrm{Pp} - \mathrm{Ph}) \text{ For z} < 11{,}000 \text{ ft} \tag{18}$$

$$\mathrm{Sh} = [(1 + \mu^2)^2 + \mu)]\text{^}2 \times (\mathrm{Sv} - \mathrm{Pp}) + \mathrm{Pp} \tag{19}$$

$$\mathrm{Sh} = (1 - \emptyset) \times (\mathrm{Sv} - \mathrm{Pp}) + \mathrm{Pp} \tag{20}$$

Where (μ) is the coefficient of the internal friction angle that can be obtained from internal friction angle by $\mu = \frac{1+\sin(\Phi)}{1-\sin(\Phi)}$.

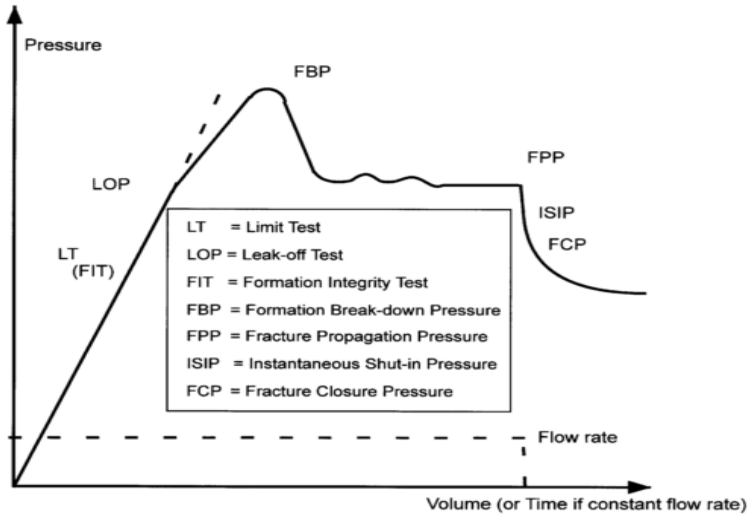

Figure 3.1. Leak-off test (Zoback, 2010).

3.5.3.Maximum Horizontal Stress. There is no direct way to directly measure the Maximum Horizontal Stress (SH) so estimation of SH is based on indirect methods (Aadnoy & Hansen, 2005). Similar to the least principal stress methods presented in Section 3.6.3, there are two separate measurements types. The first involves the approaches that alter the in-situ rock conditions, (i.e. wellbore hydraulic tests). The second methods are based on the rock behavior observations under various circumstances such as; borehole breakout, statically-derived equations and earthquake focal mechanism (Ljunggren et al., 2003).

Each method has its own limitations and drawbacks when it is implemented in real life situations. The empirical-derived methods are often established for a particular area and under specific assumptions that might be not applicable in another field, or it can result in erroneous outcomes. For example, the wellbore breakout width correlation is relied on the rock failure observation which is not necessarily due to the stress contrast (Ljunggren et al., 2003). Thus, a considerable attention should be paid to this technique when it uses for the SH estimations.

Several equations have been empirically developed by different authors and perspectives to obtain maximum horizontal stress magnitudes and directions. Equation 21 was developed to determine SH based on the wellbore breakout width (Blanco & Turner,

2011; TeufeL and Blenton, 1985). Also, Equation 23 was introduced to calculated the SH base on the types of fault regime, the values of Sv and Sh (Peng, 2007). Number of correlations being included in Appendix A.

$$SH = ((\mathrm{UCS} + 2P_p + \delta p) - S_h(41 + 2cos2\theta_b))/(1 - 2cos2\theta_b) \quad (21)$$

$$2\theta_b = \pi - W_{bo} \quad (22)$$

$$\mathrm{SH} = m \times (\mathrm{Sv} - \mathrm{S_h}) + S_h \quad (23)$$

Where (δp) is the differential pressure between borehole and pore pressures, (θ_b) is maximum angle of breakout, (W_{bo}) is the breakout width (Barton et al., 1988), and (m) is constant depended on the type of faulting regime range 0-2 (In normal fault, it is equal to 0.5) (Peng, 2007).

3.5.4.Stress Polygon. The constraint of the maximum horizontal stress magnitude in upper and lower bound respectively can be enacted by using the stress polygon technique (Zoback et al., 1986). This method depends on the friction strength theory, by which the stress magnitude is calculated at a given depth throughout manipulating; the overburden stress, pore pressure and coefficient of internal friction angle (μ) (Zoback et al., 2003). The polygon construction includes the probable existing three faulting regimes (normal faulting, strike-slip, reverse faulting) that can be represented by the diagram as shown in Figure 3.3. The SH and Sh are the domains of the polygon, and these stresses can be computed from one of the Equations 24, 25 and 26. The lower part of the vertical line in the diagram (at normal faulting area) is represented by the value of Sh from Equation 24 while the upper horizontal line (at reverse faulting area) is indicated the highest value of SH from Equation 26. The point in which the SH=Sh=Sv is considered the transition point between these faulting regimes based on the following facts. In Normal Faulting (NF) the stresses are: (Sv>SH>Sh) in Reverse Faulting (RF) the principal stresses are (SH>Sh>Sv), eventually, in Strike-Slip (SS) the in-situ stress are (SH>Sv>Sh).

Fundamentally, the stresses state is located in the area of the polygon as long as the reign of investigation in friction equilibrium state which is a normal state in most tectonically relaxing areas (Zoback, 2007). However, a modification of the polygon area can be achieved by taking into account the state of stress as well as the pore pressure change that might be shortening or widening the shape of polygon base on increasing or decreasing in the pore pressure, respectively. Also, by inserting the constraint of stresses value from the breakout width calculations of SH in the stress polygon can narrow down the possible range of SH.

The key function of the polygon is the possible bounded range of SH obtained by placing the best value of calibrated Sh (which might be obtained from the leak-off test) in the X-axis of polygon domain and measuring the corresponded values of SH in the stress polygon in Y-axis.

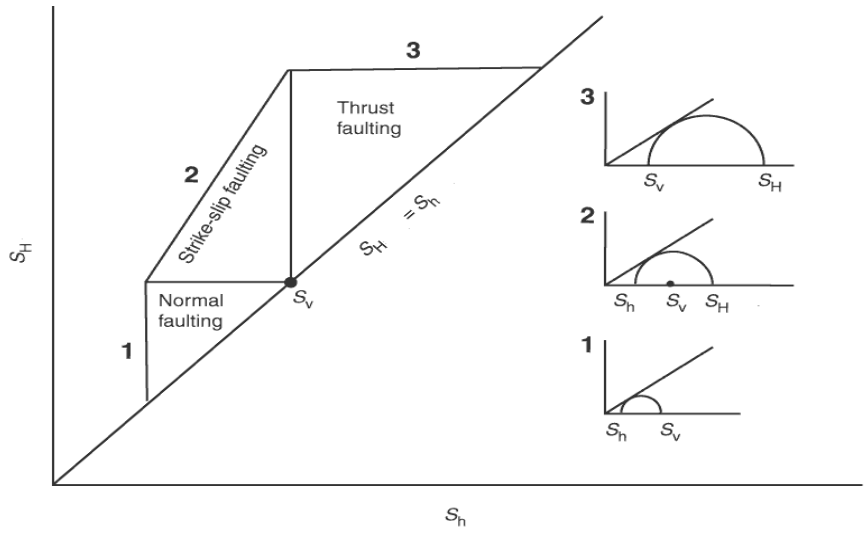

Figure 3.2. Stress polygon (Zoback et al., 2003).

$$\frac{S1}{S3} = \frac{(Sv - Pp)}{Sh - Pp} \leq (\mu^2 + 1)^{0.5} + \mu)\text{^}2 \text{ For NF regime} \qquad (24)$$

$$\frac{S1}{S3} = \frac{(SH - Pp)}{Sh - Pp} \leq (\mu^2 + 1)^{0.5} + \mu)\text{^}2 \text{ For SS regime} \quad (25)$$

$$\frac{S1}{S3} = \frac{(SH - Pp)}{Sv - Pp} \leq (\mu\text{^}2 + 1)\text{^}0.5 + \mu)\text{^}2 \text{ For RF regime} \quad (26)$$

3.5.5.Principal Stresses Around The Wellbore. Primarily, the stresses concentration around wellbore is different from the near wellbore region. The in-situ stresses concentrations are gradually converted to wellbore principle stresses as to get closer to wellbore‘s circumference because of the circular borehole geometry (Aadnoy, 2010). This state of stresses is also formed, due to the virgin rocks in the well being removed, and the parent rocks are replaced by the wellbore drilling fluid. Accordingly, it is contributed to form stress acting tangentially to the borehole named as hoop stress ($S_{\theta\theta}$) and stress acting perpendicular to the borehole named as radial stress (S_{rr}) as well as stress acting along of the borehole axis called axial stress (S_{zz}). Furthermore, in deviated and horizontal wells, the shear stresses (τ) come up to have effectiveness on the local wellbore stresses.

The determination of these stresses deems a crucial task in the wellbore analysis because the rock deforms in shear/tensile failure is mostly related to the magnitude of wellbore principal stresses. Shear failure evolves if the hoop/axial/radial stress is exceeding the shear strength of the rock. In the same regard, the tensile failure occurs when the hoop/axial stress is reached to the value of tensile strength (Fjar et al., 2008). So that the explicit knowledge of these stresses can assist to form a safe mud window in the drilling operation by avoiding the causes of wellbore failure when the drilling fluid density is appropriately selected.

3.6. STRESS TRANSFORMATION

In wellbore analysis, different types of coordinate systems in the vicinity of the wellbore that is required to be transferred to the borehole reference system. Understanding

these coordinate systems and their directions might give unmistakable diagnostics of the state of stresses around the wellbore (Aadnøy & Looyeh, 2011). Therefore, convenient transformation equations is used to transfer the stress tensor from the global coordinate system (Sv, SH, Sh) to the arbitrarily oriented wellbore Cartesian coordinate system (S_x, S_y, S_z) representing the stresses in x,y,z direction, repectively. Then the result is transformed to cylindrically wellbore coordinate system ($S_{\theta\theta}, S_{rr}, S_{zz}$) based one Kirsch solution of impermeable rock by Equations 27, 28, 29, 30, 31, 32, 33,34, 35, 36 and 37 (Aadnoy & Chenevert, 1987).

$$S_x = (SH \times cos^2\varphi + Sh \times sin^2\varphi)\, cos^2\gamma + Sv \times sin^2\gamma \quad (27)$$

$$S_y = SH \times sin^2\varphi + Sh \times cos^2\varphi \quad (28)$$

$$S_z = (SH \times cos^2\varphi + Sh \times sin^2\varphi) sin^2\gamma + Sv \times cos^2\gamma \quad (29)$$

$$\tau_{xz} = 0.5 \times (SH \times cos^2\varphi + Sh \times sin^2\varphi - Sv) \times sin2\gamma \quad (30)$$

$$\tau_{xy} = 0.5 \times (Sh - SH) sin2\varphi \times cos\gamma \quad (31)$$

$$\tau_{yz} = 0.5 \times (Sh - SH) sin2\varphi \times sin\gamma \quad (32)$$

$$S_{\theta\theta} = (Sx + Sy - \Delta pw) - 2 \times (Sx - Sy) \times cos2\theta - 4 \times \tau xy \times sin2\theta \quad (33)$$

$$S_{rr} = \Delta pw \quad (34)$$

$$S_{zz} = Sz - 2 \times \nu \times (Sx - Sy) cos2\theta - 4 \times \upsilon \times \tau xy \times sin2\theta \quad (35)$$

$$\tau_{r\theta} = \tau_{rz} = 0 \tag{36}$$

$$\tau_{\theta z} = 2 \times (\tau yz \times cos\theta - \tau xz \times sin\theta) \tag{37}$$

Where τ_{xz}, τ_{xy}, τ_{yz}, $\tau_{r\theta}$, τ_{rz} and $\tau_{\theta z}$ are the shear stress in x-z plane, shear stress in x-y plane, shear stress in y-z plane, shear stress in r-θ plane, shear stress in r-z plane, and shear stress in θ-z plane, respectively. The variables γ, φ, and θ are the well inclination from vertical, the well geographic azimuth and the well azimuth from maximum horizontal stress directions, respectively.

Finally, the principle stresses at each point at the wellbore wall can be obtained from Equations 38 and 39.

$$S_1 = \left(\frac{S_\theta + S_{zz}}{2} + \left(\left(\frac{S_\theta + S_{zz}}{2} \right)^2 + \tau_{\theta z}^2 \right)^{0.5} \right) - Pp \tag{38}$$

$$S_1 = \left(\frac{S_\theta + S_{zz}}{2} - \left(\left(\frac{S_\theta + S_{zz}}{2} \right)^2 + \tau_{\theta z}^2 \right)^{0.5} \right) - Pp \tag{39}$$

3.7. ROCK TENSILE STRENGTH

The critical of the rock tensile strength is related to the wellbore failure pose, when the principal stresses (hoop or axial) reach the value of the tensile strength as seen in Equation 40. However, sedimentary rocks ability to withstand tensile stress is small and the presence of natural fractures causes the rock tensile strength to vanish. Therefore,

tensile failure is commonly assumed to occur when either hoop stress or axial stress reach zero (Aadnoy & Chenevert, 1987; Bradley, 1979).

$$S_{\theta\theta \text{ Or } zz} \geq T_o = 0 \quad (40)$$

3.8. SOURCE OF STRESS AROUND THE WELLBORE

The main contributors to the failure are caused by stress, strength or pore pressure alterations. The well trajectory design, with respect to far field stress and the drilling fluid weight being used, is profoundly responsible for mechanical wellbore failures. The pore pressure alterations have an influence on the rock's strength and eventually deteriorate the wellbore stability that might possibly induce due to chemical effect. The state of stress in the well also could be changed by thermal effect. Finally, the anisotropic nature of the rock leads to variations in rock strength according to test directions. Thus the strength of the rock is directionally dependent.

3.8.1. Chemical-Induced Stress at the Wellbore Well. The chemical effect is caused by the interaction of continuous phase of drilling fluid with either formation rock or fluid. This interaction leads to either stress or pore pressure alteration around the wellbore, which is weakening the rock in some cases (Hale et al., 1993). The shale behaves as a non-ideal semi-permeable membrane, which governs the ion /solvent movement between the continue phase of the drilling fluid and the shale (Yew & Wang, 1992). These actions depend on the activity of water phase (aw) in the drilling fluid, shale activity (as) (the fresh water has chemical activity equal to 1 while salty water is less than 1) permeability, temperature (T), confined pressure as well as reflection coefficient (I_m), that indicates whether solute or solvent flow in the shale membrane or both. (Chen & Chenevert, 2001; Tan et al., 1996). (i.e. if the reflection coefficient is one, the membrane allows water flow only, while when it is equal to zero, the water and ions move freely in membrane).

Due to the movement of the ions or solvents between formation and borehole by chemical interaction, the ions (solute) moves from the medium of the higher-ions concentration (high salinity) to the lower-ions concentration (low salinity) to reach

equilibrium. However, the solvent (water) moves from the lower salinity medium to the higher and the osmotic pressure difference develops as a consequence (Tan et al., 1997; Tan et al., 1996), which is defined as the pressure needed to prohibit the water movement in a semi-membrane medium. For instance, if the drilling fluid activity is less than the shale activity thus the osmotic pressure is developed. Consequently, the solvent moves from the shale to the drilling fluid by the desorption process which leads to escalating in the shale dehydrate, decrease in the pore pressure, an increase in both the hoop ($S\theta\theta_{ch}$) and the axial stresses (Szz_{ch}). On the other hand, if the drilling fluid activity is greater than shale activity the osmotic pressure acquires, and the solvent moves from the drilling fluid to the shale, which leads to the shale hydrate (adsorption) the pore pressure increase, and the hoop ($S\theta\theta_{ch}$) and axial stresses (Szz_{ch}) are reduced. These phenomena might to some degree induce wellbore instability in the vicinity of the wellbore during shale hydration and dehydration. (Zhang et al, 2006, Hale et al., 1993a; Hale et al., 1993b; Chenevert et al., 1975). Nevertheless, the drilling fluid induced dehydration (desorption) might contribute in stabilizing the wellbore in a fractured shale (Kell et al., 1968). The primary alteration that causes wellbore failure due to the chemical effect results in potential change in tensile and shear strength, pore pressure, Young modulus and stress alteration (Zhang et al., 2006). Mathematically, analytical equations have been developed to calculate the induced stress due to the osmotic chemical effect in equations 41, 42 and 44.

In addition to the chemical potential different, there are other chemical and hydraulic transportations mechanisms behind the potential of chemically-induced failure, ,that are out of the research scope such as; the capillary pressure, the pressure diffusion, the advection, and the swelling pressure (Al-Bazali et al., 2009; Asef & Farrokhrouz, 2013; Chenevert & Pernot, 1998; Lal, 1999; Mody & Hale, 1993; Tan, 1997; Zhang, 2008).

$$P_{\pi} = -I_m \times \left(\frac{RT}{V_M}\right) \times \ln\left(\frac{aw}{as}\right) \tag{41}$$

$$S\theta\theta_{ch} = S_{\theta\theta} + \frac{1 - 2 \times \upsilon}{1 - \upsilon} \times P\pi \tag{42}$$

$$Szz_{ch} = S_{zz} + \frac{1 - 2 \times \upsilon}{1 - \upsilon} \times P\pi \quad (43)$$

$$\sigma rr_{ch} = 0 \quad (44)$$

Where P_π is the osmotic potential, R is the universal gas constant that equal to 8.314 Pa.m3/(mol.K) , and V_M is the water molar volume equal to 18.104 m^3.

3.8.2. Thermal Stress. The thermal stress is induced at depth mainly by heat transfer between the cooler drilling fluid and the warmer formation, which causes a reduction in the hoop ($S\theta\theta_{Th}$) and axial stresses (Szz_{Th}) (Tang & Luo, 1998). Simultaneously, this high-temperature drilling fluid will heat up the shallower rock temperature during the drilling fluid circulation, and ultimately cause an increase in the hoop ($S\theta\theta_{Th}$) and axial stresses (Szz_{Th}). A high-temperature of drilling fluid might increase the formation pore pressure due to the larges different between expansion factors of the pore fluid compare to the rock matrix (Ayoub et al., 2003).

The cooling effect of the drilling fluid might cause micro fractures initiation during drilling fluid circulation, which might induce seepage losses (Tang & Luo, 1998). On the other hand, since the drilling fluid gets warmer, these micro fractures are closed, and the drilling fluid inside them pushes back to the wellbore, which might be misinterpreted as an unexpected kick. (Zoback, 2010). The drilling fluid cooling effects leads to compressive stress reduction, while it increases the tensile stress that makes the wellbore more stable in terms of shear failure, yet it could be more likely fail in terms of tensile failure (Tao & Ghassemi, 2007).

It is worth to mention; there are other sources of thermal stress during the drilling operation, such as drill string drag induced thermal stress and the drilling bit heat source. These conduction and convection heat transfer takes place from the center of the wellbore to the formation, and the drilling fluid is the only isolation between these two mediums. The friction heat source is created from the contact between the drill string and the formation, especially in the deviated well. (Nguyen et al., 2010) . The mechanical friction in the drill bit with the formation contributes in rising the drilling fluid temperature because

the bit is in direct contact with the drilling fluid. On the other hand, the thermal effect induces failure can transfer away from the wellbore rock, and it has a higher diffusivity nature than the hydraulic invasion effect (Chen et al., 2001). Hence, a simple analytical solution has been introduced to account for the hoop ($S\theta\theta_{Th}$) and axial stress (Szz_{Th}) alterations due to thermal exchange by the equations 45 and 46 (Zoback, 2010).

$$S\theta\theta_{Th} = S\theta\theta_{ch} + \frac{\alpha_M \times E \times (T - To)}{1 - v} \quad (45)$$

$$SZZ_{Th} = Szz_{ch} + \frac{\alpha_M \times E \times (T - To)}{1 - v} \quad (46)$$

Where α_M is the volumetric thermal expansion coefficient for shale assumed $2.58 \times 10^{-6}\ k^{-1}$ (Kadyrov & Tutuncu, 2012), T and To are the drilling fluid circulation temperature and the formation temperature both in k.

3.8.3. Rock Anisotropic Induce Wellbore Failure. This type of effect induces wellbore stability problems, especially in deviation and horizontal wells. Clearly, the mechanical properties of certain kinds of rocks are directional dependent. These properties are; Young Modules, Poisson ratio, shear, and tensile strength (Aadnøy & Looyeh, 2011). These variations in the properties can induce several shear and tensile failures during highly deviated well penetration. In this regard, the plane of weakness being introduced in geomechanics studies of the wellbore stability proposes that there is a weak plane in which the rock fails under specific circumstances (Jaeger & Cook, 2007). The severity of the bedding-related failure is based on; the wellbore attack angle on the bedding planes, the normal stresses around the wellbore, formation dipping and wellbore azimuth (Aadnoy et al., 2009; Wu & Tan, 2010; Økland & Cook, 1998; Shamsuzzoha, 2015).

Furthermore, this effect is more prone when the well azimuth is in direction or close to the maximum principal stress direction (In Normal Faulting Environment). In other

hand, the well is more stable (in terms of shear failure) when it is drilled in the direction of least principal stress. The optimum well trajectory should be around 45 degrees from maximum horizontal stress (Aadnoy et al., 2009a; Shamsuzzoha, 2015).

Thus, an extensive analysis of the bedding related wellbore failure is required. A specific lab tests determine horizontal and vertical elasticity and rock's mechanical properties such as; Young modulus, UCS, internal friction angle, and cohesion. For simplicity, Equations 47 accounts for the change in the coherence of the rock with a different attack angle then it can be converted to UCS by equation 48. (Jeager, 1960; McLamore, 1966).

$$C_o = C_1 - C_2 \times (\cos(2 \times (\psi - \psi m))) \quad (47)$$

$$UCS = 2 \times Co \times tan(45 + \frac{\phi}{2}) \quad (48)$$

Where (C_1, C_2) are maximum and minimum cohesion, respectively. (ψ) is the angle between the bedding plane and S1 (maximum principle stress), and the ψm is the minimum angle of the ψ corresponding to minimum cohesion value.

3.9. FAILURE CRITERIA

Several authors have suggested that the Mogi-Coulomb failure criterion is representative of wellbore failure (Gholami et al., 2014; Al-Ajmi & Zimmerman, 2006; Rahimi & Nygaard, 2014). Figure 3.4 shows the logical domain of the Mogi Coulomb failure criterion.

Equations 53 gives the Mogi-Coulomb failure criterion. While Equations 49, 50, 51 and 52 are; the strength constant related to both cohesion and internal friction (a), and

the strength constant related to internal friction (b), the mean normal stress (S_{OCT}),and the octahedron shear stress (τ_{oct}).

$$a = 2 \times C_o \times \frac{\sqrt{2}}{3} cost(\phi) \tag{49}$$

$$b = 2 \times \frac{\sqrt{2}}{3} \sin(\phi) \tag{50}$$

$$\tau_{oct} = \frac{1}{3}((S_1 - S_2)^2 + (S_2 - S_3)^2 + (S_3 - S_1)^2)^{0.5} \tag{51}$$

$$S_{OCT} = \frac{S_1 + S_2 + S_3}{3} \tag{52}$$

$$\tau_{oct} = a + b \times S_m \tag{53}$$

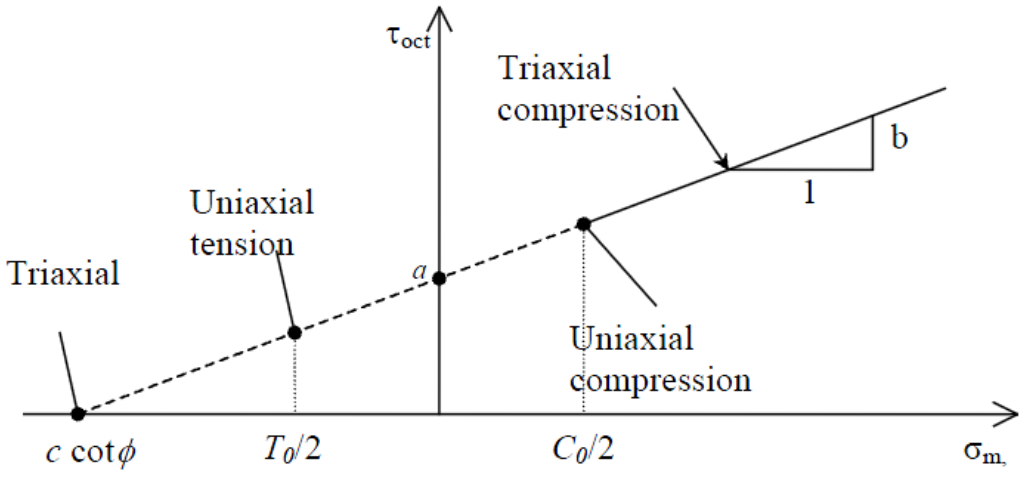

Figure 3.3. Mogi-Coulomb FC. Domain.

3.10. MAIN TYPES OF WELLBORE INSTABILITY RELATED PROBLEMS

There are different kinds of wellbore instability related problems that are commonly encountered in the drilling operations: stick pipe, caving, tight hole and lost of circulation. The stuck pipe problems cause non productive times and in more severe cases tracking or losing the well. Hole cavings might lead to inaccurate well logging reading, improper hole cleaning, and insufficient cement volume pumping. The tight spots cause unscheduled wiper trip or reaming that eventually increases the NPT. The drilling fluid loss lead to extend the well expenditure and kick or blowout in severe scenario (Escobar & Santander, 2014; Maury et al., 1987).

Collapse failure arises, when the formation in the vicinity of wellbore falling is due to shear failure (Fjaer et al., 2008). Consequently, the wellbore is packed off if the drilling ferments are not adequately transported out of the hole in brittle shale (due to insufficient drilling fluid properties, flow rate, or string rotation), and a pack off stick pipe might be encountered. Nevertheless, hole erosion is another source of washout if the flow rate is too high, especially in unconsolidated rocks. A reduction of boreholes might experience due to yield in the plastic zone around the well when either the drilling fluid weight and/or properties are not sufficient to support the wellbore wall or the stress contrast around the well is too high repecting to the rock strength (Tare & Mody, 2002). The details description of the shear and tensile failure were explaining in Appendix A.

3.11. TYPES OF STUCK PIPE

The stock pipe is defined as the inability of pulling the drill string out of the hole caused by downhole obstacles even though the maximum over-pull has been applied. There are different common causes lead to pipe sticking. The two primary types of pipe sticking occur in drilling operations, which are differential sticking, or mechanical sticking. Differential sticking happens when the borehole pressure is substantially higher than the pore pressure in a permeable formation. Furthermore, the friction coefficient, inappropriate fluid loss controller as well as solid removing efficiency and BHA exposure time to the formation are intensified factors to the differential sticking (Rabia, 2010). In other hand,

the mechanical sticking is usually experienced due to physical restriction of the drill string (Cunningham, 2012). Technically, there are various types of the mechanical stick but in this research, borehole instability and drill pipe pack off were investigated. Mechanical sticking often called pack off when the cuttings and caving are wrapping around the drill stem and prevent the movement.

The pack off happens mainly due to improper hole cleaning, or formation degradation. Typically, the drill cutting related stuck pipe befalls during pull out of the string by different sources such as hole washout (low flow rate), or inefficient fluid properties. As the hole over-gauges, the annuluss' velocity is reduced. Thus, the solid particles tend to settle down in the upper part of the drill string tool joint because of hole restriction (Warren et al., 1940). With regard to the drilling fluid deficiency, the insufficient suspending agent in drilling fluid could lead to the cuttings being transported up to the surface aggregated, resulting in pack off sticking. However, if the well highly deviates a considerable care should be taken to the flow rate and the drilling fluid properties because of the rock fragments lifting tends to roll within the lower well side, so it needs high energy to get diligent transportation (Devereux, 2012). The bore hole potentially suffers form pack off sticking in shale formation. if the chemical and physical properties react with the drilling fluid properties, forcing the shale to stick (or gummed) to the pipe.

3.12. WELLBORE INSTABILITY PARAMETERS

Several authors have categorized factors that cause wellbore instability into controllable and uncontrollable parameters shown in Table 3.1 (McLean, 1996; Fjaer, 2008; Pašić et al., 2007). The stability of the wellbore is achieved by choosing the controllable parameters for the optimum well design such as; drilling fluid properties, density, well trajectory and well casing design. These parameters can be used as valuable tools to determine the best solutions in order to prevent failure. Also, the designer will have a clear pictures regarding the parameters that can be adjusted to avoid the instability problems. For example, the in-situ parameters cannot be adjusted or modified, but it

effectiveness might be mitigated indirectly based on the controllable factors (appropriately selection of the controllable parameters (i.e. drilling fluid density and casing design)).

Table 3.1. Controllable parameters

Uncontrollable factors	Controllable factors
Low strength rocks	Drilling parameters
Stress anisotropy	Mud chemical properties
Naturally fracture	Rock Erosion
Faulting regime	Mud temperature
Chemical properties of the rock	Drill string vibration
Thermal gradient	Borehole transient pressure
Unconsolidated formation	ECD and static density
Formation mobility	Well casing design
Overpressure zones	Well trajectory design

From the drilling perspective, the uncontrollable effects have a direct or indirect effect of escalating the wellbore instability diagnostic and solution. For instance, increasing the drilling fluid pressure to handle the pressure increase in abnormal pressure zones might lead to initiate tensile failure on the other weak zones. In other hand, the unconsolidated rock and natural fracture might potentially induce rock fragments to fall during drilling by either drill string vibration or BHA design that consequently lead to stick pipe. Hence, the diagnostic of the main source causing hole failure is a highly important task in term of the treatment selection. Since this problem frequently poses by a combination of different effects so that a proper understanding of these influences is required (Fjaer, 2008; Pašić et al., 2007).

3.13. STEPS TO PREVENT PIPE STICKING

Various approaches and procedures have been carried out in the oil industry to prevent the pipe sticking incidents. The well-trained rig personnel and new technologies/material can be helpful in reducing the likelihood of the pipe sticking. Recently, the comparison of the drilling data between Measurement While Drilling (MWD) with the rigs' surface sensors can give clear insight regarding the downhole obstacles (Bailey et al., 1991; Falconer et al., 1989; Bible et al., 1991). For example, if the real-time monitoring of the Wight on bit and drag logs from the MWD different from the rig surface measurements, this case can be an earlier indication of pipe sticking. The drill string friction log, compile with ROP can also be beneficial in predict the onset pipe sticking (Bailey et al.,1991). The real time caliber log has been mounted in Log While Drilling tools (LWD) to determine the change in hole diameter during the drilling and the subsequence problems (Elahifar et al., 2012; Orban et al., 1991). The continue circulation technique can be helpful in reducing the borehole pressure related instabilities with respect to surge and swab effects. The chemical additive has widely used in drilling operation to minimized the shale stabilizes due to chemically-related wellbore failure.

3.14. SHALE TIME DEPENDENT-FAILURE

Several authors investigated the shale behavior after prolonged exposure time to the drilling fluid. It turned out the longer contact with water base mud fluid, the higher the likelihood of shale failures with time (Hardy er al., 1959; Horsurd et al., 1994; Nes et al., 2015; Tare et al., 2001). Different mechanisms might potentially induce time-dependent failures such as; hydrodynamic consolidation, creep, shale-fluid interaction, and temperature (Horsurd et al., 1994). The consolidation is mostly related to pore pressure alteration due to the change in state of stress, and it is a function of permeability, porosity, and rock/fluid stiffness. The creep is phenomena, in which the rock strain change over time with respect to constant effective stress and it comes from viscoelastic effect. The last two mechanisms were discussed in the sections 3.9.1 and 3.9.2, respectively.

3.15. QUANTITATIVE RISK ANALYSIS IN GEOMECHANICS MODEL

The quantitative risk analysis (QRA) is frequently employed in petroleum related geomechanics because there is much uncertainty in the geomechanics input variables (MckLellan & Hawkes., 1996; Ottesen et al., 1999). This approach is conducted by identified the range of the probability for the input data then, Monte Carlo simulations is performed, and the model result is represented by probability plots (Moos et al., 2003). The detail description of this method is out of research scope.

3.16. DRILLING PRACTICE OPTIMIZATION

The downhole pressure is fluctuated during the tripping operation due to surge and swab effects. These phenomena can result in different wellbore instability issues such as drilling fluid losses or pipe sticking (Mitchell, 1988). Physically, the surge pressure can be defined as the increment in bottom hole pressure due to the drill tools (casing, drill pipe) being lowered into the well. Contrarily, the swab pressure is described as the reduction in the bottom hole pressure because the drilling tools are pulled out of the hole (Bourgoyne, 1986). Therefore, it is essential to include a safety factor or trip margin to account for the surge and swab pressure in the well construction stage. Different factors contribute in tripping related pressure alterations, such as tripping velocities, drilling fluid properties, drill string eccentricities, wellbore geometry variations, and types of flow regimes (Mitchell, 1988; Srivastav et al., 2012). Numerous mathematical model has been innovated base on different disciplines to consider the drilling fluid density alterations by the tripping operation.

4. DRILLING OPTIMIZATION LITERATURE REVIEW

4.1. DRILLING OPTIMIZATION BACKGROUND

The drilling operational parameters are optimized to increase the rate of penetration in order to reduce the drilling time and the associated problems. The drilling improvements are not only accomplished by enhancing the drilling conditions but also through choosing proper drilling tools for an individual formation (Hareland et al. , 2007) . The ROP can be increased when the WOB, RPM, and hydraulic factors to some extent are incremented. The WOB building up led to further bit teeth embedment into the virgin formation and ROP improvement. Also, the increase in both RPM, and hole cleaning parameters result in a significant enhancement in ROP (Hareland & Nygaard, 2007). On the other hand, it is decreased if the hole size, drilling fluid density, rock strength and bit worn out factors are increased. The larger the bit size, the higher weight on bit distribution on the parent rock, then less ROP drives. As the drilling fluid gets denser, the chip holds down effect is intensified, and consequently, the ROP is lowered. The rock aggressiveness to penetration is elevated if the rock strength, or the bit wear increase (Defined as the damage in the bit components), which lead to a reduction in ROP (Hareland & Nygaard, 2007). Different techniques have been developed in the oil industry to optimize the drilling condition from various disciplines, such as the drill off test, multi-regression analysis, and drilling optimization simulators (DROPS) (Rashidi et al., 2008). Other common drilling optimization techniques are either mechanic specific energy method (MSE) or drill-off test to simulate ROP (Rashidi et al., 2008). The detail information can be founded in Appendix A. There are different types of the drill bit have been developing to increase the ROP such as Drag bits and roller cone bits. However, the details descriptions of the drag bit-Polycrystalline Diamond Compact (PDC) has addressed in this research since the majority of production section being drilled by PDC (according to the research data set).

4.2. POLYCRYSTALLINE DIAMOND COMPACT (PDC)

The PDC bit is made up from hard matrix body with a blade, where the man-made diamonds (cutters) are mounted, and it has opened areas that allow the drilling fluid and

rock cutting to pass into the annulus (junk slot area) (Hareland et al. , 2007). The drilling mechanism of this bit is shearing the breakage rock, which means less energy is required (WOB) and less bit wear induced. There are some factors should be considered to improve the PDC performance based on the drilling environment such the bit geometry and the cutter geometry, that shown in Figures 4.1 and 4.2. The number of blades is mostly related to the rock hardness, in which the number of blades in soft formation PDC are usually fewer than the hard one. In addition, the soft rock tends to drill in PDC bit with larger junk slot area for hole cleaning purposes comparing with hard rocks. The fewer number of cutters and smaller cutter diameter are used in PDC soft rock bit (to improve cleaning efficiency in soft rock) when it compared with hard rocks PDC bit. The back rake and side rake angles are defined as the cutter face orientation with respect to vertical and left/right direction, respectively. The back rake angle is lowered the ROP and bit wearing when it increases, while the side rake angle is often small, and it mechanically improves the hole cleaning by oriented the rock cutting into the annulus (Rabia, 2010). The cutter thickness is mostly related to cutter abrasiveness to resist wearing. Eventually, the exposure is cutter bottom space, that available to peel off the rock without contacting with the bit body (Bourgoyne et al., 1986).

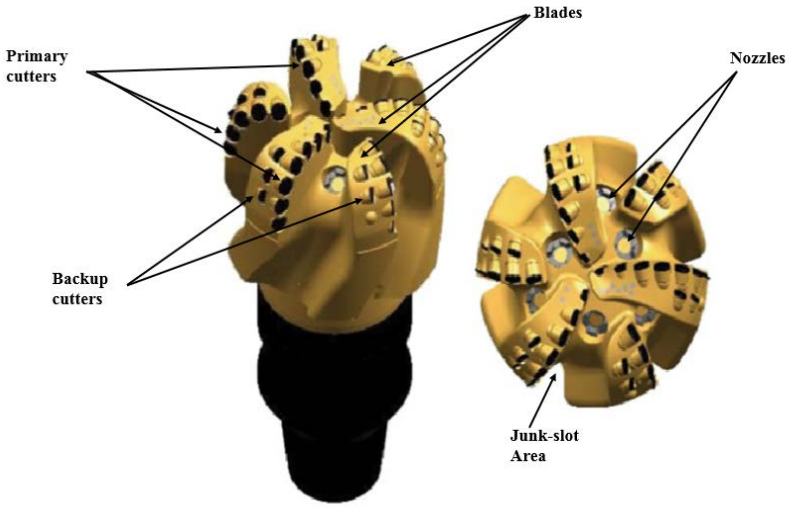

Figure 4.1. PDC bit elements (Baker Hughes)

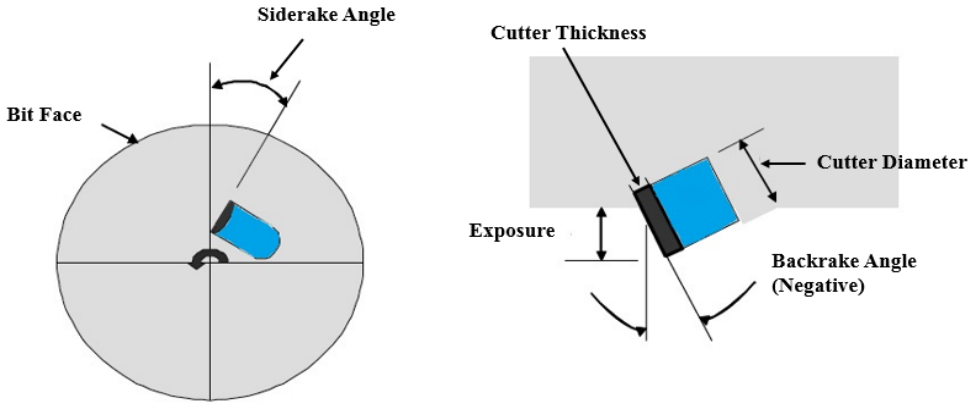

Figure 4.2. PDC cutter design parameters, Siderake, Backrake, Cutter thickness, Cutter diameter, and Exposure (Bourgoyne et al, 1986).

4.3. MULTI-REGRESSION ANALYSIS TO PREDICT ROP

Bourgoyne and Yound (1974) introduced a mathematical model to optimize the drilling activity base on multi-regression analysis of offset wells data. They proposed the model of dependent ROP variable could be derived from the following independent factors; formation strength, depth, compaction, well differential pressure, bit operation conditions (diameter and weight), rotary speed, bit wear and hydraulic. Then the optimum selection of this variables can be beneficial in the drilling processes improvement.

The drilling variables can be linearly regressed to get the independent variable coefficients and the model intercept. Each coefficient represents the anticipated value of the dependent variable (ROP) for a unit change of single independent variable (drilling datum) when the other variables keep constant. The least square estimation typically used to solve the multi-variances coefficients and to construct the model (Montgomery, 2013).

4.4. REVERSE RATE OF PENETRATION MODEL

The rate of penetration model has frequently used to predict the bit performance and the apparent strength logs (ARSL) based on geological and operational conditions. A modified model to simulate different types of the bit is included to anticipate the ROP for

each bit type. The drilling environment data that affected the ROP should be involved meter by meter from offset wells as well as the lithology description. The bit specifications and evaluations are required as input data to the simulator. By compiling all the previously mention information, the apparent strength log can be generated from inversion rate of penetration model (Hareland & Nygaard, 2007; Nygaard & Hareland, 2007). Once the ARSL is estimated, than the theoretically computed ROP is validated with field 's ROP to ensure preciseness of the simulator (Nygaard et al., 2002).

The bit wear and rock strength are provided by the DROP under drilling operation environment can be used to optimize the future wells. The drilling input data can be modified in planning well to increase the operation performance and reduce the expenditure. The program allowed selecting a wide verity of; the well geometry design, hydraulic, drilling operation, and bit specification (unpublished source of MST drilling optimization class).

The drag (PDC) bits are commonly used in production section. Therefore, the theoretical ROP model of this bits has only covered in this research (The roller cone bit model is covered in Appendix). The shear failure of PDC bit relies on; the WOB, cutter geometry, Cutter placement, bit wear, rock properties, and the operation conditions (Hareland & Nygaard, 2007; Hareland & Rampersad, 1994). The PDC cutting efficiency also has an impact on the ROP, and it is related to back rake angle, formation properties, and the depth of cutter (Hareland et al., 2007). The ROP model for PDC bit is expressed mathematically in equation 54. The mathematical model of Roller cone bit addressed in detail in Appendix A.

$$\mathrm{ROP} = \mathrm{W_F}\left(f_c(hyd)\left(\frac{f(bit)\times a_i \times D_B^2 S^{(2-b_e)}}{RPM \times WOB^{(2-b_e)}}\right)\right)^{-1} \tag{54}$$

Where ($\mathrm{W_F}$) is wear factor, a_i and b_e are the model constant, (D_B) is the bit diameter, ($f_c(hyd)$) and $f(bit)$ are the hydraulic and bit factors, respectively.

5. METHODOLOGY

5.1. AVAILABLE DATA

In this analysis, different types of data have been used to construct the geomechanical model and to optimize the drilling variables. Due to the variation in subsurface conditions in southern Iraq fields, a base field has been selected and analyzed in this research according to the following sources;

5.1.1. Daily Drilling Report. The wellbore instability events have been evaluated based on the Daily Drilling Report (DDR) from 45 wells in a field located in southern Iraq. These reports usually included the drilling operation progress and other available data such as the BHA profile and the drilling parameter being used. The trip in and trip out drilling conditions, the associated time have been obtained from this data, the same as for the down reaming and the back reaming information. The hole caving has been quantified from the DDR. In addition, it is the source of drilling data for both drilling file of the drilling optimizer and the input data of the tripping model.

5.1.2. Well Logging Data. Wireline data have been reviewed such as the porosity, density, caliber, Gamma Rays, image and sonic logs that are the main building blocks of this research in terms of geomechanics part.

5.1.3. Mud Logging Data. These reports provide the lithology descriptions of each interval. The cutting type and percentage were obtained from Mud Logging Report (MUDR) that also uses in lithology file of the drilling optimizer.

5.1.4. Pore Pressure Data. The pore pressure gradient value has been obtained from offset wells calculated and recorded data that has been estimated by Eaton/Ratio methods in Tanuma formation. It has been validated, throughout the pore pressure tests measurement in underlying limestone section (repeated formation test (FRT), formation pressure while drilling (FPWD)).

5.1.5. Final Well Report. The total productive and nonproductive time were obtained from the final well reports, which can be used as powerful tools in quantitative and qualitative in the majors of drilling problems. The lessons learned in this report has been summarized to improve the future well performances. Moreover, the bits'

evaluation reports for each bit being run, have been collected in the final well report, which utilizes in the drilling optimizer ‘s bit file.

5.2. STUCK PIPE ANALYSIS

Diagnostic analysis of different types of pipe sticking that occurs during the drilling operation was conducted to construct the stuck pipe worksheet based on pre-stuck and post-stuck pipe drilling variables. This worksheet also provides an explanation based on monitoring of the drilling observations when the stuck pipe events occurred. The worksheet considers only three type of pipe stick that might potentially take place (Differential stuck, pack off stuck, geomechanics related stuck). Furthermore, three codes have been manipulated to describe the weighted value of certain drilling circumstances on each stuck pipe type. Thereby, digit two in the Table refers to the highest likelihood of a symptom occurrence with respect to the stock type, while digit one indicates that the event is less likely to occur with a stuck pipe. Finally, zero digits indicate that it is not existent or was not experienced with this kind of stuck pipe. As a result, the pipe sticking with the highest score is the most likely induced stuck pipe mechanism.

5.3. GENERAL OVERVIEW FOR GEOMECHANICS MODEL AND THE DRILLING OPTIMIZATION METHOD

To build the geomechanical model, the pore pressure was obtained from the offset wells’ pore pressure gradient for the Tanuma shale. Equation 1 has been used to calculate the pore pressure in Tanuma formation according to the pore pressure gradient in this zone.

The available log measurements such as those for the density, sonic,and neutron logs, have been utilized in empirical equations to obtain the in-situ stress magnitudes. Also, the fluid injection test has been used to validate the log-derive values when it comes to minimum horizontal stress estimation. Conversely, the maximum horizontal stress has been concluded from an empirical equation that is validated by the history matching procedure.

The principal stresses around the wellbore have been determined from the transformation equations based on the Kirsch solution for impermeable rock. The other source of stresses around the wellbore was also computed by analytical equations from literature such as the thermal and chemical induced wellbore failure. The strength anisotropy effect has been included in the model to account for shale property variations (cohesion and UCS) with respect to well angle.

The rock elastic properties have been calculated based on available log-derived correlations for shale in different regions. Mogi-Coulomb failure criteria were used to obtain the optimum drilling fluid density to prevent onset shear failure.

The drilling optimization was performed to reduce the shale exposure time during the drilling the production section and to improve the drilling practice during tripping. Beside the swab pressure calculation, two types of drilling optimization techniques have been employed from different disciplines to reduce the shale exposure time such as multi-variances analysis, and DROPS drilling simulators. The empirically derived swabbing model and the suggested tripping parameters have used to mitigate the reduction in drilling density related to swabbing effect.

5.4. ROCK MECHANIC PROPERTIES.

The rock elastic and mechanical properties have been obtained from the Log-derived methods nor the static approaches.. To start with, The only possible sonic measurement is the compressional travel time. Therefore, Equation 3 has used to get the shear wave velocity from compressional wave velocity. Once the shear travel time was determined, the Poisson was computed by Equation 4. The dynamic Young was calculated through equation 5. After that, the static Young modulus was obtained from the dynamic one by Equation 6.

The internal friction angle and cohesion of the shale formation were obtained by using Equations 11 and 47, respectively.

Additionally, Equations 7, 8, 9, and 10 were used to calculate the unconfined compressive stress from sonic log parameters then Equation 8 was ultimately selected in the model analysis.

5.5. THE IN-SITU STRESS OF THE GEOMECHANICAL MODEL

The total overburden stress was calculated using Equation 13 based on the bulk density gradient in overlying rocks. Technically, the bulk densities were obtained from density log in each interval, were the primary components in Sv estimation; Nonetheless, these values are not available from the surface to the bottom of the Tanuma formation, instead of, the density measurements usually started from the intermediate hole (Lower Dammam formation). Hence, the available measurements of the Neutron log and the mud logging reports for rocks percentage in each surface layers were combined in Equation 12 to get the bulk density of the surface intervals.

The total minimum horizontal stress was determined by drawing Equations: 14, 15, 16, 17, 18, 20 and 19, then the most decent value was verified by the available Leak-off Test in the upper formations to represent Sh.

Furthermore, the maximum horizontal stress was concluded from Equation 23, which has been validated by forty-five wells history matching. The stress polygon was established to constrain the value of maximum horizontal stress based on the estimated minimum horizontal stress and the designated faulting regime. Appendix A contained the stress polygon for southern Iraq field. Ultimately, all accessible data such as image log and caliber log are hard to interpret due to high well inclination angle, so the orientation of horizontal stresses was obtained from history matching procedure.

5.6. HISTORY MATCHING PROCEDURE

This method was used in this analysis to get the uncertain values of geomechanical model input such as the maximum horizontal stress magnitude and its orientation relying on the field data. The magnitude of the maximum horizontal stress is bounded between the Sh and Sv in the normal faulting regime. Therefore, after the geomechanical model is fed with all necessary inputs (the SH orientation set to zero), the values of SH are supplied to the model within Sh (as lowest bound) and Sv (as highest bound). Then, the drilling fluid density, which is the model output, is recorded at each time when the SH values have changed until the closest fitting has been achieved between the model drilling fluid density and the field drilling fluid (in stuck-free wells). After the best SH has been determined, the

orientation of the maximum horizontal stress is changed in the model input data until the best fitting between the drilling fluid density output and the field density used in the stuck-free wells. It has been concluded that this value is approximately close to the tectonic movement in the Arabian plate. Also, these values suggested drilling fluid density higher than the field density for the well that has experienced pipe sticking in the Tanuma shale.

5.7. STRESS TRANSFORMATIONS

The stresses were transformed from the far field domain (Sv, SH, Sh) to the arbitrarily oriented wellbore Cartesian coordinate system (S_x, S_y, S_z) by Equations 27, 28, 29, 30, 31,and 32. subsequently,the la terally mentioned coordinate was transferred to the cylindrically wellbore coordinate system ($S_{\theta\theta}$, S_{rr} , S_{zz}) by using Equations: 33, 34, 35, 36 and 37.

5.8. CHEMICAL AND THERMAL-INDUCED STRESSES

These stresses have been computed analytically without taking into consideration the coupling effects of each one to the other. Analytical equations are manipulated accounting for thermal and chemical induced hoop stress as well as axial stress by using Equations: 42, 43, 45 and 46, respectively. A worst-case scenario of the Gulf of Mexico sloughing shale has been assumed to be equivalent to the one in the Tanuma formation to account for chemical effect by using the shale activity of GOM shale from (Zhang et al., 2008). The water activity of the KCL polymer mud was obtained from the literature (Zhang et al., 2008). The geothermal gradient is available from the offset wells data, and it has been used in thermal stress equations. To sum up, these influences have algebraically added to the hoop and axial stress that come from mechanically induced effects.

5.9. BEDDING RELATED WELLBORE INSTABILITY

For this effect, the core analysis from horizontally and vertically cored sampled should be conducted. However, the leakage in this kind of core test leads to simplifying

this failure as much as possible by relating this effect to directional alteration in unconfined compressive stress and cohesions. Equations 48 and 47 were utilized to consider this failure by changing these values with respect to well inclinations and azimuths in the input model (Cohesion and UCS). Where C_1 is obtain from the UCS reading, and C_2 Obtain from the assumed minimum UCS value which equal to 3.17 Mpa.

5.10. DRILLING FLUID WEIGHT ESTIMATION

The appropriate drilling fluid density was estimated by compiling all previously mentioned stresses and rock strength parameters with the Mogi-Coulomb failure criterion. In the case of collapse failure prevention, the principal stress of each point around the wellbore was extracted by using Equations 38 and 39 based on the $S\theta\theta_{Th}$ and SZZ_{Th} as input from Equation 55 and 56. By including the S_{rr} , the maxuimum, intermadaite, and lease pricipal stress were determined at each point around the wellbore. After that, the maen normal and the octahedron shear stress were calculated by using Equations 49, 50, 57, and 53. Then, the maximize value of the S_1, S_2, S_3 , S_{OCT} ,and τ_{oct} from all the points around wellbore were determined. Eventually, these values are plugged in Equation 53 with iteration process to find out the optimum drilling fluid weight to prevent onset shear failure when the mechanical, chemical, thermal and anisotropic effects were taken into considerations as shows in Figure 5.1.

In the case of the tensile failure, the least value of the hoop stress or the axial stress at all points around wellbore was chosen to represent the worst-case scenario for onset tensile failure. Consequently, drilling fluid weight iteration based on Equation 40 was conducted to find out the maximum allowable drilling fluid weight.

5.11. UNCERTAINTY ANALYSIS FOR GEOMECHANICAL MODEL

The Solver™ plate-forms add-on in Excel™ was used to perform a risk analysis on the input data based on Monte Carlo simulations. The unconfined compressive strength, the angle of internal friction, Poisson ratio, maximum horizontal stress magnitude and

orientations were investigated to represent the uncertain variables in this analysis. The range of these variables was chosen to be +10% and -10% as the input in probability distribution function.

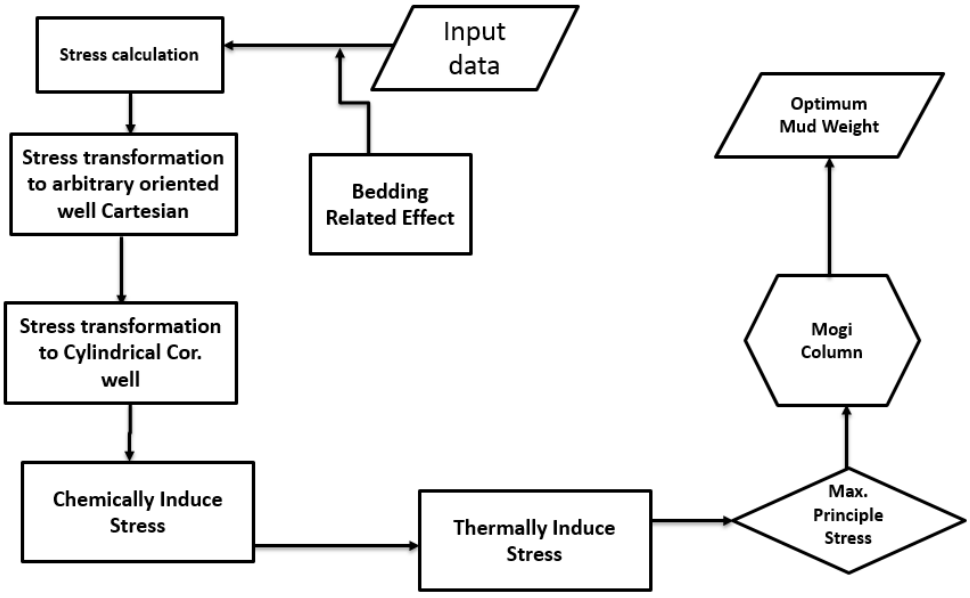

Figure 5.1. Geomechanical Model workflow

5.12. DRILLING OPTIMIZATION

The drilling optimization for the production section was undertaken by using the multi-regression analysis of drilling data and DROPS ™ drilling simulation optimizers. The drilling data from 25 well were collected from the previously mentioned data such as WOB, TFA, RPM, MWT, and ROP. These parameters were fed to JMP® statistical software, and based on the least square estimation method; the regression coefficients were solved to obtain the empirical model equations. In additional, the screening and sensitivity analysis methods were performed to the input data to ensure model confidentiality. The DROPS drilling optimizer used to improve the drilling efficiency and consequently reduce the Tanuma exposure time. The software was provided by the bit, lithology and drilling ACII files; then the drilling data was alternated to ROP optimization. The sensitivity

examination of each operational and bit factor was conducted by change one variable when other factors keep constant. Star plots were constructed for this purpose to show up the normalized effects for the variables. Eventually, the operational and bit variables were optimized by DROPS.

5.13. TRIPPING VARIABLE OPTIMIZATION MODEL

The swab effect on the bottom hole pressure was accounted depend on the drilling observations and empirical equations. Numbers of wells were implemented to investigate the influence of drilling practice, tool, and material on the borehole pressure. The combination of the drilling fluid density, yield point, plastic viscosity, BHA size, slip to slip time, tripping speed and the depth of investigations was used as input data. The mathematical formulas from (William et al., 2015) were utilized in this research to consider the swabbing effects during the tripping. According to problems free-wells data, the JMP® software was used to construct a swabbing model that can predict the drilling fluid reduction for a certain tripping variables. The software was fed with MWT, FL, WOB, TFA and RPM to get the drilling density reduction by swabbing effect based on standard linear least square method. Then, suggested tripping variables and the geomechanical model densities were plug in the swabbing empirical model to mitigate this effect.

6. WELLBORE COLLAPSE FAILURE INVESTIGATIONS IN SOUTHERN IRAQ

6.1. DRILLING EVENTS ANALYSIS

Highly deviated wells have been experiencing major wellbore instability problems in Tanuma shale, have been analyzed to determine the primary source of the problems. Drilling events in three wells experienced the severest wellbore collapse failure in the Tanuma interval have been reviewed. After that, the diagnostic table has been set up to recognize the stuck pipe type. Furthermore, the drilling progresses charts of thirteen wells have exhibited to present the seriousness of Tanuma stability problems. Finally,other wellbore instability events in all sections in some wells have been addressed.

6.2. STUCK PIPE PROBLEM IN A-50

The pipe sticking problem was experienced in this well despite carefully drilling practice. It took place in the 8 ½ section after reaching 2,927m MD (measured depth) in the parameters that are illustrated in Table 6.1. As a general practice, low and high viscous pills were pumping in every stand being drilled for the hole cleaning purposes. In addition, reaming and back reaming procedures were frequently performed after each stand. According to the drilling plan, the drill string Pull out of Hole (POOH) was conducted from 2,972 m up to 2,863 m, yet fifteen tons over pull were suddenly noticed, and then, the string was stocked at the transition zone between the top of Khasib and the bottom of the Tanuma formations. Instantly, an attempt to run the string down the hole was undertaken, but without any result. Afterward, a trip in and pumping out processes were tried even though there was no return circulation associated with this problem. The jar was worked down as well as the weight of 25 tons was slacked off with no successes. As a consequence, a decision was made to pull out and slack down 200 and 25 tons, respectively. However, there was no progress with the drilling fluid returned or pipes rotated. Finally, back off as well as side track procedures were performed to a new trajectory.

6.3. STUCK PIPE PROBLEM IN A-51

Stuck pipe occurred in this well in the following sequence: the directional drilling in the 8 ½ section continued to a depth 3,312 m MD with the parameters that shown in Table 6.1. Reciprocating drill string combined with the low and high viscous pills were pumped periodically to enhance hole cleaning. Noticeably, high torque and drag were experienced while drilling this section. Thus, the BHA was run out of the hole with fluid circulation to the bottom of Tanuma formation where a 45 ton over pull was observed, and the string unexpectedly got stuck. Meanwhile, the standpipe pressure went up to 3,500 psi without fluid return. Jarring up and down were tried with circulation and rotation several time without any result. Eventually, fishing procedures were performed to release the BHA, but there was no positive eventuation so the backoff process was conducted and side truck was drilled to.

6.4. STUCK PIPE PROBLEM IN A-52

Two stuck pipe problems was recorded while tripping out of the production section specifically during the reaming and short trip. The first issue arose after the production section drilled to 2947m with the parameters shown in Table 6.1. A high viscous pill and wash up were undertaken with reaming down for each half stand being drilled. A high torque, together with excessive shale in the shale shaker was observed. Therefore, the string was pulling out of the hole while back reaming, but both the standpipe pressure and the torque increased. Subsequently, the relief valve on the mud pump was fired when the string got stuck at 2,911m (at the top of the Khasib formation). Several slick off weight and failed POOH were performed without progress despite firing the jar up and down several times with a maximum weight of 175 tons. Other attempts were conducted by increasing the torque up to 27,000 ft. Ib with firing the jar up and down, but the situation did not change. Therefore, the back off procedure was conducted, and the cement plug was seated to drill a side track.

The second problem happened while pulling the string out of the hole when the string reached a depth 3,240 m in the sidetrack path with parameters given in Table 6.1.

Several tight spots were observed from a depth of 3,240 m to 2,871 m. Thus, a procedure of reaming and back reaming was performed on every stand with multi-viscous pill sweep. At a depth of 2,871 m (in the Tanuma formation) a sudden increase in standpipe pressure up to 1,500 psi with no return was detected. Hence, the jar was firing up and down with a pull of 175 tons but with no succes. In addition, a combination of left-hand torques up to 24 KN-m and the drill string pull up / down was applied, but that was not successful. Therefore, a slinging off weight of 25 tons and pulled the string up to 180 tons were carried out, but the situation was still same. After that, the multiple activation bypass system (PBL) was activated and started to pump up to 1,600 L/m, resulting in enhancement in terms of the drilling fluid return. However, the BHA was not released so back off and side track was applied to a new trajectory.

Table 6.1 Drilling parameters during drilling production section in Different wells

Well	WOB (ton)	Flow RATE L/m	SSP psi	RPM	Torque KN*m	Avg ROP m/hr	Inc. Deg.	Azm Deg.	MWT sg	CL X1000 (mg/l)
A-50	8-12	2000	3000	170	19-24	5-8	58	240	1.25	150
A-51	8-10	2500	3670	120	22-28	14	50	243	1.25	114
A-52	3-6	2300	3250	90	17-22	15-20	53	97.3	1.25	112
A-52	3-10	1800	2300	60	16-23	10-15	53	97.3	1.28	106

6.5. WELLBORE INSTABILITY DIAGNOSTIC

The detail drilling events associated with the Tanuma formation issues have been collected and investigated, as shown in Table 6.2. As a result, the shear failure related to pipe sticking is the dominant type of this formation.

However, the pack off sticking is mostly induced by the bad hole cleaning to either the drilling spalling and/or the rock fragments being yielded. Therefore, the geomechanics and pack off related to pipe sticking are not independent, but are affected by each other.

Finally, the key seat has not been discussed in this analysis due to the drilling experience do not indicate such type of pipe sticking.

Table 6.2. Stuck pipe diagnostic analysis of 16 stuck pipe incidents showed similar behavior caused by shear failure. A = Stuck Caused by Shear failure, B= Differential Stuck, B= Stuck Pipe Due to Pack Off.

	Symptoms	**A**	**B**	**C**
Primary Analysis	Shale Formation	2	0	1
	Permeable Rock	0	0	0
Pre-Stuck Analysis	High Drag and Torque	2	0	2
	String Reciprocating	2	0	1
	Mud Properties Change	0	0	0
	Large Cutting Size	1	0	1
	Over Sized Hole	2	0	1
Post-Stuck Analysis	No String Rotation	2	1	1
	No String Reciprocating	2	1	2
	No Circulation	2	0	1
	Out of Gauge Hole	2	1	1
	Excess Cement Required	2	0	2
	Total	19	3	13

6.6. OTHER WELLBORE INSTABILITY EVENTS

There are some stability issues that occur during drilling operations in southern Iraq fields that caused to change the well design or increase in the non-productive time. Seemingly, the stuck pipe is the most time-consuming in the production section, shown in Figure 6.1. However, the loss of circulation is equally important in the intermediate section. As mentioned in Chapter 2, the third section suffers from thief zones (i.e. Damam and Hartha formations). Also, severe drilling fluid losses have been reported during the

intermediate section cementations, but have not been accounted for in Figure 6.2 (the vast majority of intermediate hole cementation has either partial of complete losses). On the other hand, several reaming and back reaming have been recorded in different zones such as the Em-Eruduma zone due to a tight spot. Washout and differential stuck also other sources of operational problems in some wells. Figure 6.2 summarizes analysis from thirteen wells in the field of study.

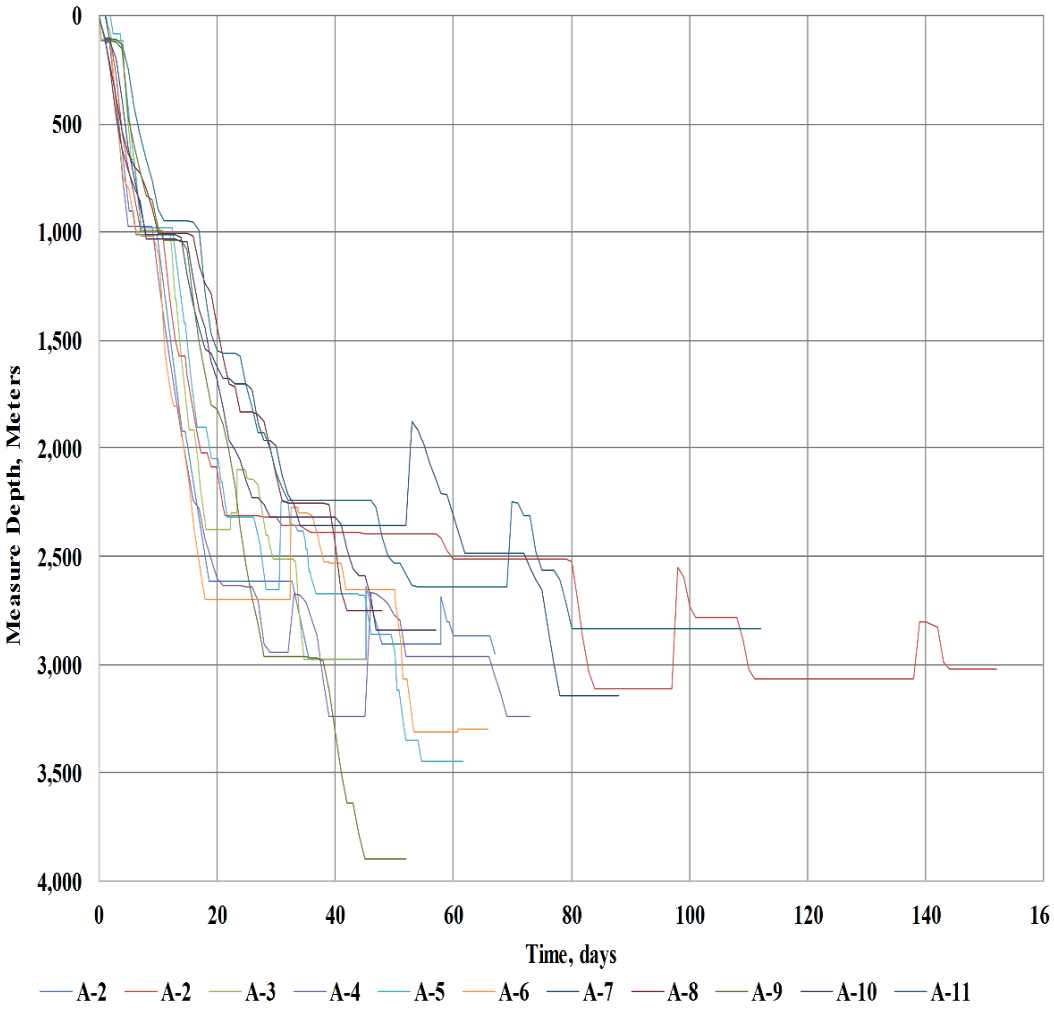

Figure 6.1.Wells performance plot.

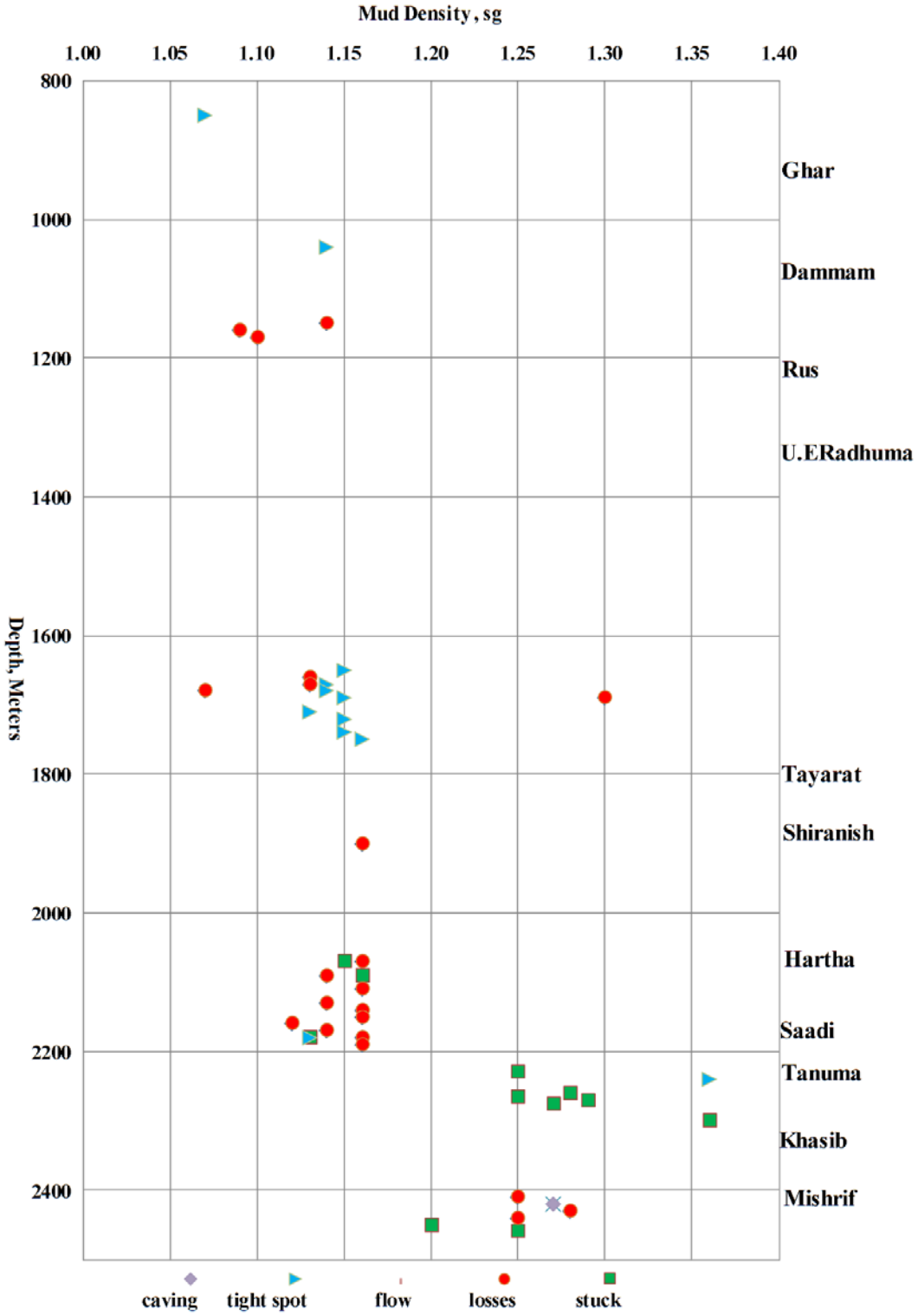

Figure 6.2. Reported drilling problems from DDR and static mud density shows stuck pipe in Tanuma FM and fluid losses in Hartha FM Summary (Stuck pipe in Tanuma shale).

7. GEOMECHANICAL SOLUTION FOR THE WELLBORE INSTABILITY IN SOUTHERN IRAQ

7.1. INTRODUCTION

The area of research being divided into three sections based on the depth of Tanuma formation tops. Similarly, some of the mechanical properties are different in each group. In addition to variations in wellbore instability variables, the drilling practices are miscellaneous in each well, yet the drilling fluid weights are almost in a limited range or constant in the majority of wells. With respect to drilling practice analysis, the swab pressure model was established to account for the drilling fluid reduction during the drilling practice. By compiling the knowledge of geomechanical and drilling practice, new design parameters have been proposed to mitigate wellbore failure.

7.2. GROUP ONE ANALYSIS

This group is characterized by the shallowest Tanuma tops in depth of 2212 m. The vertical stress and pore pressure magnitudes of the group-1 wells are shown in Figure 7.1. The pore pressure reaches it maximum in the Tanuma section of 26.43 MPa. The drilling fluid density is slightly higher than the pore pressure within all sections.

The minimum and maximum horizontal stresses in this group have been depicted in Figure 7.1. As can be seen, the values of the horizontal stresses are different base on the corrolations used (i.e. Eaton and Holbrook show a reverse behavior in the production and intermediate section). However, the general trend of all equations is increased linearly with depth. Overlying LOT showed the Breckels and Van Ecklenen are the best representative of Sh in the field of investigation. Several shale empirical equations were used in base case well in group-1. As can be seen the shale volume increases the unconfined compressive stress decreases and severe washout is recorded in the caliber log. An increase in UCS was noticed at different intervals at Tanuma because of an increase in limestone content. The rocks' elastic properties are given in Figure 7.3. Similar to UCS, the behavior of increase in Young's modulus and a decrease in Poisson ratio are seen in the limestone stinger sections.

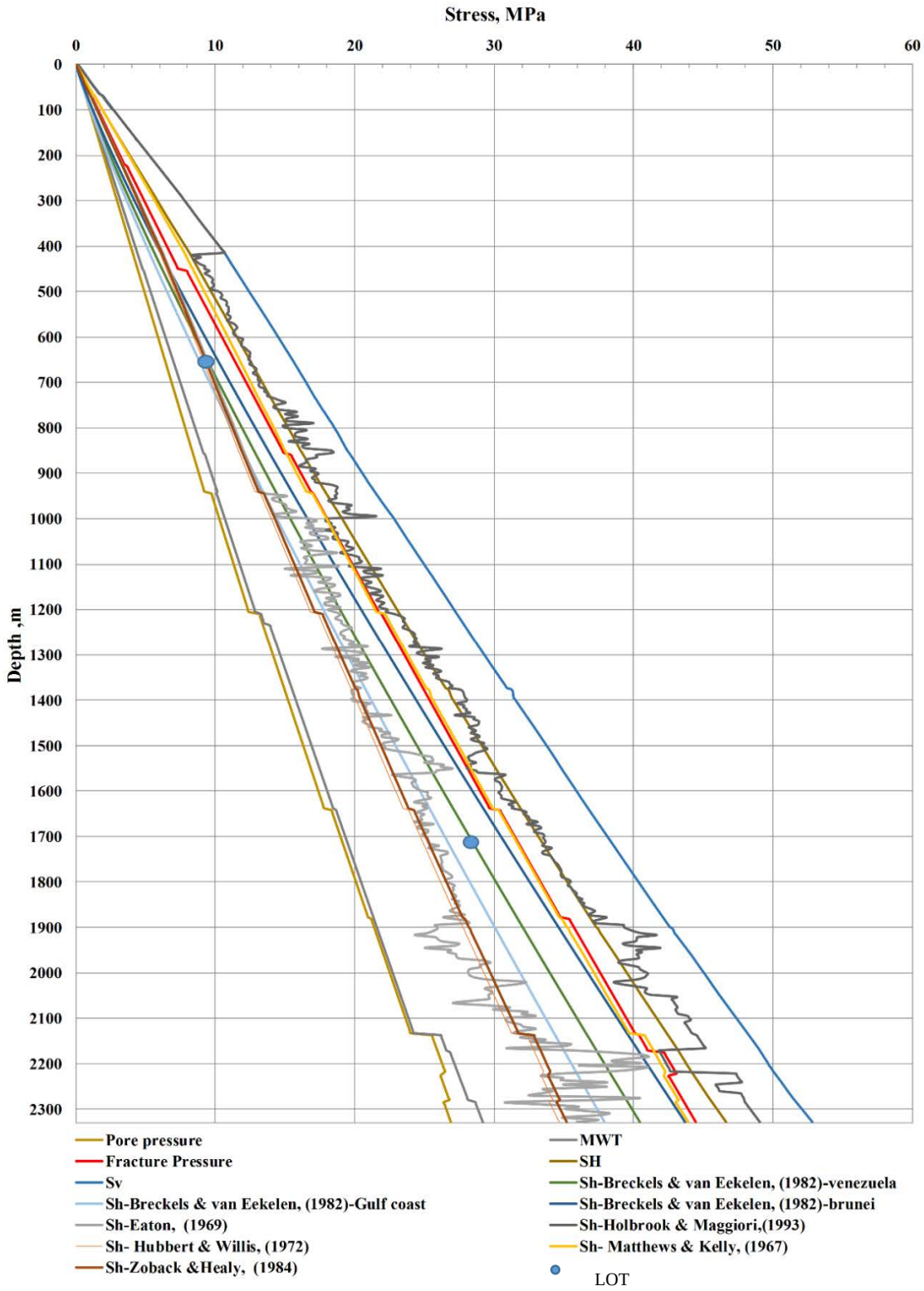

Figure 7.1. In situ stresses and pore pressure in southern Iraq, LOT test were overlaid and the Sh-Breckels & van Eckelen was chosen for Group-1 wells.

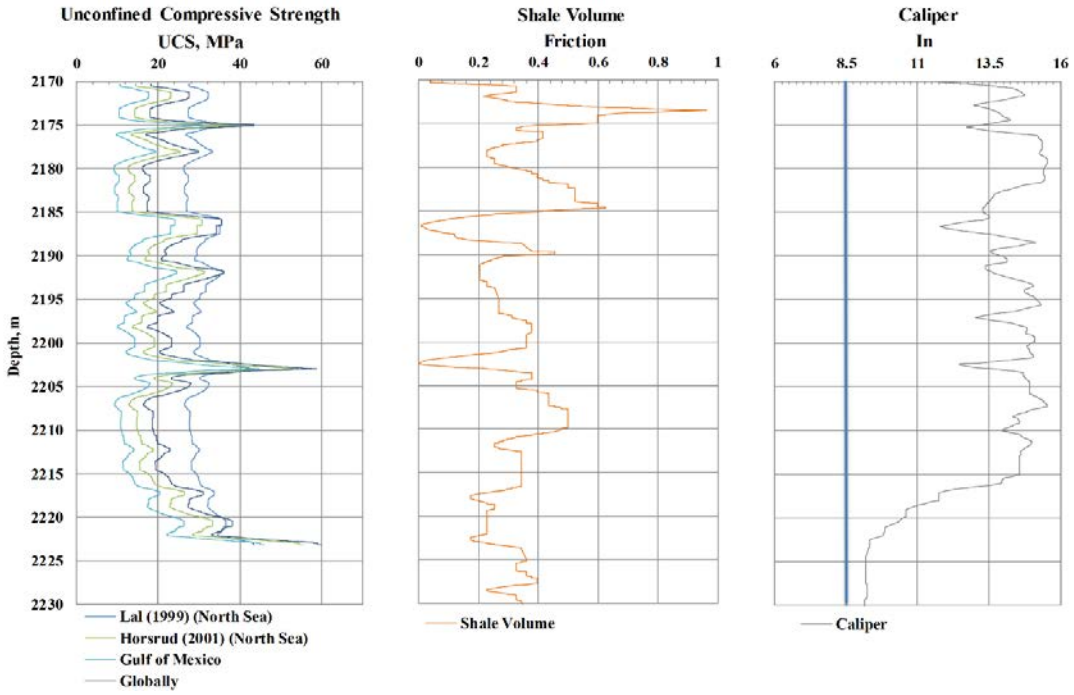

Figure 7.2.Tracks-1 shows the UCS values from different Empirical equations; Track-2 represents the shale volume from GR reading;Track-3 shows the Caliper log for Group-1.

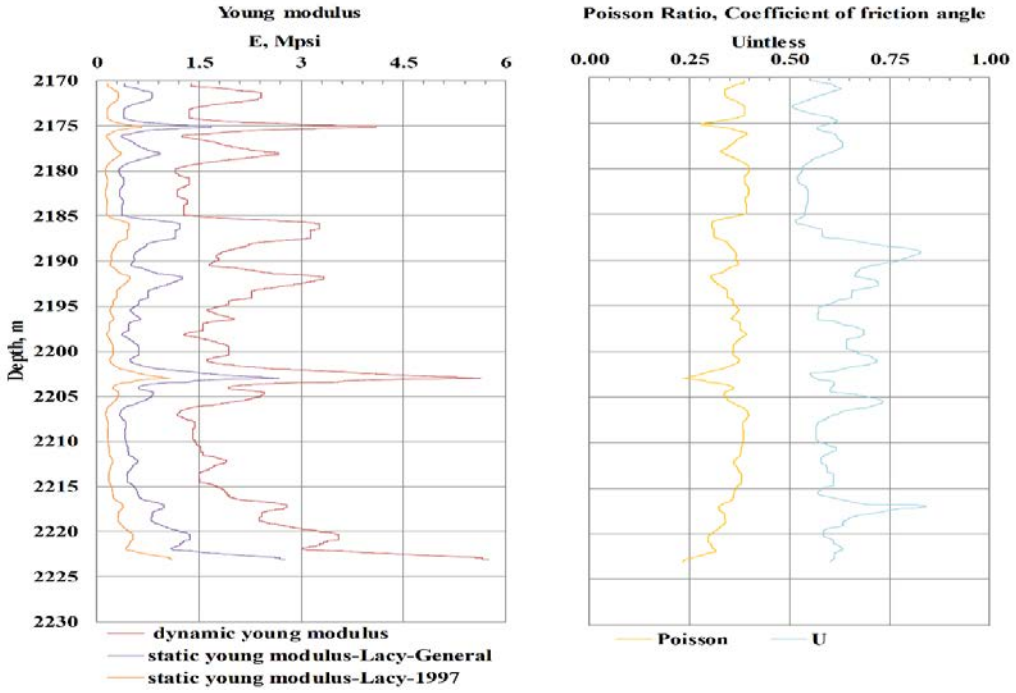

Figure 7.3.Track-1 shows the static and dynamic Young modulus, Track-2 represents Poisson ratio and coefficient of internal friction for Group-1.

7.3. DRILLING FLUID WEIGHT PREDICTION

The appropriate drilling fluid design has been estimated on the geomechanical model analysis and drilling parameters investigations in this group. Table 7.1 summarizes the model input data and the source of each variable. Afterward, the model drilling fluid weight has been compared with both the field static/dynamic drilling fluid density and the drilling fluid reduction caused by the swabbing effect in Table 7.2. This drilling fluid density reduction is deteriorating the wellbore stability status in Tanuma shale. It has come out that, the vast majority of the wells enduring drilling fluid weight is lessening along with different types of well instability. An investigating the tripping parameter shows, that the reduction in drilling fluid by the swabbing effect, in some well is mostly related to fast tripping out of the hole and large BHA diameters (i.e. well A-13). On the other side, the predicted drilling fluid density is higher than the field drilling fluid density in the majority of the wells, suffering from wellbore instabilities issues which means the inappropriate drilling fluid density might be the potential cause for wellbore failures. In addition, the predicted drilling fluid density varies with respect to well inclination and azimuth. Contrarily, the field drilling fluid is slightly changed with trajectory parameters, as shown in Table 7.2. However, a few well have been predicted to have drilling fluid weight a little less than the field density (i.e. wells A-17, A-20, and A-21). The well diagnostic analysis revealed these well have either no wellbore instability in Tanuma or suffer from instability issues after the entire section is completed. Therefore, it can be concluded that these wells failed due to the prolonged exposure of shale to the drilling fluid. Eventually, the well trajectory design is equally important as illustrated by the polar plots in Figure 7.4 , and Figure 7.5. The wells are more likely safe when they are drilled in the direction of the minimum horizontal stress while it is potentially riskier to drill in the maximum horizontal stress direction.

Table 7.1. Group-1 Model input data for Tanuma FM based on typical well

Parameters	Value (Unit)	Source
Depth	2212 m	
Sv	50 MPa	
SH	44 MPa	
Sh	38 MPa	(Breckels & van Eekelen, 1982)
Pp	26.43 MPa	
Internal Friction Angle	0.6	
UCS	29.9 MPa	(Lal,1999)
Poisson Ratio	0.36	
Water Activity	0.94	(Zhang et al., 2008)
Shale Activity	0.82	(Zhang et al., 2008)
Formation Temp.	356 K	
Volumetric Thermal Expansion Coefficient	2.58*10^-6	(Kadyrov & Tutuncu, 2012)
Sh Orientation	335 Degree	
Young Modulus	5711 MPa	

Table 7.2. Group-1‘s result, (1=stuck, 2=stuck free, 3=caving, 4= Tight spot)

Well #	Field Mud sg	Mud sg	Mud Without effects Sg	Swab Effect Sg	ECD Sg	Azm Deg.	Inclin. Deg.	Problems
A-51	1.25	1.27	1.23	1.236	1.41	243	50	1
A-13	1.25	1.31	1.27	1.182	1.29	304	38	2
A-14	1.28	1.35	1.31	1.269	1.33	97	53	1
A-15	1.3	1.32	1.28	1.292	1.38	237	55	1
A-16	1.27	1.42	1.41	N/A	1.31	246	70	1
A-17	1.25	1.2	1.19	1.244	1.32	120	20	3
A-18	1.28	1.35	1.31	1.272	1.3	170	45	4
A-19	1.28	1.3	1.25	1.274	1.32	199	31	2
A-20	1.25	1.2	1.19	1.240	1.33	329	7	3
A-21	1.25	1.21	1.18	1.243	1.3	70	32	3
A-22	1.28	1.21	1.20	1.273	1.33	149	15	
A-23	1.25	1.28	1.26	1.242	1.3	322	33	
A-24	1.25	1.35	1.32	1.240	1.29	280	53	2
A-25	1.25	1.4	1.38	1.237	1.36	317	62	4
A-26	1.25	1.31	1.28	1.242	1.35	353	37	
A-13-S2	1.25	1.35	1.30	1.170	1.34	33	51	2
A-27	1.28	1.36	1.32	N/A	1.37	354	47	other
A-28	1.28	1.36	1.32	1.272	1.36	37	55	4
A-29	1.25	1.40	1.35	1.240	1.34	16	55	4
A-30	1.28	1.37	1.34	1.269	1.32	165	51	4
A-31	1.25	1.25	1.32	1.242	1.34	135	47	3
A-32	1.25	1.38	1.37	1.203	1.39	199	53	3

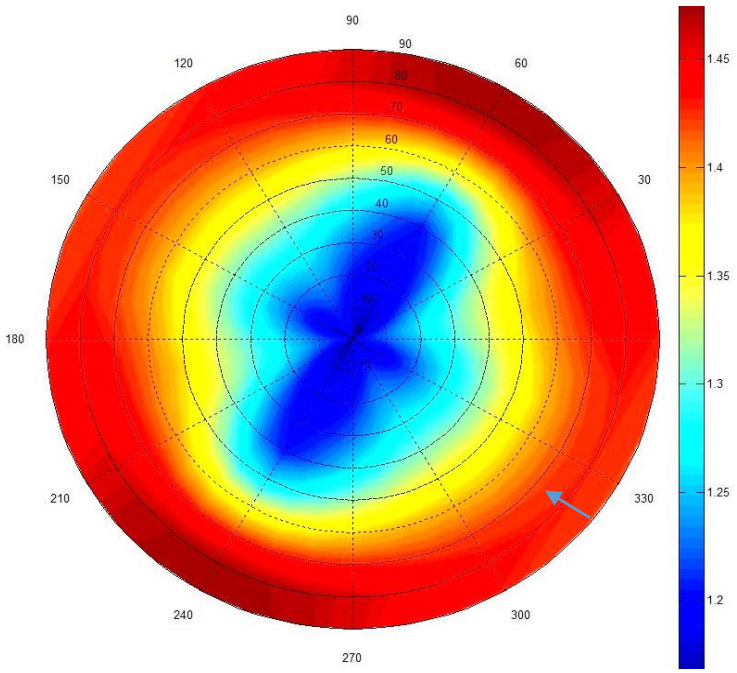

Figure 7.4. Polar plot of the model mud weight to prevent shear failure in Tanuma FM for Group-1 (Including effects- thermal and chemical induced stress as well as strength anisotropy), the wormer color repersents the higher requires fluid density (NW).

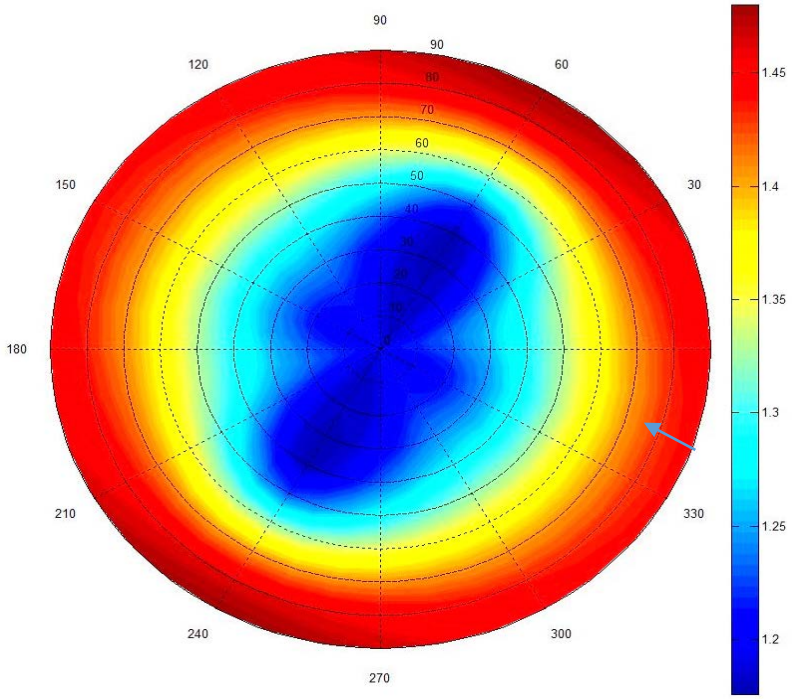

Figure 7.5. Polar plot of the model mud weight to prevent shear failure in Tanuma FM for Model-Group-1, the wormer color repersents the higher requires fluid density (NW).

7.4. GROUP TWO ANALYSIS

These groups represent the well that has moderate Tanuma tops depths. In these wells, the Sv values developed proportionally with depth in spite of an interval in the intermediate section where Sv increased dratistically as illustrated in Figure 7.6. The pore pressure in the group-3 wells increased in the entire production section, especially in the Mishrif formation. The fluid field density was slightly over the pore pressure in the surface section but in the other sections the pressure differences increased.

The calibrated equations were used to calculate the maximum and minimum horizontal stresses via the same method in previous sections. Similar to Sv, the horizontal stresses increase linearly with depth, and one interval showed up out of the trend behavior in the SH track, as shown in Figure 7.6.

According to Figure 7.7, the UCS log displays two major peaks and several flactuated intervals with a reduction in shale volume in caliber log reading. These abnormal behaviors belong to some limestone stringers in this interval, as can be observed in shale volume log. Also, the over-gauge hole was observed within the Tanuma interval, particularly in the clay-rich interval. Young modulus, Poisson ratio, and the coefficient of internal friction are displayed in Figure 7.8. Various interval increased in Young's modulus and the internal friction coeffecient, while there was reduction in Poisson's ratio.

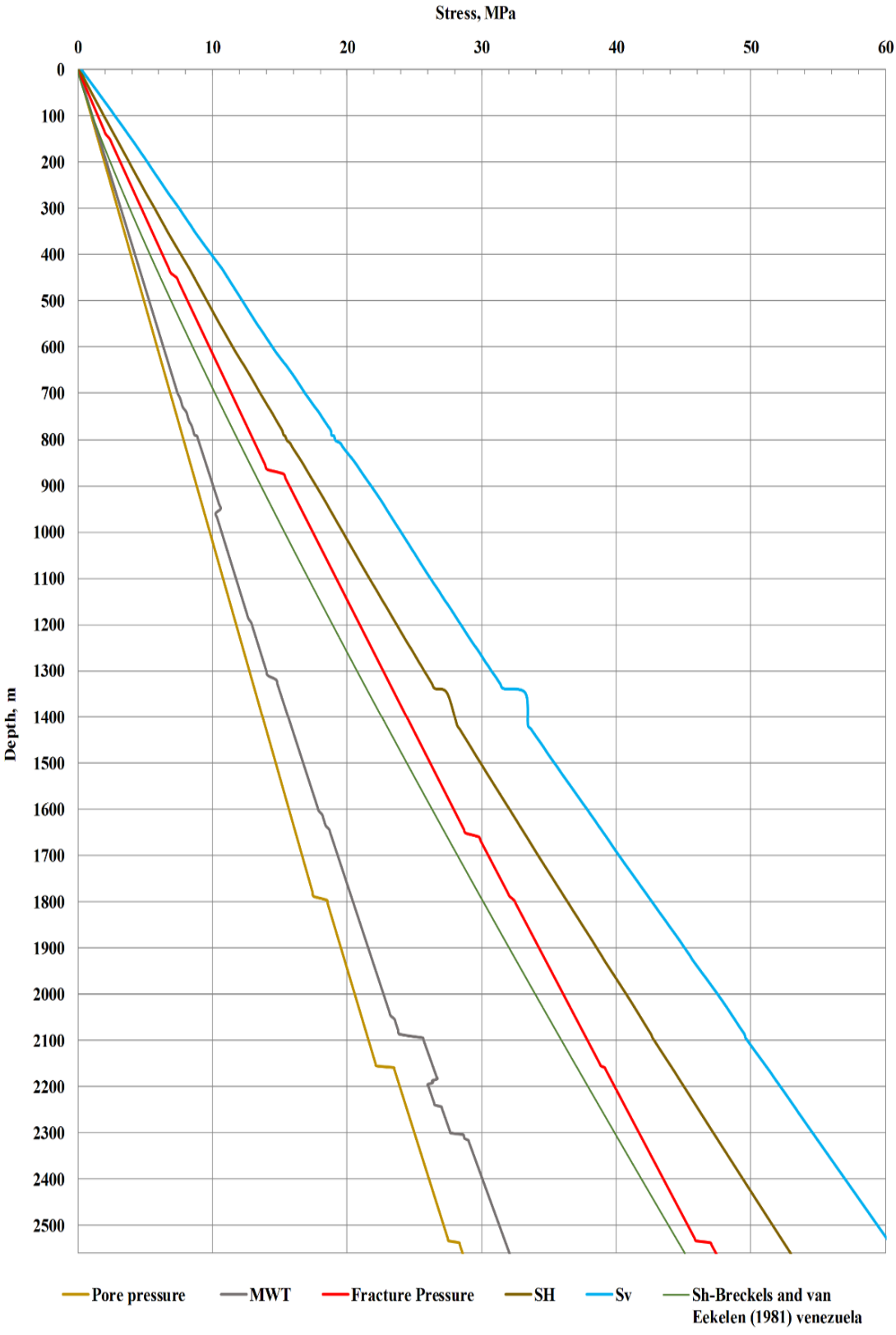

Figure 7.6. The borehole and subsurface stress in Group-3 well

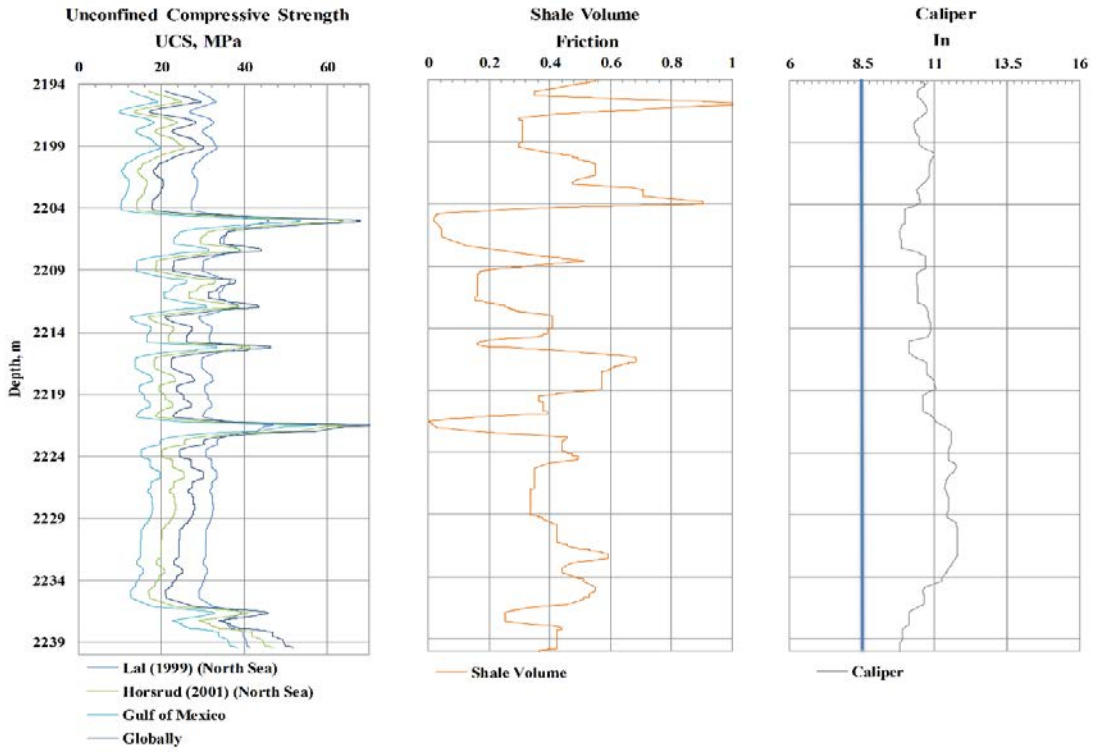

Figure 7.7. Tracks-1 shows the UCS values from different Empirical equations; Track-2,3 represents the shale volume and the Caliper log respectively for Group-3.

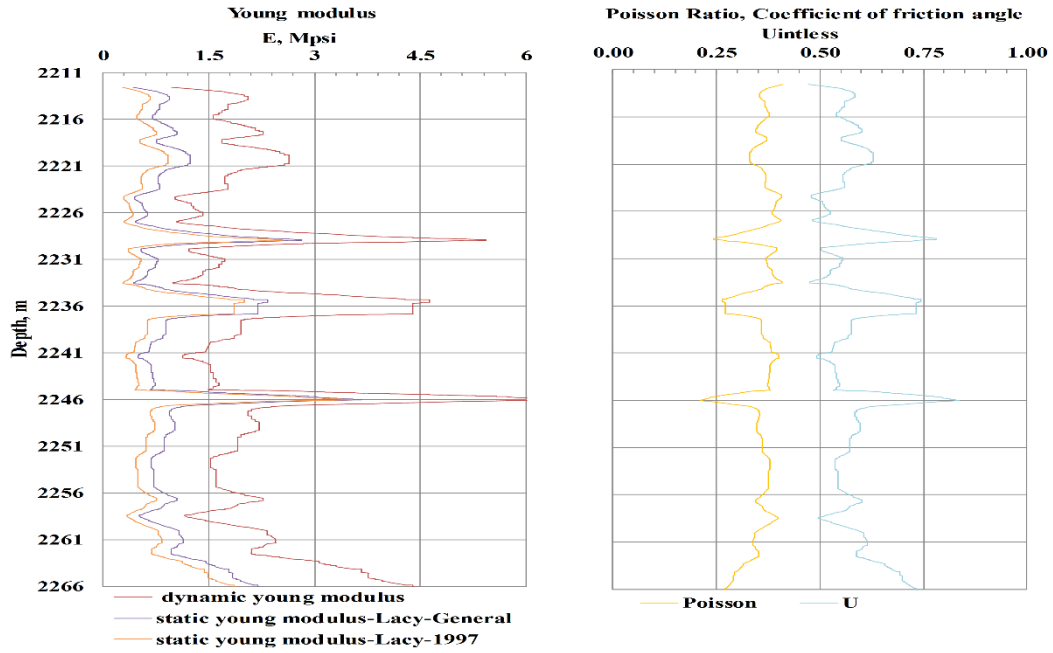

Figure 7.8. Track-1 shows the static and dynamic Young modulus; Track-2 represents Poisson ratio and coefficient of internal friction for Group-3.

7.5. DRILLING FLUID WEIGHT PREDICTIONS

The model suggests drilling fluid weight based on the input data Table 7.3 (the FM temperature used 356 k). The model output revealed drilling fluid densities higher than the field static drilling fluid densities, and these wells encountered wellbore instability events, as displays in Table 7.4. This result indicates the field drilling fluid density was randomly changed, and there was no insufficient support from the borehole pressure. However, one well (A-40) subsequently experienced washout and stuck, in spite of the predicted drilling density being less than the field density, but according to the DDR investigation for this well, these events mostly occurred after the entire hole was drilled, and the shale might be suffering from poor drilling fluid properties. The data analysis has revealed that, the extensive reaming and back reaming procedure in the Tanuma formation can deteriorate the wellbore stability in some wells. The contrast stress effects on the well trajectory design, the rock strength anisotropy has a substantial impact on changing the required fluid density for a particular direction as shown in the difference between Figure 7.9, and 7.10. These parameters follow the same trend of the previous groups when it comes to fluctuation due to limestone stringers interbedded with shale. Finally, one well (A-45) shows a severe lowering to the drilling fluid density while tripping out of the hole procedure.

Table 7.3. Geomechanic Model input data for Group-3 to Tanuma FM

Parameters	**Value (Unit)**	**Source**
Depth	2234 m	
Sv, SH	54, 46MPa	
Sh	38.6 MPa	(Breckels & van Eekelen, 1982)
Pp	26.06 MPa	
UCS	29.79 MPa	(Lal,1999)
Poisson Ratio, Coeff. Of internal friction	0.36, 0.6	
Water, shale Activity	0.94,0.82	(Zhang et al., 2008)
Volumetric Thermal Expansion Coefficient	2.58*10-6	(Kadyrov & Tutuncu, 2012)
Young Modulus	6019 MPa	

Table 7.4. Group-3 results, 1=stuck, 2=stuck free, 3=caving, 4= Tight spot

Well	Field Mud	Mud With Effect	Mud Without	SWAB Effect	Ecd	Azm	Inclin	Problems
#	Sg	Sg	Sg	Sg	Sg	Deg.	Deg.	
A-40	1.28	1.19	1.18	N/A	1.31	135.00	3.00	2
A-41	1.28	1.27	1.22	1.269	1.35	220.00	40.50	
A-42	1.28	1.35	1.32	N/A	1.42	251.04	56.80	4
A-40	1.25	1.19	1.18	1.243	1.31	135.85	2.47	3
A-43	1.28	1.33	1.30	1.270	1.35	290.15	44.10	2
A-44	1.28	1.41	1.38	1.268	1.37	314.72	54.82	4
A-45	1.27	1.38	1.35	1.241	1.37	129.32	49.23	4
A-46	1.28	1.36	1.33	1.269	1.34	97.70	51.93	4
A-47	1.28	1.34	1.33	N/A	1.36	78.16	57.06	4
A-48	1.28	1.35	1.31	1.271	1.32	282.72	48.53	
A-49	1.25	1.32	1.26	1.241	1.34	18.90	31.00	3
A-53	1.25	1.29	1.26	1.242	1.35	58.90	53.47	4
A-54	1.26	1.34	1.30	1.250	1.39	352.50	39.50	3
A-55	1.25	1.36	1.31	1.239	1.35	36.74	51.38	3
A-56	1.25	1.34	1.29	N/A	1.36	37.45	48.65	3

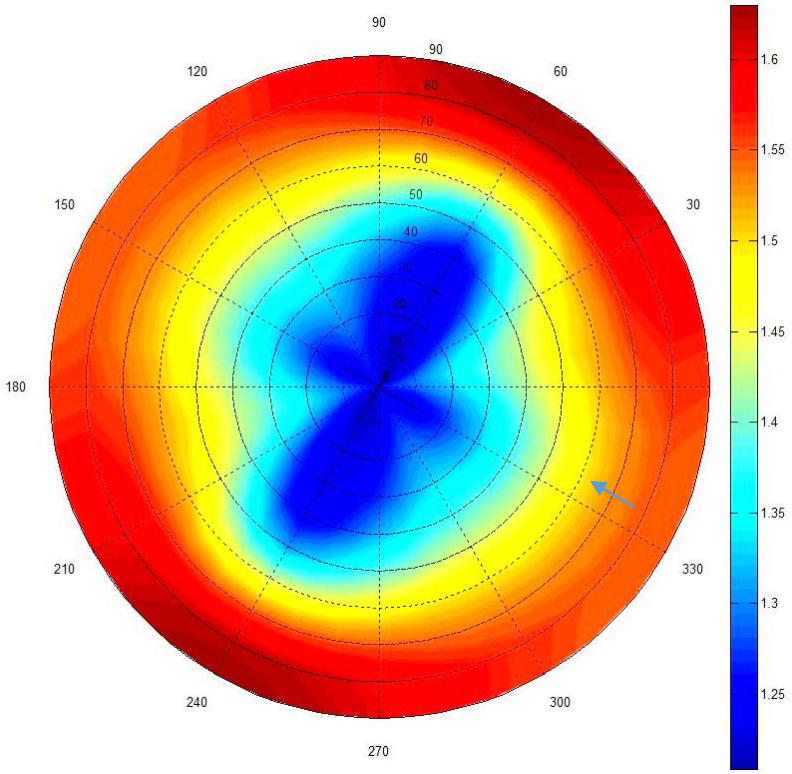

Figure 7.9. Polar plot of the model mud weight to prevent shear failure in Tanuma FM for Group-3 (Including effects- thermal and chemical induced stress as well as strength anisotropy), the wormer color repersents the higher requires fluid density (NW).

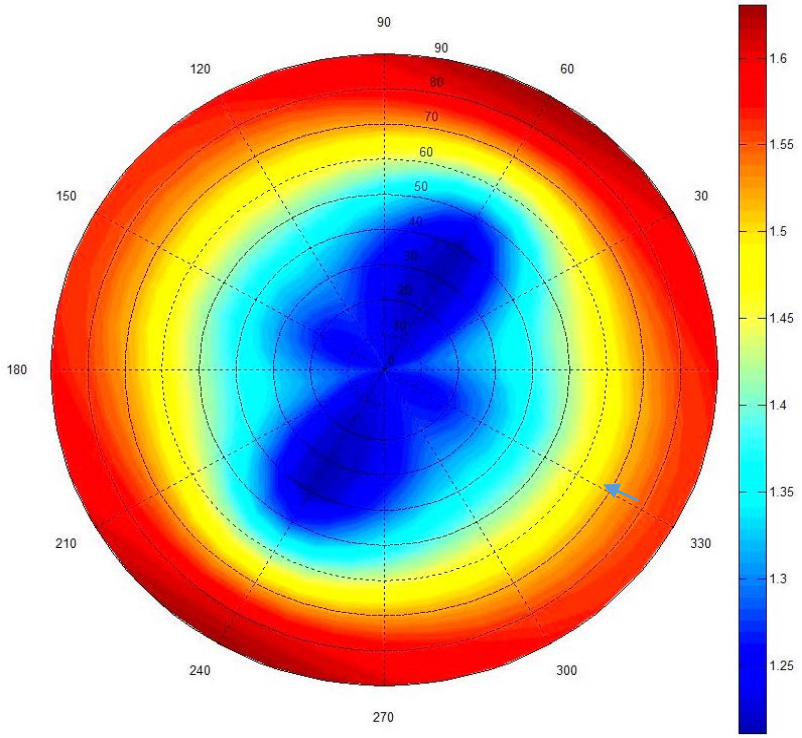

Figure 7.10. Polar plot of the model mud weight to prevent shear failure in Tanuma FM for Group-3.

7.6. GROUP THREE ANALYSIS

The deepest Tanuma tops (2241 m) distinguish the wells under this category. The calculated vertical stress and the pore pressure for group-2 wells have been drawn in Figure 7.11. It is important to highlight that these values are higher than the values of the greoup-1 because the depth of investigation is greater. The Sv is proportionally related to depth and the pore pressure trends in this group are similar to group-1, but it increases drastically in the Sadi and Tanuma formation while it decreases in the Mishrif formation. The drilling fluid density being used is close to the value of the pore pressure along the whole well depth.

The validated correlation of SH and Sh are illustrated in Figure 7.11, and it can be concluded, the linear tend of the horizontal stress is dominated with depth along the entire well depth. The fracture gradient is located between the maximum and minimum horizontal stresses.

The rock strength property, shale volume and caliber log are displayed in Figure 7.12. As can be noticed, the excessive washout in the caliber log is mostly related to a high clay percentage as well as the low rock strength magnitudes. The UCS values are at these depths have types of rocks other than shale (i.e. marl, limestone). Figure 7.13 shows the rock elastic parameters and the coefficient of internal friction angle. The three depths have been distinctive of increasing Young modulus and angle of friction, yet decreasing Poisson‘s ratio.

7.7. DRILLING FLUID WEIGHT PREDICTION.

The optimum drilling fluid weight was determined based on the input data in Table 7.5. In addition, the model output has been summarized in Table 7.6. It can be seen that, the anticipated drilling fluid density is greater than the static drilling fluid used in the field and the majority of these wells have experienced wellbore instability problems. Despite two wells showing a different trend (Wells A-33 and A-37), but the shale failed in these well after the long exposure to the drilling fluid. Therefore, it might be an indication of time-dependent failures. The swab effect slightly changes the drilling fluid densities but it might affect the wells’ integrity. Also, the wells present wellbore instability with respect to well azimuth and inclination thus require that the drilling fluid be denser in a certain direction (maximum horizontal stress) as shown in Figure 7.15, and 7.15. It is important to allude that, according to DDR, the extensive procedure was conducted while drilling and tripping out of the Tanuma shale in this group, which might potentially increase the likelihood of the shale eroded and time dependency failures.

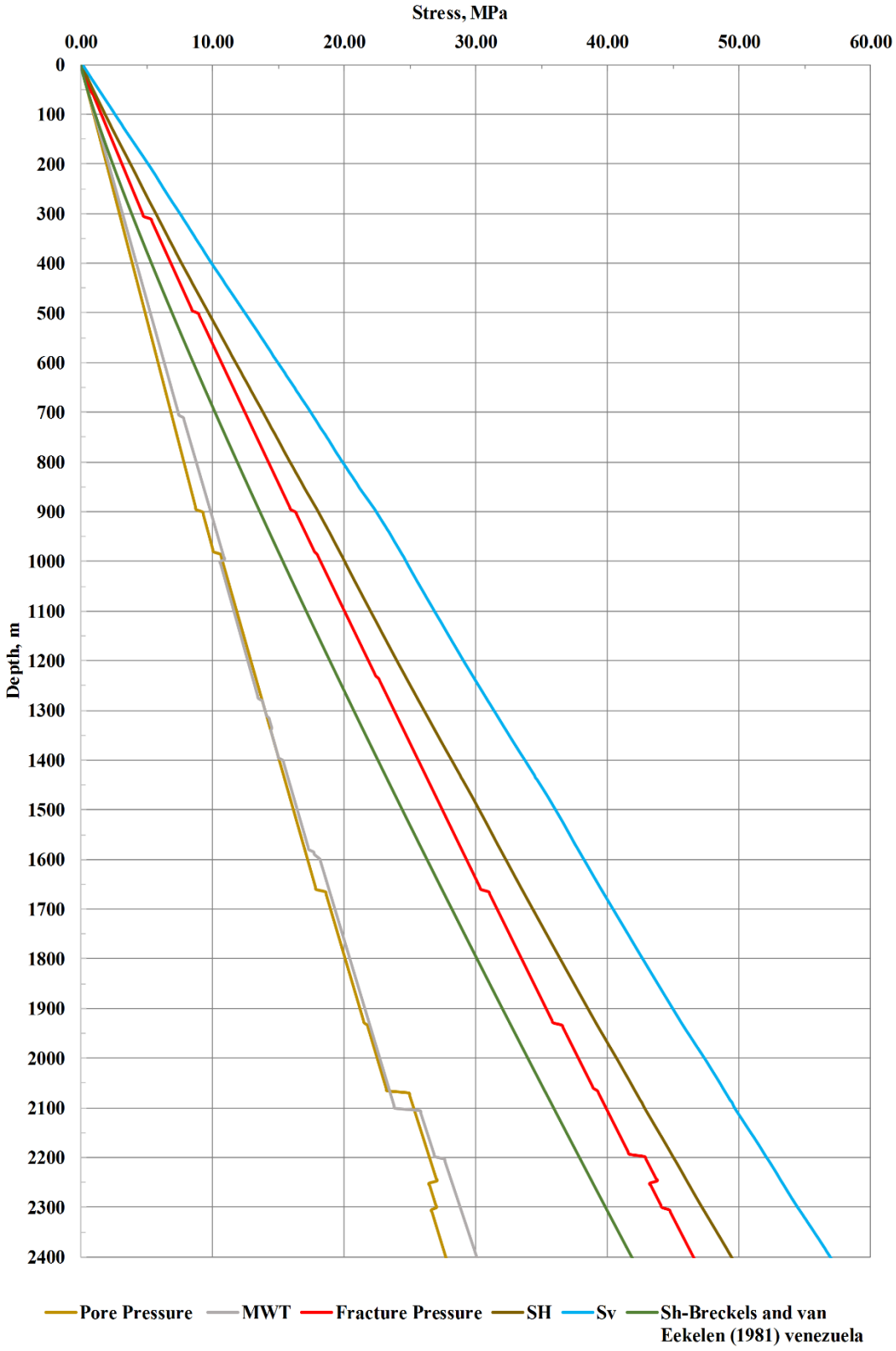

Figure 7.11. The borehole and subsurface stress in Group-2 wells.

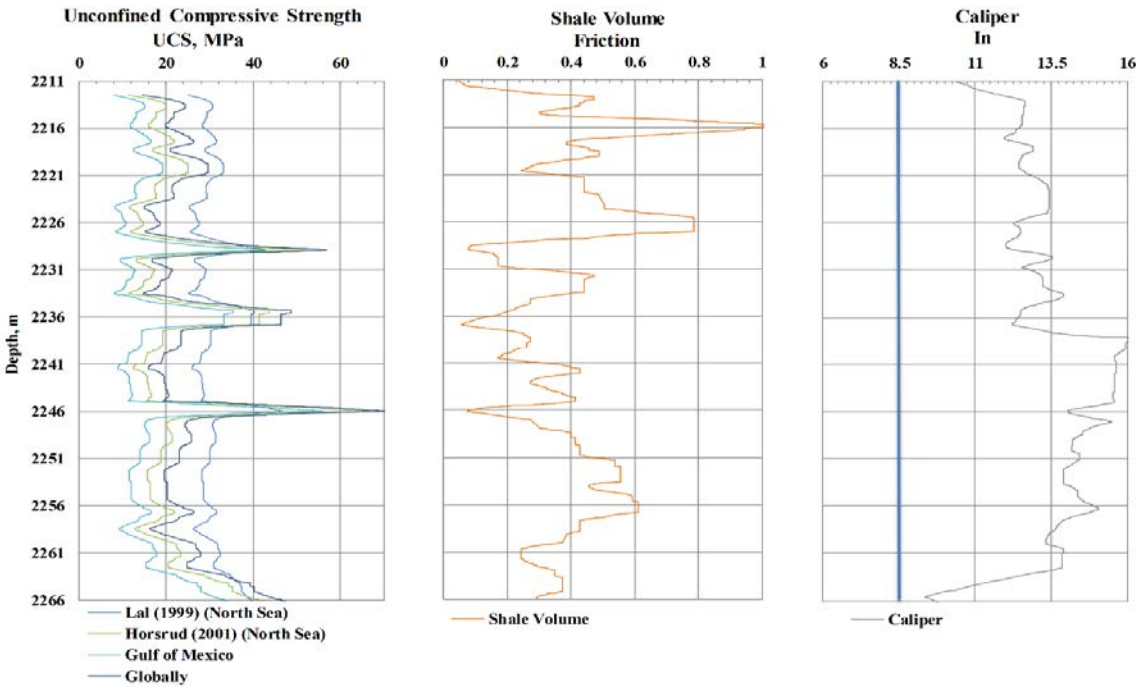

Figure 7.12. Tracks-1 shows the UCS values from different Empirical equations; Track-2,3 represents the shale volume and the Caliper log respectively for Group-2.

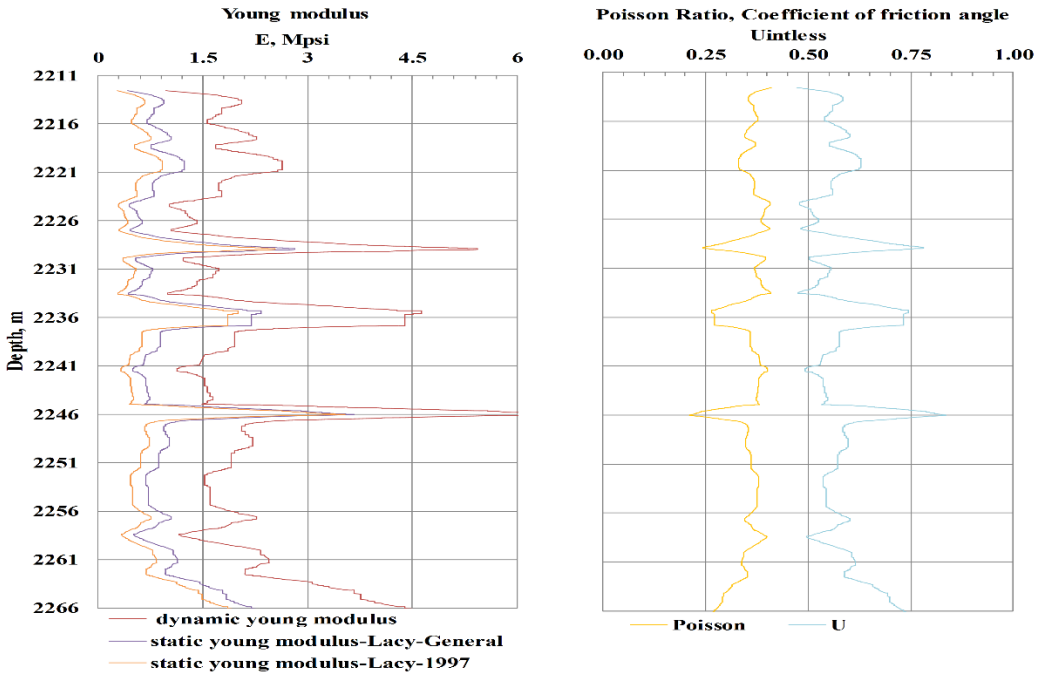

Figure 7.13. Track-1 shows the static and dynamic Young modulus; Track-2 represents Poisson ratio and coefficient of internal friction for Group-2.

Table 7.5. Model input data for Tanuma FM based on typical well for Group-2

Well	Field Mud	Mud With Effect	Mud Without	Swab Effect	ECD	Azm	Inclin.	Problems
#	Sg	Sg	Sg	Sg	Sg	Deg.	Deg.	
A-33	1.25	1.24	1.23	1.241	1.30	256	30.00	2
A-34	1.27	1.35	1.32	1.257	1.37	230	51.83	3
A-35	1.25	1.33	1.32	1.243	1.33	313.27	34.37	
A-36	1.28	1.30	1.29	1.273	1.33	287.94	31.05	3
A-37	1.25	1.40	1.34	1.241	1.29	241.00	59.00	1
A-37-S	1.25	1.24	1.22	1.239	-	244.00	37.00	other
A-38	1.27	1.29	1.27	N/A	1.33	217	31.00	2
A-39	1.28	1.28	1.27	1.272	1.36	256.23	42.44	3

Table 7.6. Group-2‘s result, (1=stuck, 2=stuck free, 3=caving, 4= Tight spot)

Parameters	Value (Unit)	Source
Depth	2241 m	
Sv	53.1 MPa	
SH	45.91 MPa	
Sh	38.74 MPa	(Breckels & van Eekelen, 1982)
Pp	26.35 MPa	
Coeff. Internal Friction	0.6	
UCS	26.06 MPa	(Lal,1999)
Poisson Ratio	0.39	
Water Activity	0.94	(Zhang et al., 2008)
Shale Activity	0.82	(Zhang et al., 2008)
Formation Temp.	356 K	
Volumetric Thermal Expansion Coefficient	2.58*10-6	(Kadyrov & Tutuncu, 2012)
Sh Orientation	335 Degree	
Young Modulus	4043 MPa	

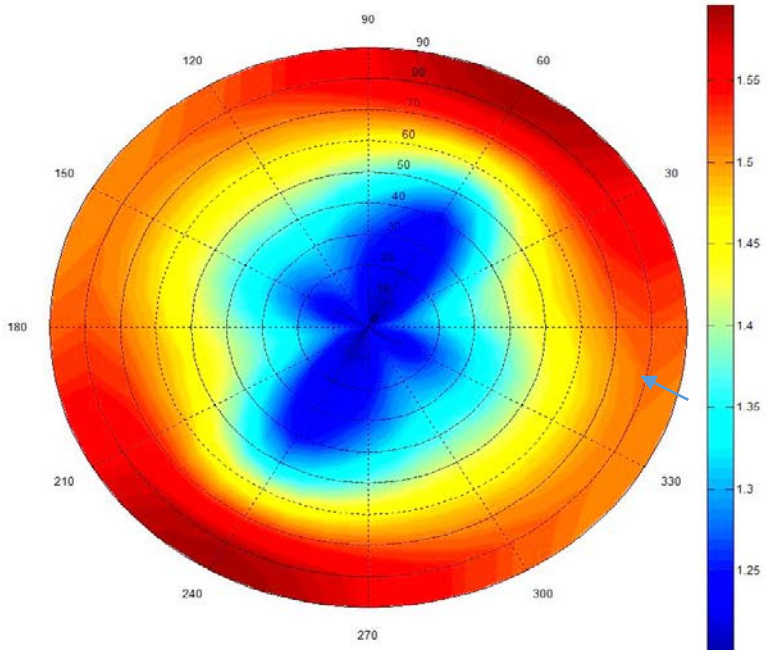

Figure 7.14. Polar plot of the model mud weight to prevent shear failure in Tanuma FM for Group-2 (Including effects- thermal and chemical induced stress as well as strength anisotropy, the wormer color repersents the higher requires fluid density (NW).

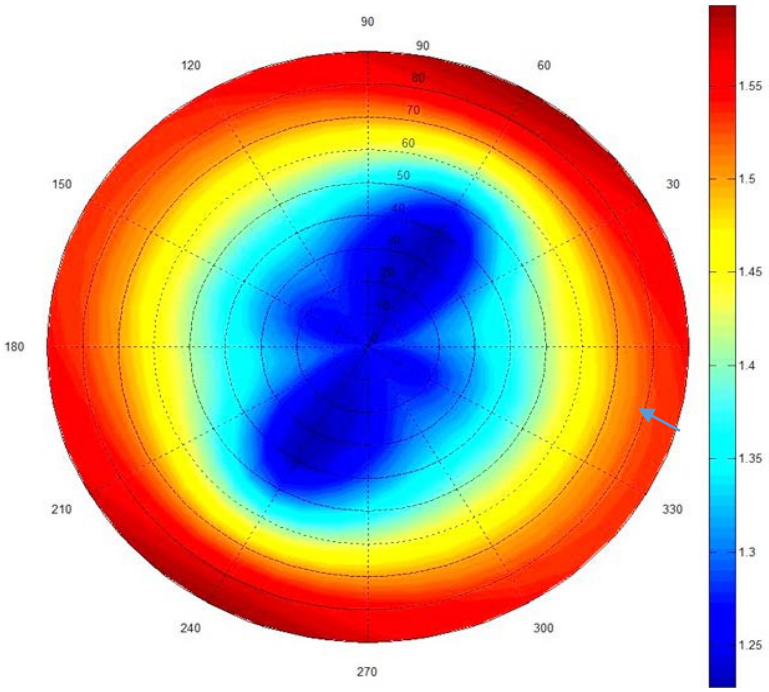

Figure 7.15. Polar plot of the model mud weight to prevent shear failure in Tanuma FM. for the Model-Group-2, the wormer color repersents the higher requires fluid density (NW)

7.8. THE TENSILE FAILURES IN UPPER AND TARGET FORMATION SECTIONS

The tensile failure of the weak zones in the production section has been examined to ensure the predicted fluid density in the safe operational mud window. According to the formation integrity test (FIT) that was conducted in the last casing shoe, the model‘s fluid densities are lower than the value of FIT (1.43 sg). Thus, the modeled drilling fluid densities are in the range of the operational mud window. Furthermore, the Polar plots for the maximum drilling fluid pressure to onset tensile failure in the Sadi and Mishrif (target) formations have demonstrated the predicted drilling fluid used to prevent the shear failure in the Tanuma section is less than the Tensile failure drilling fluid in other formations at the same section, as depicted in Figure 7.16 ,and 7.17.

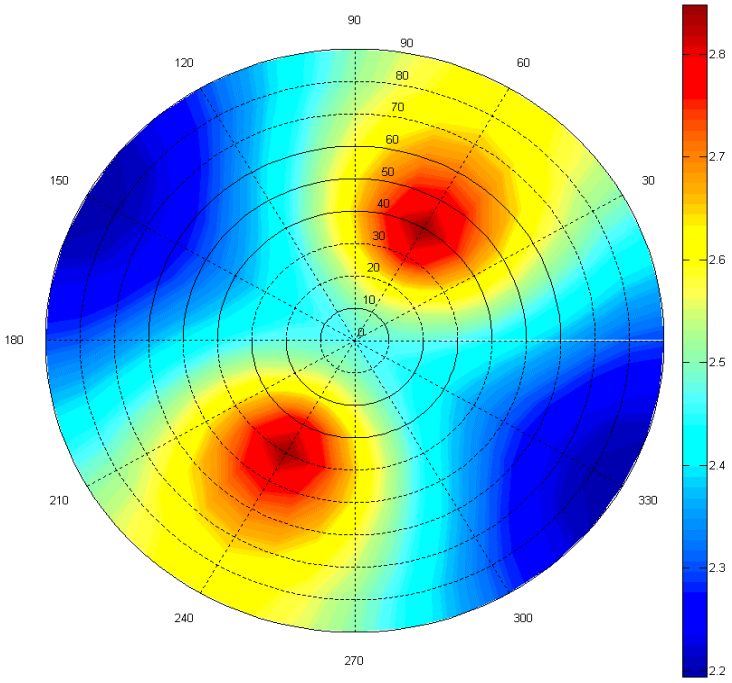

Figure 7.16. Polar plot of the model mud weight to prevent tensile failure in Upper Sadi FM , the wormer color repersents the higher requires fluid density to induce tensile failure (NW).

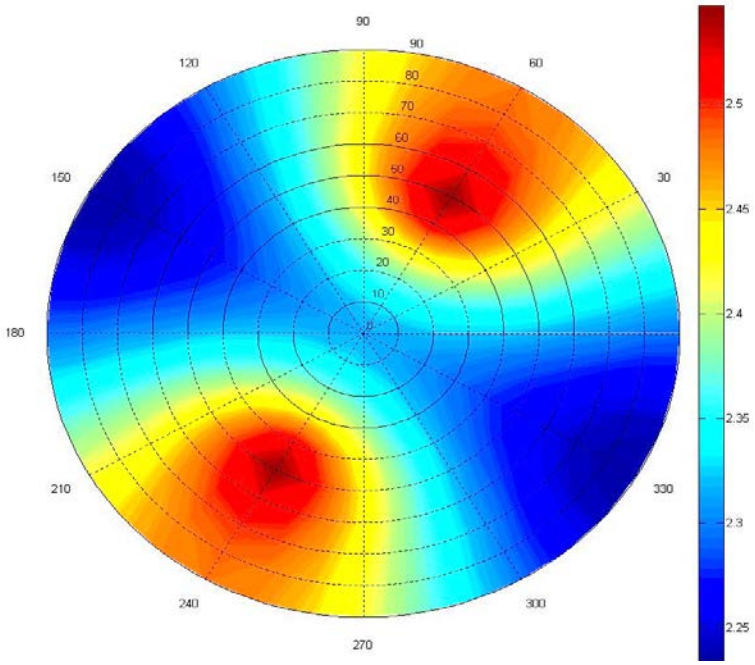

Figure 7.17. Polar plot of the model mud weight to prevent tensile failure in Lower Mishrif FM.

7.9. THE UNCERTAINTY ANALYSIS FOR GEOMECHANICS MODEL

The probability distribution of the of the geomechanical model to prevent onset collapse failure in Tanuma shale illustrated in Figure 7.18, and 7.19 according to 10000 trialls. As can be observed, the likelihood of having drilling fluid density less 1.19 Sg and greater than 1.39 were 7.87 % and 1.5% respectively. These ranges were the lowest and the highest values predicted by the geomechanical model, that meant to prevent onset shear failure there was the probability of 90.63% to have drilling fluid density between (1.19-1.39) sg. The uncertainty analysis for certain input variables shown in Figure 7.20, which demonstrated the SH, UCS, Poisson ratio, and friction angle were the most influence on the magnitude of the minimum drilling fluid density to prevent shear failure. The sensitivity analysis for the all input data shown in Figure 7.21. It shows the chemical effect component is slightly affected the required drilling density.

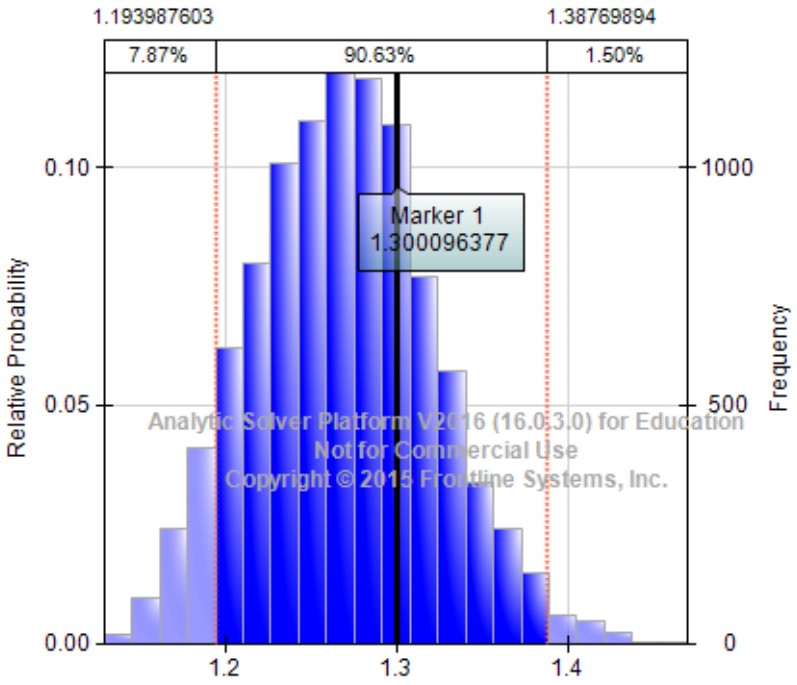

Figure 7.18. Probability density distribution chart for the drilling fluid density to prevent collapse failure in Tanuma FM.

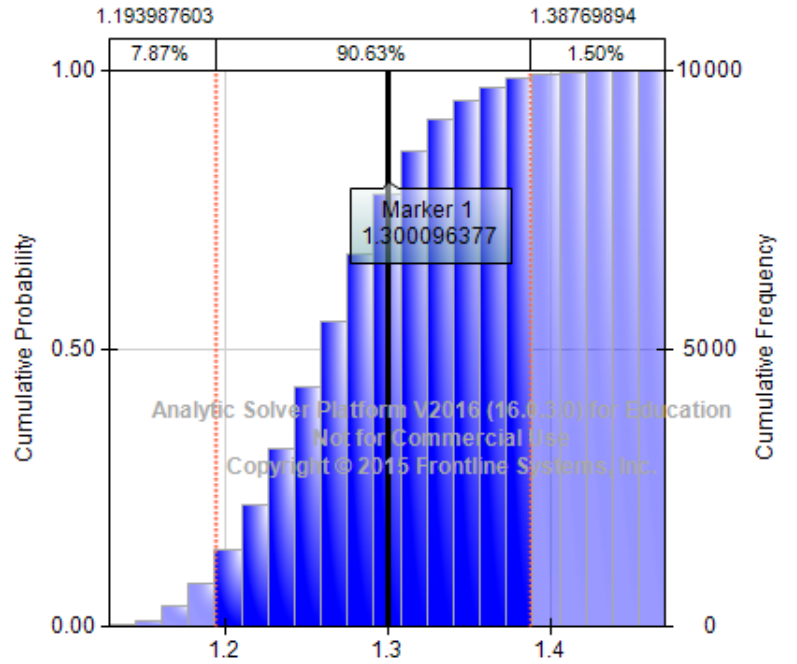

Figure 7.19. Cumulative Probability density for the drilling fluid density to avoid collapse failure in Tanuma FM.

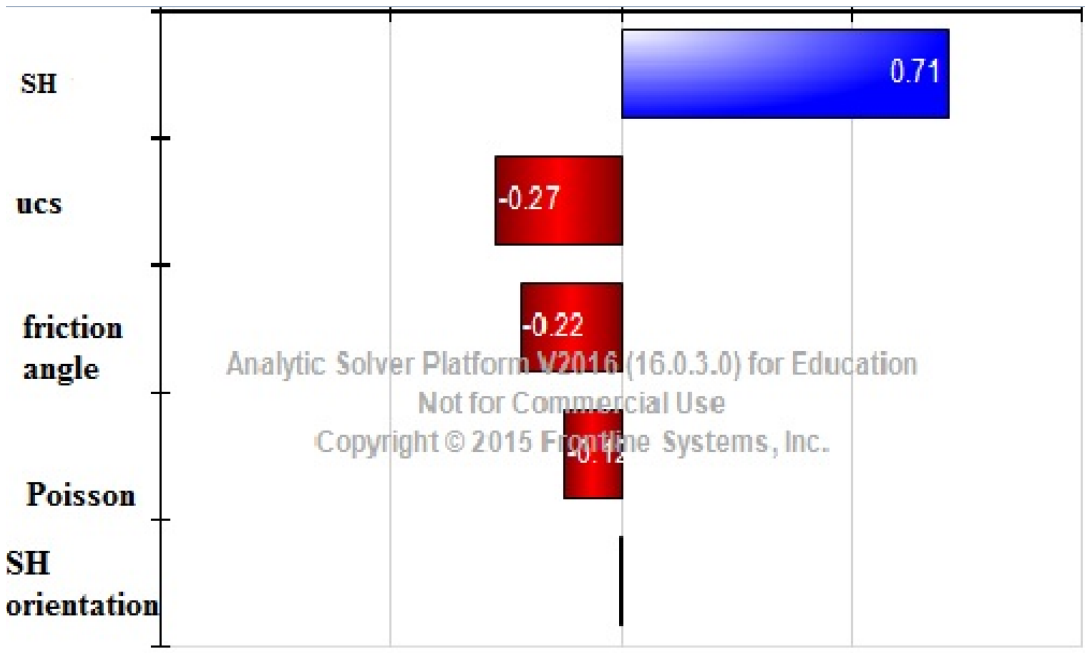

Figure 7.20. Tornado charts for the uncertain variables.

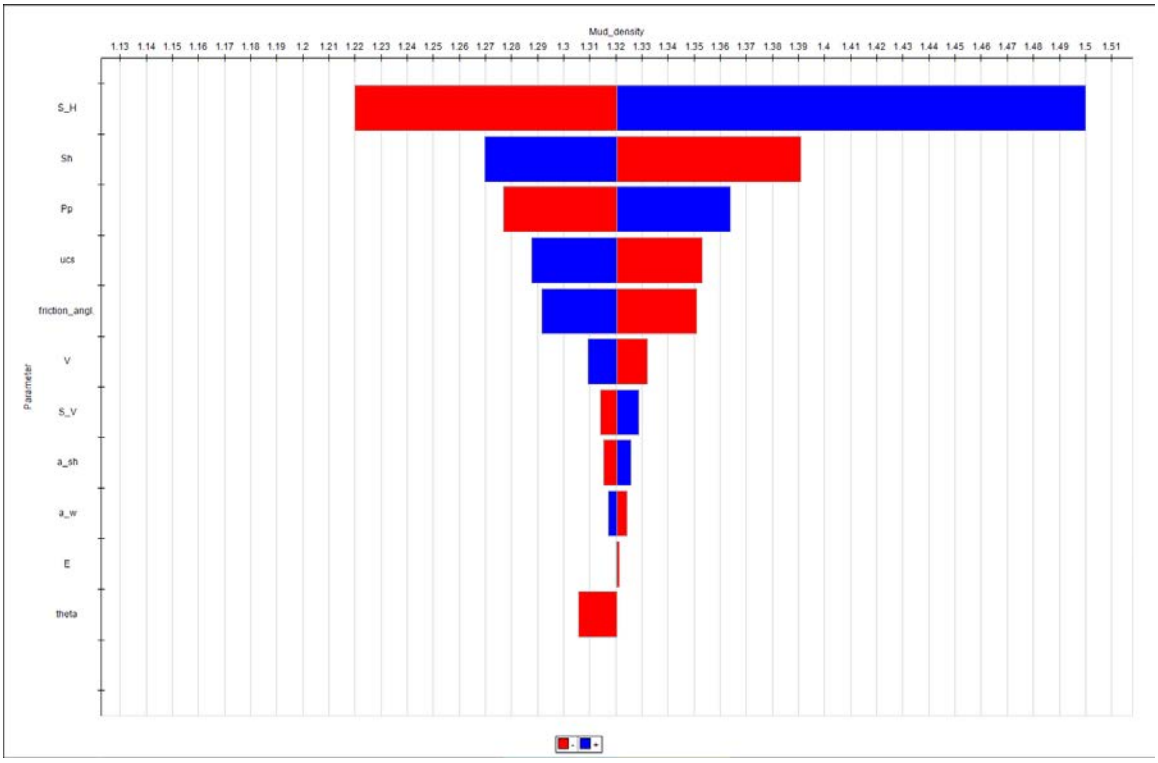

Figure 7.21. Sensitivity analysis of the input for Geomechanical model

8. DRILLING OPTIMIZATION SOLUTION FOR WELLBORE PROBLEMS

8.1. MULTI REGRESSION ANALYSIS

The drilling data from 25 wells have been analyzed to enhance the drilling performance and consequently the ROP. As the rate of penetration develops, the shale exposure time reduces, and a more stable wellbore is potentially achieved. The multi-regression analysis for the field data was conducted using JMP software. The pre-analyses of the drilling parameters with respect to ROP are illustrated in Figure 8.1, 8.2, and 8.3. According to these figures, the ROP has a positive slope with the following factors: WOB, TFA, and FR. In these figures, the blue dashed line represents the mean of ROP while the solid and dashed red lines represent the fitted model and the confidence interval, respectively. Additionally, Table 8.1, 8.2, and 8.3 provides the sensitivity analyzes and the statistical model variable that is used to predict the ROP from Equation 58. It is important to emphisized, the previously analysis were conducted to Tanuma shale formation while the limestone part of the procuction section was obtained by Equation 59 and the detail description of the drilling variable shown in Appendix A.

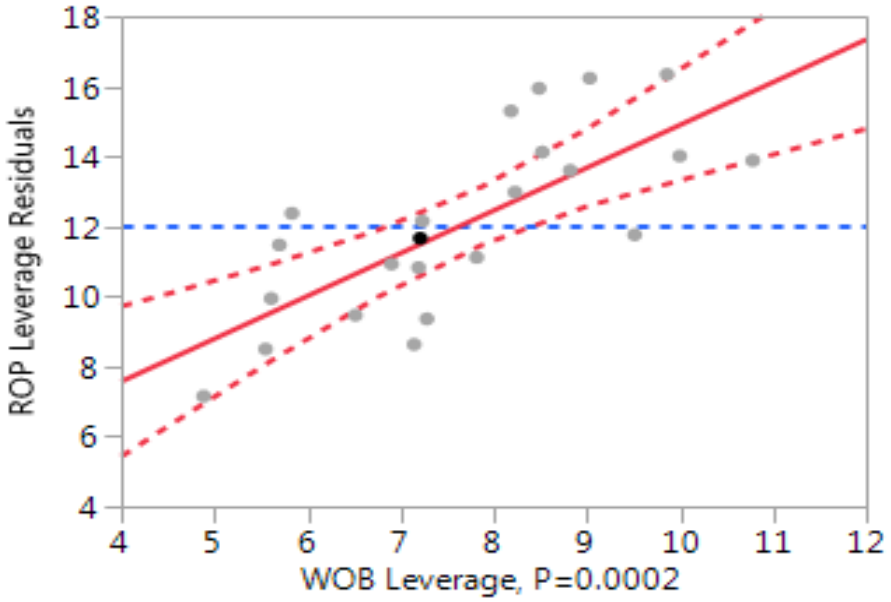

Figure 8.1. The weight on bit effect on the ROP of the field data.

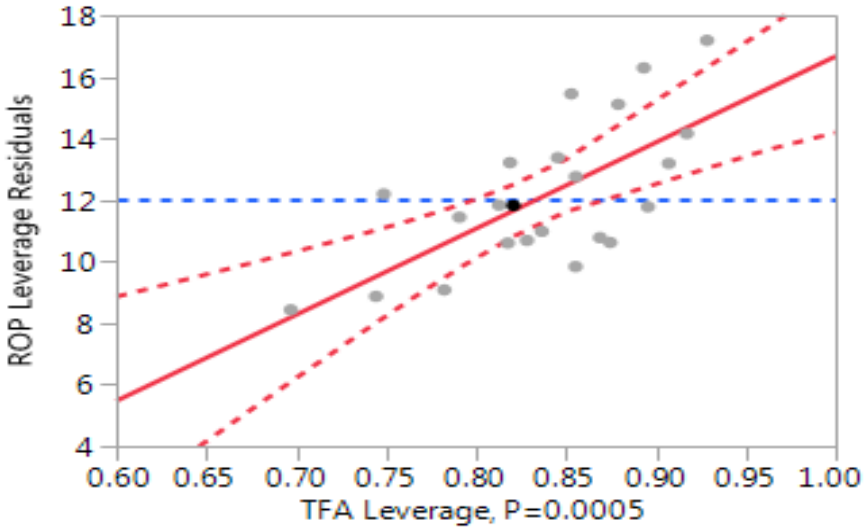

Figure 8.2. Total flow area effect on the ROP.

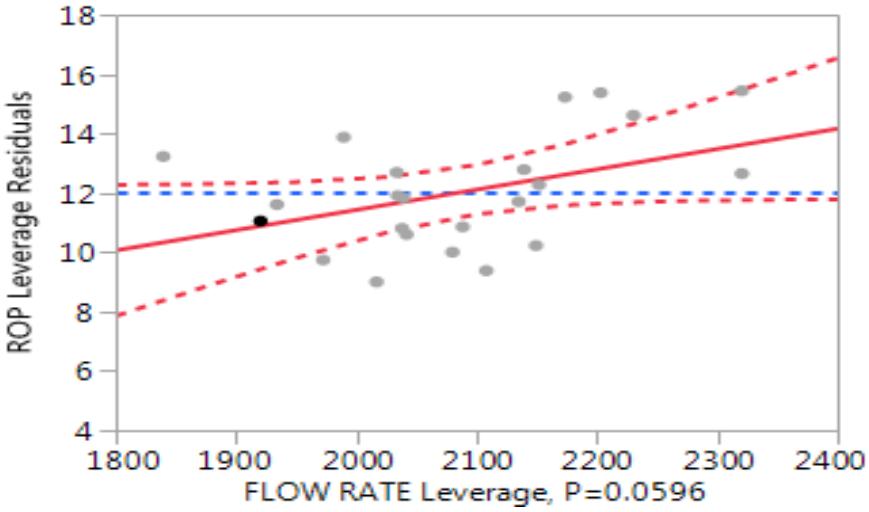

Figure 8.3. Flow rate effect on the ROP.

Table 8.1. Model sensitivity variables

Source	LogWorth	PValue
WOB	3.784	0.00016
TFA	3.263	0.00055
MUD	2.656	0.00221
FLOW RATE	1.224	0.05964
rpm	0.604	0.24889

Table 8.2. Model statistical variables

Parameters	Value
RSquare	**0.732767**
RSquare Adj	0.658536
Root Mean Square Error	1.918892
Mean of Response	12.02542
Observations (or Sum Wgts)	24

Table 8.3. Multi-regression model

Term	Estimate	Std Error	t Ratio	Prob>|t|
Intercept	-204.094	53.83167	-3.79	0.0013*
MUD	138.29372	38.78055	3.57	0.0022*
FLOW RATE	0.0068317	0.003398	2.01	0.0596
rpm	-0.02442	0.020493	-1.19	0.2489
WOB	1.2211055	0.257768	4.74	0.0002*
TFA	27.991098	6.67527	4.19	0.0005*

$$ROP = 138.3 \times MUD + 0.0068 \times FL + 1.221 \times WOB + 28 \times TFA - 0.024 \times RPM - 204 \text{ . for } (shale) \quad (58)$$

$$ROP = 35.204 \times MUD + 0.00376 \times FL + 1.863 \times WOB + 9.04 \times TFA - 0.0139 \times RPM - 61.04 \text{ . for (limestone)} \quad (59)$$

8.2. DRILLING OPTIMIZATION

Two base case wells were investigated to enhance the drilling performance and reduce the shale exposure time The sensitivity analysis of each drilling variable was undertaken in which certain parameters were optimized in DROPS when the other

variables kept constant. Figure 8.4, 8.5, and 8.6 show the drilling parameters and the bit design variables star plots that can serve a significant role in choosing the best modification for each input variable to enhance the ROP. The drilling variables that improve the ROP to some extent are the WOB, HSI and flow rate. However, the increased in the drilling fluid density and the plastic viscosity have adverse effects on the ROP. With respect to PDC bit design parameters, the ROP can be enhanced if either junk slot area or exposure of the back rake cutter increase while increasing the rest of bit variables might reduce the ROP to some extent. The post-optimization analysis has resulted in triple the ROP in well-1 and well-2, respectively have shown in Figure 8.7, and 8.8, respectively. These figures represent the apparent strength logs and the optimized ROP.

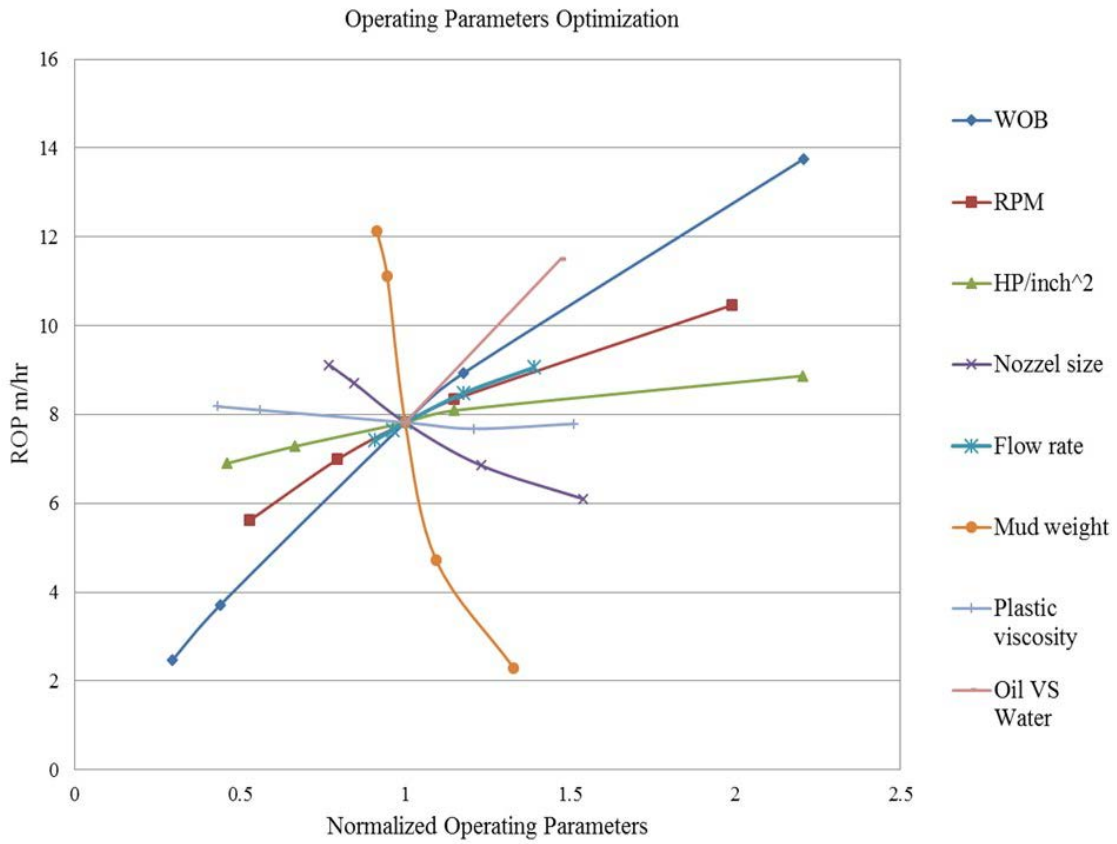

Figure 8.4. Star plot for the sensitivity of the drilling variables.

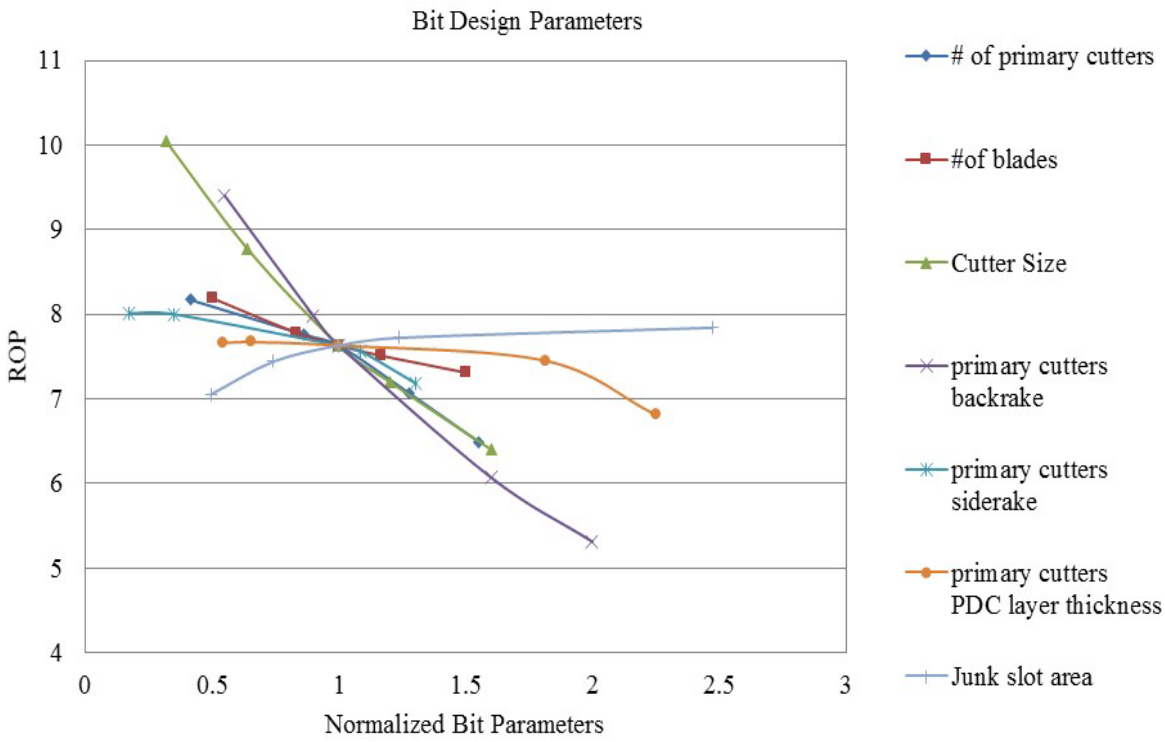

Figure 8.5. Star plot for the sensitivity of the bit designs variables-1

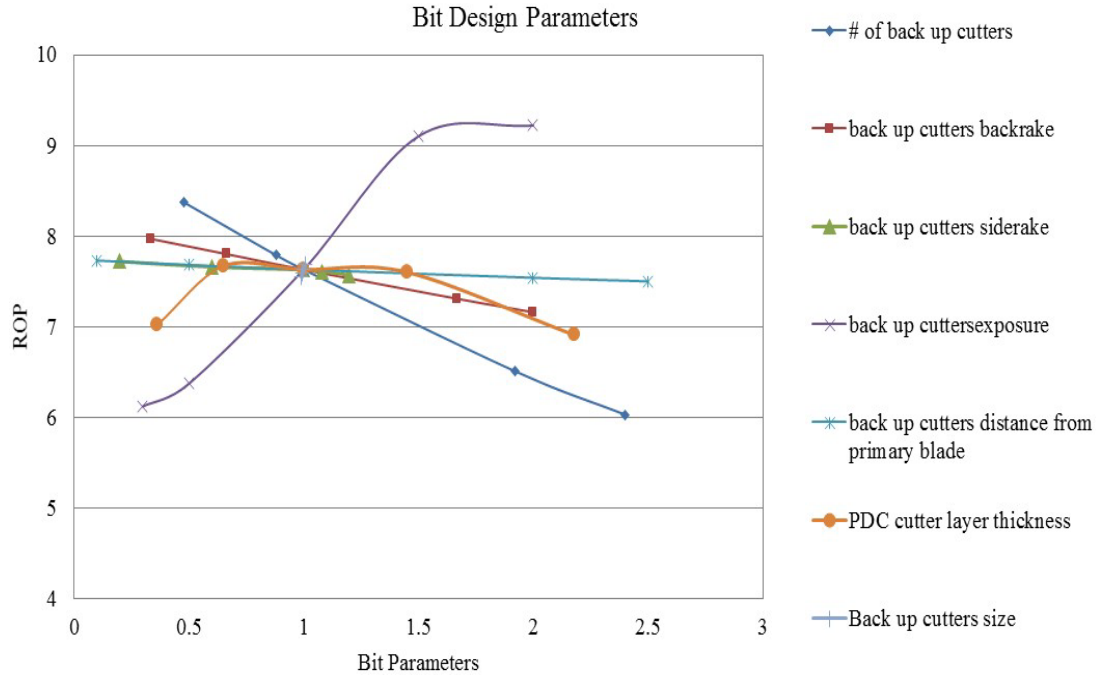

Figure 8.6. Star plot for the sensitivity of the bit designs variables-2.

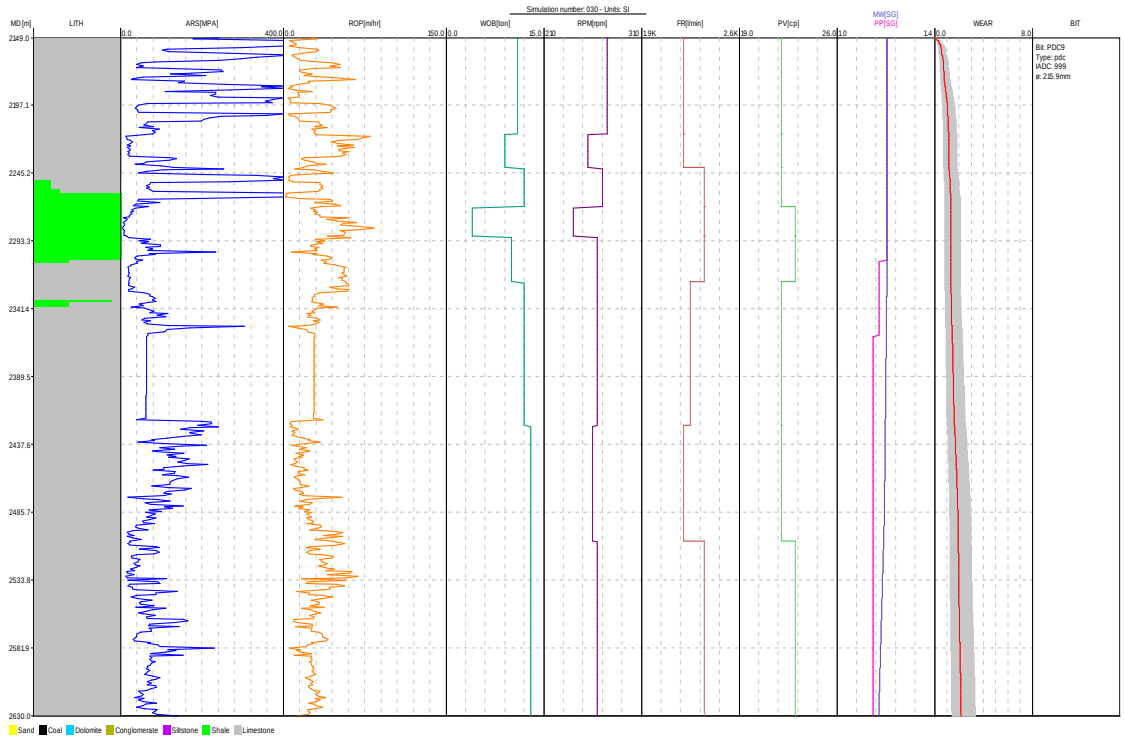

Figure 8.7. Well-1 optimization and drilling parameters.

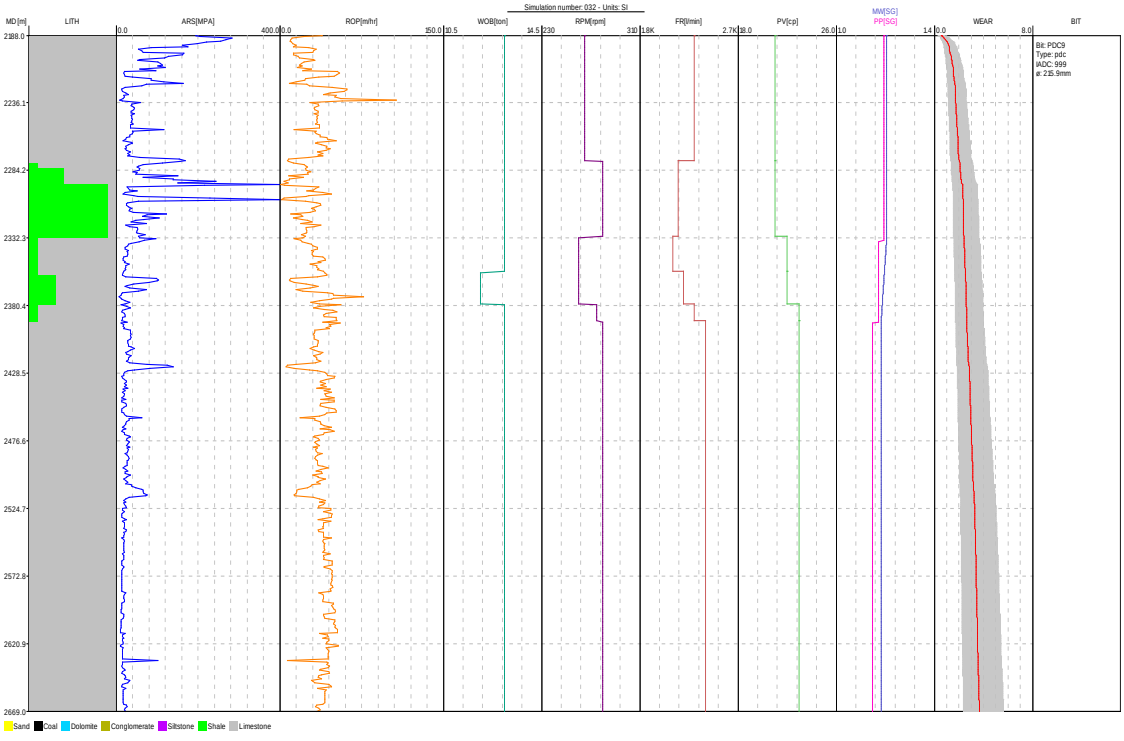

Figure 8.8. Well-2 Optimization and drilling parameters.

8.3. DRILLING OPTIMIZATION RESULT

There are a noticeable enhanced in drilling activity and the time required to complete the production section as shown in Figure 8.9 that explain the different between the fields ROP with the optimized ROP techniques. The DROPS software ROPs and multi-regression ROP are superior over the field ROPs and result in considerable reduction in drilling cost and time. In addition, the new bit design, that shown in Table 8.4, did not improve the performance much. Thus, the drilling parameters optimization is more beneficial over the bit design variables optimizations.

Table 8.4. Bit design parameters

Bit	**back rake angle (P,B)**	**Side rake angle (P,B)**	**Primary (p) Cutter Diameter**	**Back up (B) Cutter Diameter**	**Exposure**	**Junk slot area**	**Number of primary cutters**	**Number of backup cutters**
old	(15,20)	(23,25)	0.625	0.529	0	16.168	29	25
New	(18,22)	(8,10)	0.45	0.75	0.15	20	29	25

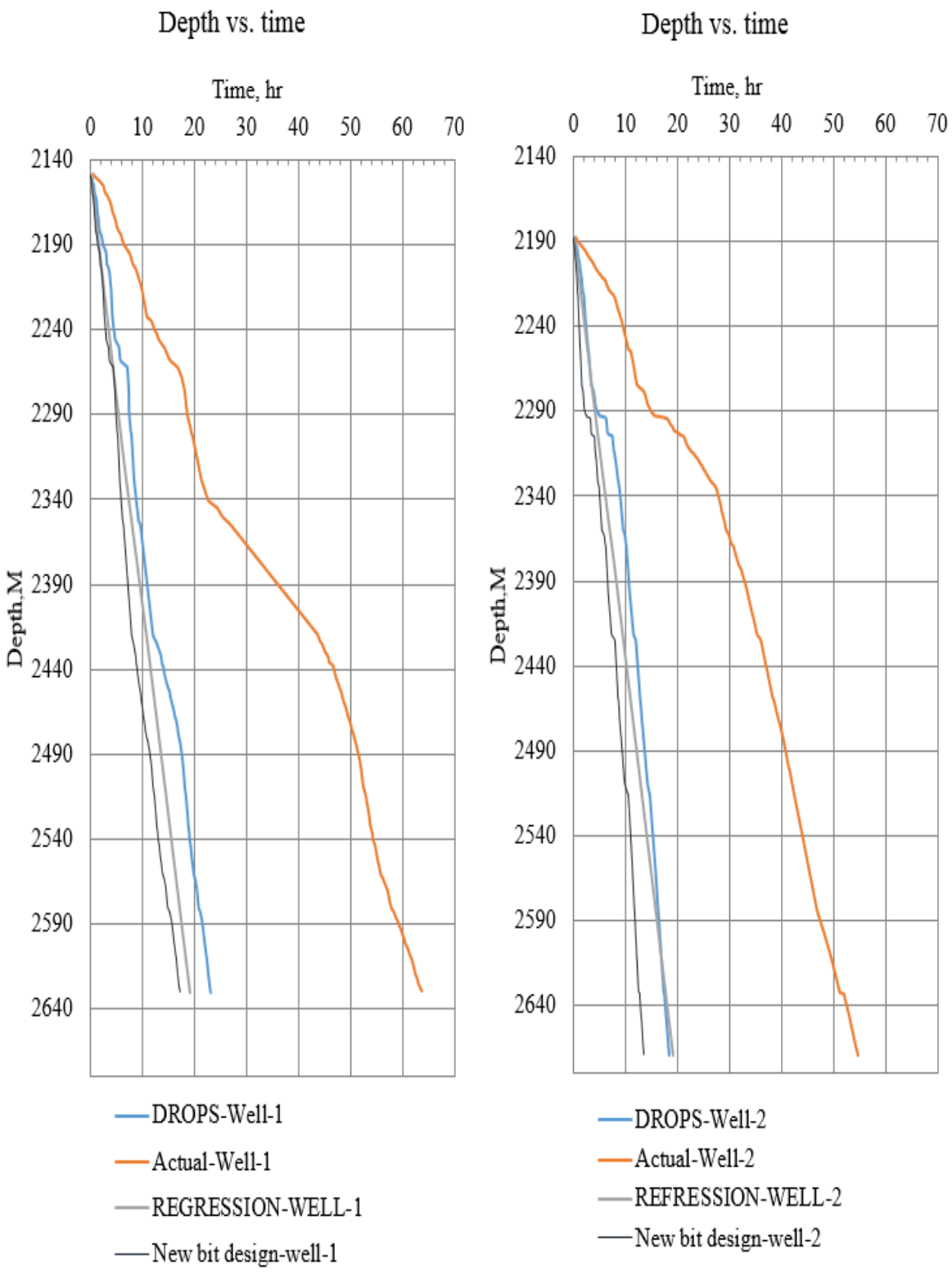

Figure 8.9. Comparison between the optimization methods for well-1 and well-2

9. DRILLING FLUID DENSITY REDUCTION BY SWABBING EFFECT

The main factors that cause reduction in bottom hole pressure have been analysis based on tripping data of 22 wells. Figure 9.1 shows trending of propositional increase of the fluid density by swabbing with the fluid density and slip to slip time (TT), but the swabbing density is negatively affected by the plastic viscosity, flow rate, and the drill collar outside diameters as shown in Figure 9.2, and 9.3, respectively. The yield point does not change the swab effect much according to Figure 9.3 The predicted model to calculate drilling fluid density reduction by swabbing effect is represented in Equation 60. The recommended tripping variables summarized in Table 9.1 and result of the swabbing model when it applied on the geomechanical model result illustrated in Table 9.2. It can be observed; the drilling fluid reduction is mitigated considerably when the suggested tripping parameters were applied in the swabbing model.

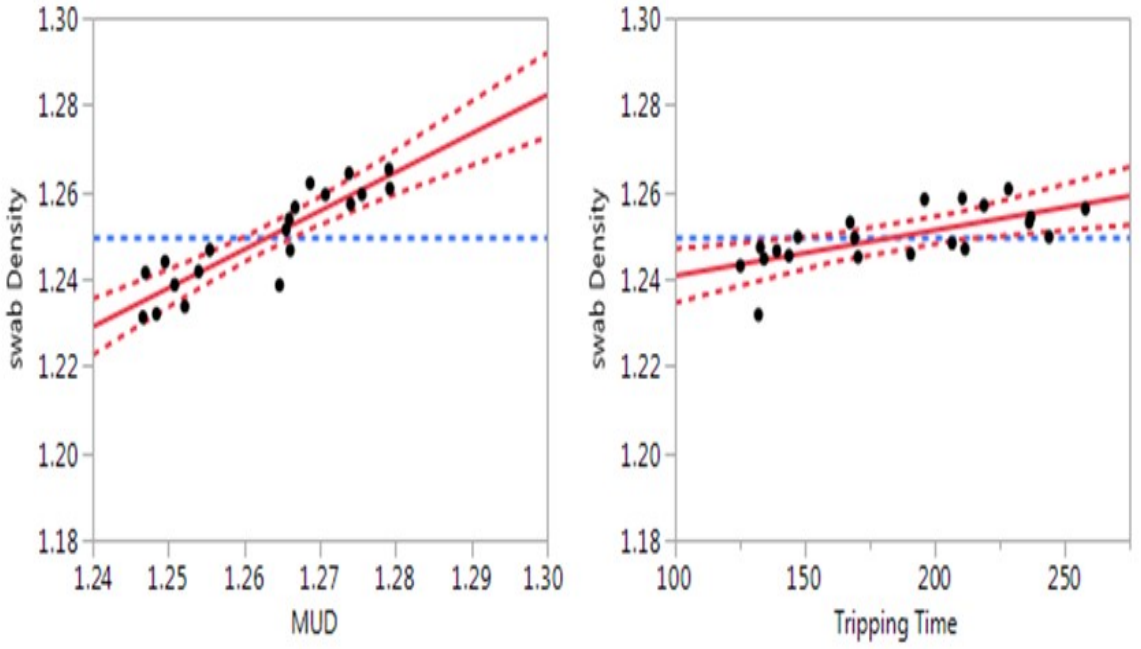

Figure 9.1. Drilling fluid density and the tripping time effects on the swab density.

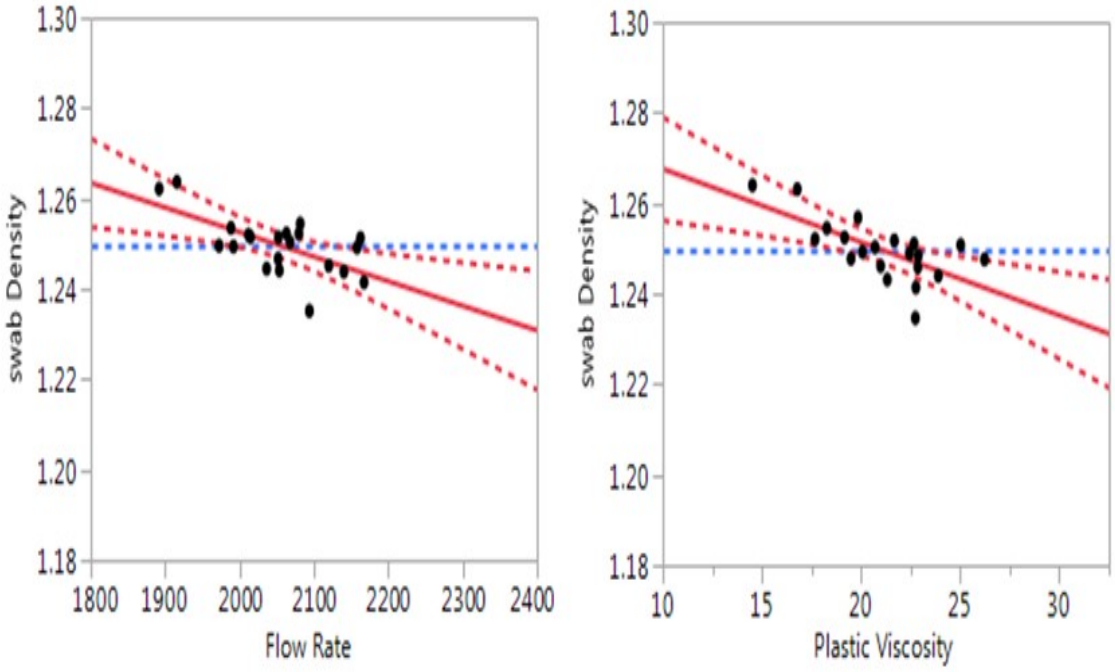

Figure 9.2. Flow rate and plastic viscosity effects on the swab density

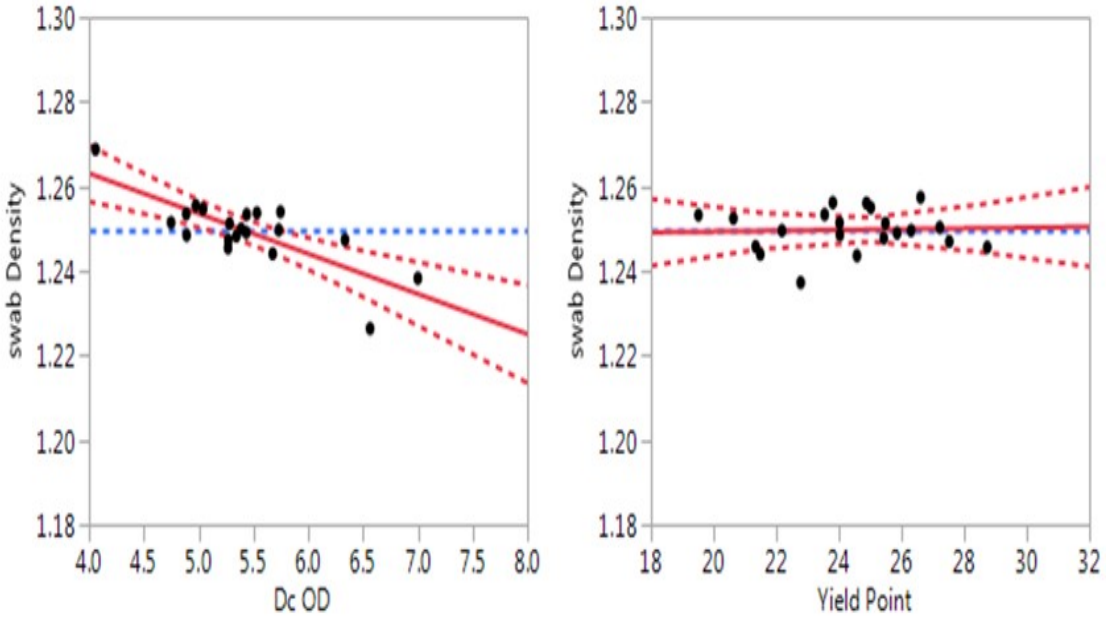

Figure 9.3. Drill collar OD and yield point effects on the swab density

Table 9.1. Tripping suggested parameters

Parameters	**Flow rate (L/min)**	**PV**	**Drill collar OD (In)**	**Slip to Slip time (sec)**
Value	2000	23	4.5	180

$$Swab_{density} = 0.30258 + 0.8885 \times density - 0.001618 \times PV - 5.439 \times 10^{-5} \times FL - 0.00949 * DC_{OD} - 0.0001048 * TT \quad (60)$$

Table 9.2. Swabing model result

WELLS	Modeled density (sg)	Swabbing model density(sg)	Field static density (sg)
A-51	1.27	1.261	1.25
A-13	1.31	1.297	1.25
A-14	1.35	1.332	1.28
A-15	1.32	1.306	1.3
A-16	1.43	1.403	1.27
A-17	1.2	1.199	1.25
A-18	1.35	1.332	1.28
A-19	1.3	1.288	1.28
A-20	1.2	1.199	1.25
A-21	1.21	1.208	1.25
A-22	1.21	1.208	1.28
A-23	1.28	1.270	1.25
A-24	1.35	1.332	1.25
A-25	1.4	1.377	1.25
A-26	1.31	1.297	1.25
A-13-S2	1.35	1.332	1.25
A-28	1.36	1.341	1.28
A-29	1.4	1.377	1.28
A-30	1.37	1.350	1.25
A-31	1.25	1.243	1.28
A-32	1.38	1.359	1.25
A-33	1.24	1.235	1.25
A-34	1.35	1.332	1.25
A-35	1.33	1.314	1.27
A-36	1.3	1.288	1.25
A-37	1.4	1.377	1.28
A-37-S	1.24	1.235	1.25
A-38	1.29	1.279	1.25
A-39	1.28	1.270	1.27
A-40	1.19	1.190	1.28
A-41	1.27	1.261	1.28
A-42	1.35	1.332	1.28
A-40	1.19	1.190	1.25
A-43	1.33	1.314	1.28
A-44	1.41	1.386	1.28

10. DISCUSSION

The appropriate drilling fluid density/variable have been estimated based on the geomechanical analysis and the drilling data optimizations. In terms of the drilling fluid estimation, it was demonstrated in section 7.3 that there is a difference between the models predicted drilling fluid density with and without wellbore stresses and strength perturbation effects (thermal, chemical and anisotropic). According to Figures 7.4, and 7.5, the anisotropic effects of the Tanuma formation caused by the bedding planes effected the magnitude of the required fluid density. In the same regard, the wells drilled in the direction of minimum horizontal stress are more stable, while the wells drilled along the maximum horizontal stress are less stable. Hence, the fluid density should be adjusted with respect to well trajectory parameters. It also can be observed that the modeled static drilling fluid density values are lower than the magnitudes of the formation integrity test in the last casing setting point and it also less than the maximum drilling fluid density used to induce tensile failure in the upper Sadi formation. By comparing, the predicted drilling fluid and the field drilling fluid in Tables 7.2, 7.4, and 7.6, it can be concluded that the modeled density is higher than actual static density especially for the wells that have reported instability problems. However, a few wells have been predicted to have drilling fluid density slightly less than the field density. But, extensive analyses for such wells have revealed two other facts. These wells were either stable in Tanuma formation or suffered from instability after the entire section was drilled. This means a time dependent failure was encountered due to insufficient drilling fluid functionalization.

The drilling practice and tripping variables can be optimized to reduce the likelihood of the time-dependent failure. As the shale exposure to drilling fluid time mitigate, the result will be insufficient time for the shale-drilling fluid chemical reactions as well as the creeping effect. The drilling parameters optimization revealed a considerable enhancement in the drilling performance but the bit design variables are slightly improved the ROP. Hence, the appropriate selection of the drilling fluid density/parameters can reduce the shale instabilities and exposure time that might be the best treatment.

The tripping data modification can also mitigate the drilling fluid density reduction while tripping out of the hole. The drill collar diameters and the high flow rate are the

dominate effected in drilling fluid reduction. Therefore, the empirically derived swabbing model combine with the tripping suggested variables contribute to noticeable improvement regarding the drilling practice and subsequently wellbore support.

11. CONCLUSIONS

This research presents a case study of severe wellbore instabilities in a shale formation in southern Iraq fields by instigation of drilling and geomechanical parameters. It has been demonstrated that the problem mostly is related to the shear failure of the wellbore. As a result, the appropriate drilling fluid selection with respect to well inclination and azimuth can likely be more helpful to solve this problem. In addition, it has concluded that the wells drilled in the direction of minimum horizontal stress are more prone to be stable to the same deviated angle. Hence, the well trajectory should be designed to avoid the maximum horizontal stress direction, or the drilling fluid density should be high enough to keep the mechanical stability of wellbore. The chemical and thermal sources of stresses have minor contributions in the stress perturbation in this research. The anisotropic nature of the rock strength/stress parameters should be considered in the drilling fluid density calculation. Also, the drilling practice should be well-optimized to avoid the shale instability deteriorations.

In this investigation, if the shale exposure time is extended, the wellbore instability issues may potentially evolve. Therefore, the ROP-related drilling parameters were optimized not only to improve the drilling performance but also to prevent the shale from being affected by the harsh ambient drilling. In brief, the drilling fluid and parameters should be optimized to reduce the shale exposure time and to prevent the destructive effect of the drilling environments.

The tripping and filling procedure are harshly affected by the borehole pressure and eventually the well integrity status. The analysis has revealed the large diameters of the BHA component and the high flow rate are magnificent during the tripping processes. Thus, the suitable BHA profile and the tripping data have to be chosen properly to reduce the likelihood of the drilling fluid weight alterations by the swabbing effect. Statistically derived swabbing model from stuck-free well was helpful in mitigate the drilling fluid reduction by tripping operations. Finally, the analysis revealed, the extensive reaming and back reaming while drilling Tanuma with unsuitable drilling hydraulic parameters leads to many stability issues.

12. RECOMMENDATIONS

The model analysis and the drilling data the following points should be evaluated and considered to mitigate the well instabilities in the production section in southern Iraq:

1. The drilling fluid density should be change with respect to well trajectory design and the well direction from maximum horizontal stress orientation.
2. The drilling fluid properties should be selected to eliminate the probability of the Shale-Fluid interaction tendency.
3. The stuck pipe prediction while drilling should be implemented in which the comparison between the drilling measurements in the surface sensors with drilling measurement downhole equipment by real-time analysis are required.
4. The dynamic drilling fluid properties and static bottom hole pressure needs to be optimized with drilling operational environment to maintain the wellbore wall integrity.
5. Pressure management while drilling or continuous circulation technique can be helpful in reducing the borehole pressure-related instabilities.
6. The lessons learned from offset wells problems need to be investigated in order to update the current drilling producer and design factors.
7. The shale exposure time should be reduced depending on the drilling optimization as much as possible.

APPENDIX

1. Minimum horizontal stress

(Fairhurst, 1967) suggested Equation A.1 to calculated Sh based on hydraulic fracturing treatment data. (Blant & Olson, 1999) developed another imperial Equation A.2 which related the elastic rock properties (Young modulus and Poisson ratio) and the rock thermal expansion effect to quantify the minimum horizontal stress as shown in Equation A.3. (Fjaer et al., 2008).

$$\mathrm{Sh} = \frac{3\mathrm{EW_{MAX}}}{4(1+\mathrm{v})\mathrm{L}}\left(2(1-\mathrm{v}) - \alpha(1-2\mathrm{v})\right)^{-1} - \mathrm{p_p} \tag{A.1}$$

$$S_h = \frac{vS_v + (1-2v)\alpha P + E\alpha_T \delta T}{1-v} + \frac{vE}{1-v} \times E_{tec} \tag{A.2}$$

$$\mathrm{Sh} = \left(\frac{\mathrm{v}}{1-\mathrm{v}}\right) \times (\mathrm{Sv} - \mathrm{Pp}) + \mathrm{P} + \left(\frac{\mathrm{E_S}}{1-v^2}(E_X + v \times E_Y)\right) \tag{A.3}$$

2. Maximum Horizontal Stress

Equation A.4 proposed by Fairhurst (1967) to estimated SH when hydraulic fracturing data available. The rock elastic parameters, as well as tectonic strain, was combined to estimate SH by Equation A.5 (Fajear et al., 2008).

$$\mathrm{SH} = \mathrm{P_c}\left(2 - \frac{\alpha(1-2\mathrm{v})}{1-\mathrm{v}}\right)\mathrm{T_o} + 3Sh \tag{A.4}$$

$$\mathrm{SH} = \left(\frac{\mathrm{v}}{1-\mathrm{v}}\right) \times (\mathrm{Sv} - \mathrm{Pp}) + \mathrm{P} + \left(\frac{\mathrm{E_S}}{1-v^2}\left(E_y + v \times E_x\right)\right) \tag{A.5}$$

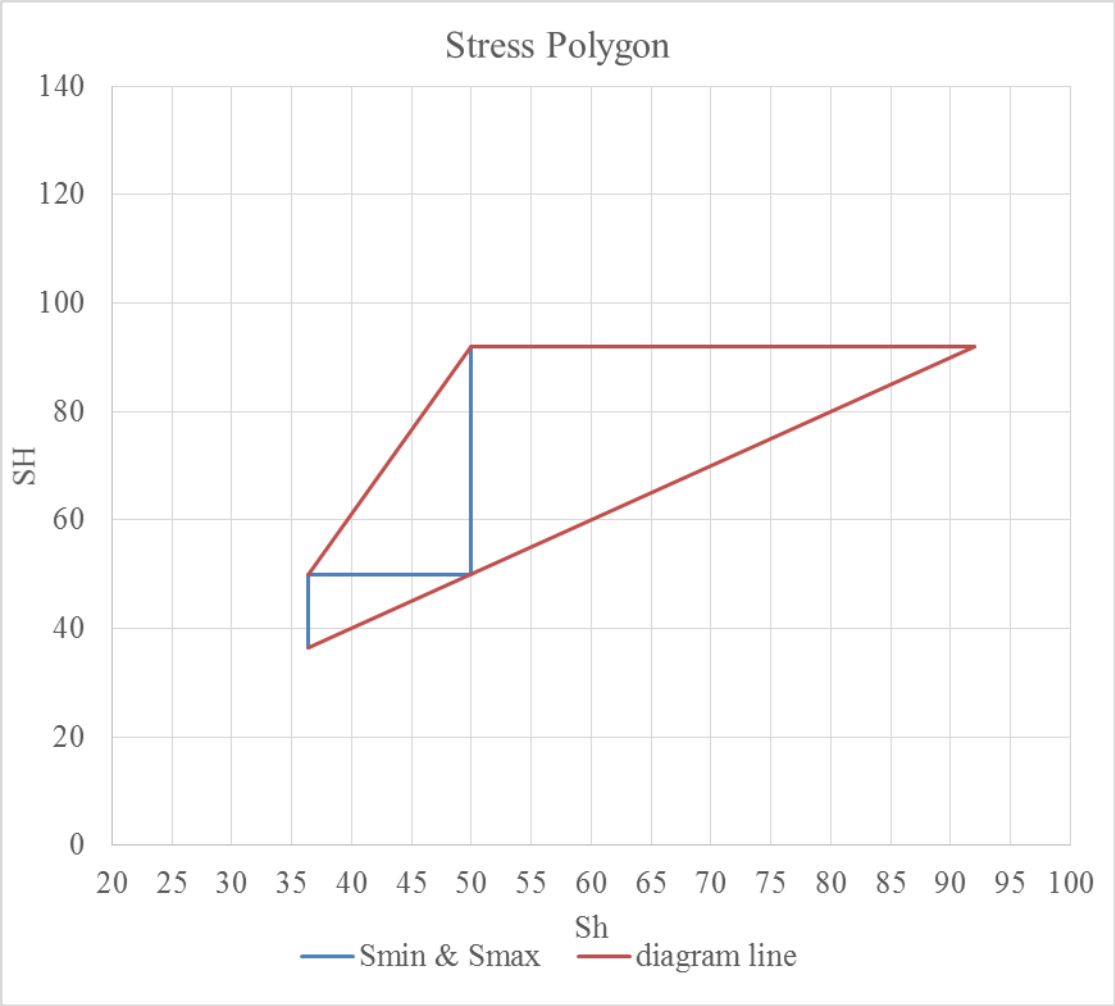

Figure.A.1 1. Stress Polygon for a field in southern Iraq

3. TYPES OF SHEAR AND TENSILE FAILURE

There are different types of shear and tensile failures associated with the wellbore failure if the drilling fluid weight is not properly selected to support the wellbore, or the principle stress contrast around the wellbore is too high (Tan et al., 1998; Guizhong et al., 2003). The divisions of the shear failure have been shown in Figure.A.1 2.Shear failure shapes. As can be seen, the breakout occurs when the hoop stress is the greatest stress around the wellbore while the radial stress is the smallest. The Toric shear poses when the axial stress is the greatest and the radial stress is the smallest. Furthermore, helical shear

failure is experienced if the axial stress is greatest but the hoop stress is the smallest. Finally, Elongated shear provokes if the radial stress is the greatest and the hoop stress is the smallest. Apart from shear failure, tensile failure has two unique types Hydraulic or drilling induce tensile failure as illustrate in Figure.A.1 3. This failure occurs when effective hoop stress is greater than radial stress and tensile strength of the rock (Chen et al., 1998). However, tensile exfoliation happens when the effective radial stress is greater than the hoop stress and tensile strength of the rock.

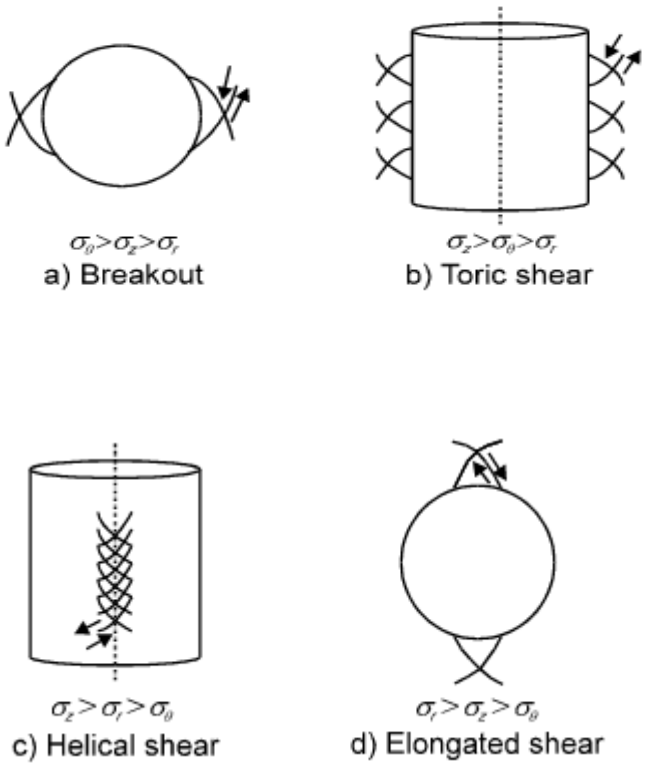

Figure.A.1 2.Shear failure shapes

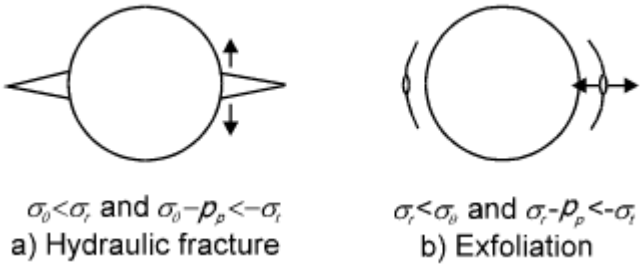

Figure.A.1 3.Tensile failure shapes

4. DRILL-OF TEST

The main function of the drill-off test is to understand the relationship between WOB and ROP under constant drilling conditions of the RPM and the fluid pressure. The driller applies pre-plan maximum WOB then the rig brake is locked down, and the WOB vs. ROP chart is recorded and monitored in the different time interval. The WOB changes base on the drill string elongations in given period, therefore, the ROP can be obtained with the corresponding WOB increment (Bourdon et al., 1989). The drill-off test is performed periodically in oil industry especially if new types of bit/formation being used or a sharp decline in ROP has recorded in a particular interval.

The threshold and flounder points are determined from the drill-off chart that defines as the minimum, and maximum applied WOB can be used to optimize the ROP, respectively. In other words, the threshold is minimum load applied to onset ROP, while the flounder point is the maximum load beyond which the exceeded in WOB do not lead to proportionally increased in the ROP (Robinson & Ramsey, 2001). These points can be used to enhance the bit performance and reduce the bit wearing if the operation condition allowed to be within their range. Also, bit balling might be avoided to some extended if the bit operated in the drill of test limitation (threshold and flounder) as well as bit vibrations.

5. MECHANICAL SPECIFIC ENERGY

The mechanical specific energy was brought to the surface by (Teale, 1965), when he proved the maximum energy required to remove a certain amount of rock was constant regardless of the drilling parameters alterations (i.e. WOB, RPM, and ROP). This concept has been employed to modify the drilling variables in order to optimize the ROP and the drilling cost. (Dupriest & Koederitz, 2005) Investigated the improvement in the drilling efficiency when real-time MSE log is monitoring. Their work allowed to diagnostic the drilling problems that evolve due insufficient energy manipulation while drilling. After that (Armenta, 2008) enlightened the drilling specific energy (DSE) by including the bit hydraulic to MSE equation. The DSE can also use to find out the abnormal drilling condition and give an improvement to MSE prediction under various operation conditions. He concluded the horsepower per square inch (HSI) had a significant contribution to

enhancing the ROP performance. It is well-recognized the lower value of MSE indicate a higher drilling efficiency, therefore, it widely uses to quantify the drilling performance. The mathematical expression of the MSE and DSE are shown in Equations A.6 and A.7 respectively.

The MSE magnitude serves as a powerful tool in prediction the confidentiality of the operational parameters while drilling. The high MSE with low ROP might be potentially due to improperly applied WOB that leads to smaller cutter-rocks embedment; consequently, a considerable amount of energy dissipated because of rock fragments re-grinded, bit wear accelerated, string vibration and high friction evolved. In other side, the suitable WOB can result in higher cutter depth penetration that produces fracturing and breaking rock mechanisms. This action contributes to increasing the ROP and reduces MSE since the input energy is mainly invested in drilling activity nor friction and cutting re-drilling. It worth to state, the bit consumes only 30-40% of the theoretically calculated input data in drilling processes (Pessier & Fear, 1992).

$$\text{MSE} = \frac{WOB}{A_B} + \frac{120 \times \pi \times RPM \times T}{A_B \times ROP} \tag{A.6}$$

$$\text{DSE} = \frac{WOB}{A_B} + \frac{120 \times \pi \times RPM \times T}{A_B \times ROP} - \frac{1980000 \times \lambda \times HP_B}{A_B \times ROP} \tag{A.7}$$

6. ROLLER-CONE BIT

The ROP model for a roller-cone bit was developed by (Warren, 1987) and it was modified by (Hareland & Hoberock, 1993). This model considers several significant effect on ROP such as; rock fragment generation and removal, CHDE, and a bit wearing. The mathematical model of modified roller cone bit is illustrated in Equation A.8. The first term in the equation refers to the rate of the rock destroyed into chips; the second term is accounted for the WOB distribution on the teeth; the third is considered the rock fragment

is removing by the hydraulic design. Other than crushing and scraping in roller cone bit, the failure mechanism in drag bit is shearing processes.

$$\mathrm{ROP} = \mathrm{W_F}\left(f_c(p_e)\left(\frac{a\,D_B^3 S^2}{RPM \times WOB^2} + \frac{b}{RPM \times D_B}\right) + \frac{c \times \rho \times u \times D_B}{I_m}\right)^{-1} \quad \text{(A.8)}$$

7. LIMESTONE MULTI-REGRESSION DATA

The limestone interval ROP model data illustrated in Figure.A.1 4Figure.A.1 5Figure.A.1 6Figure.A.1 7. The sensitivity and statistical data shown in Table A.1 1, and A.1 2.

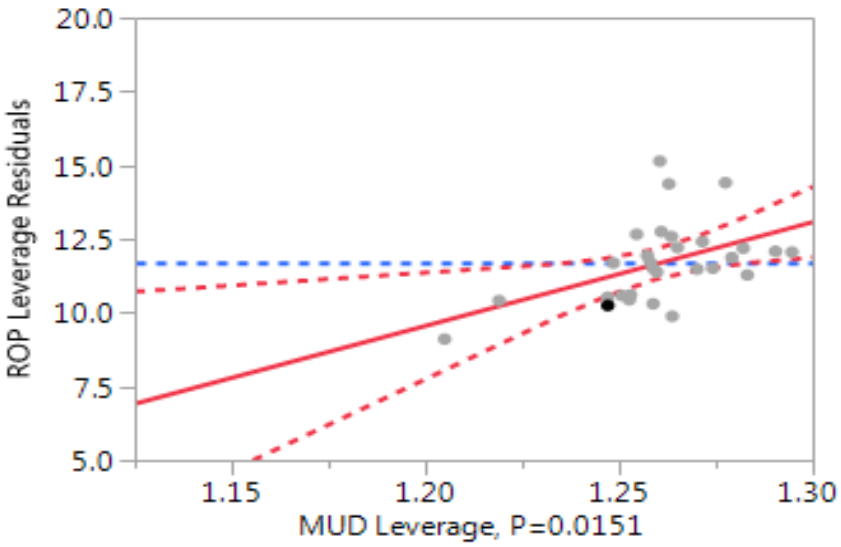

Figure.A.1 4. The weight on bit effect on the ROP of the field data

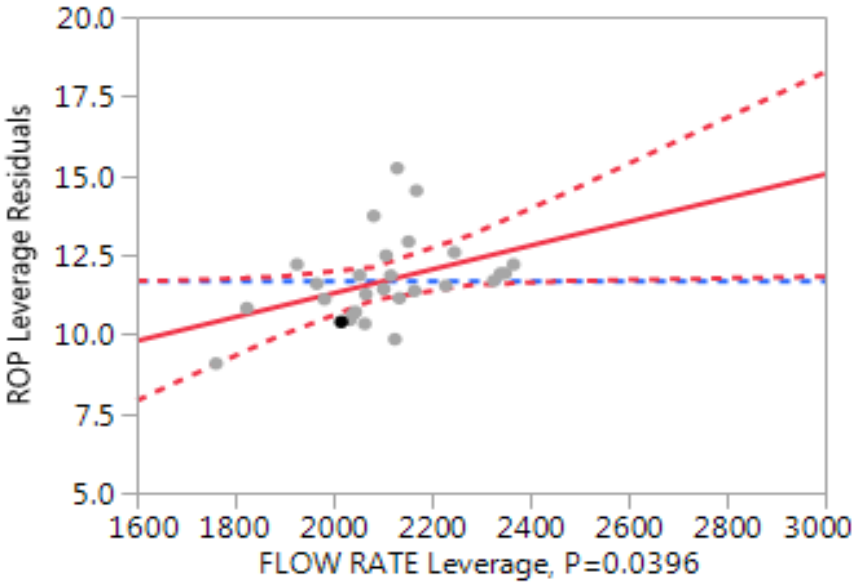

Figure.A.1 5. The flow rate effects on the ROP

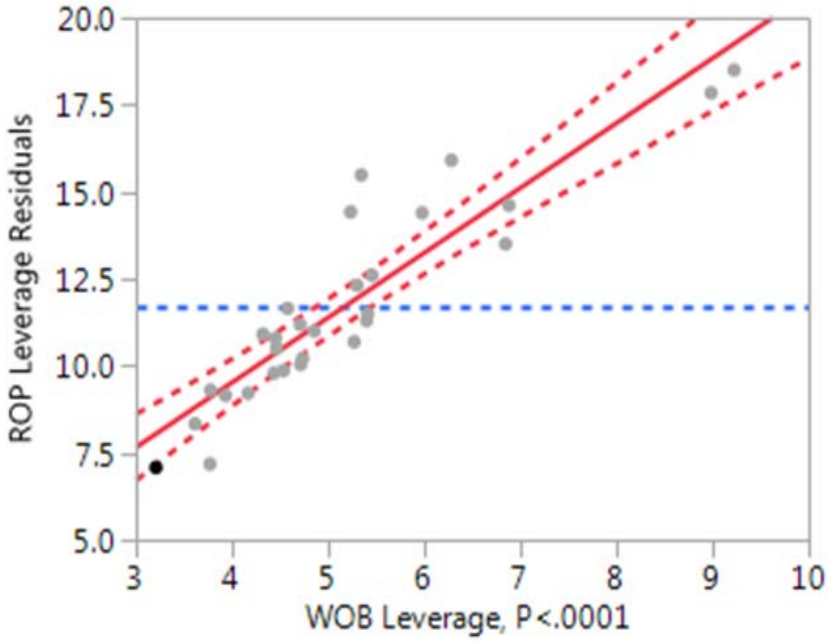

Figure.A.1 6. The effects of the WOB on The ROP

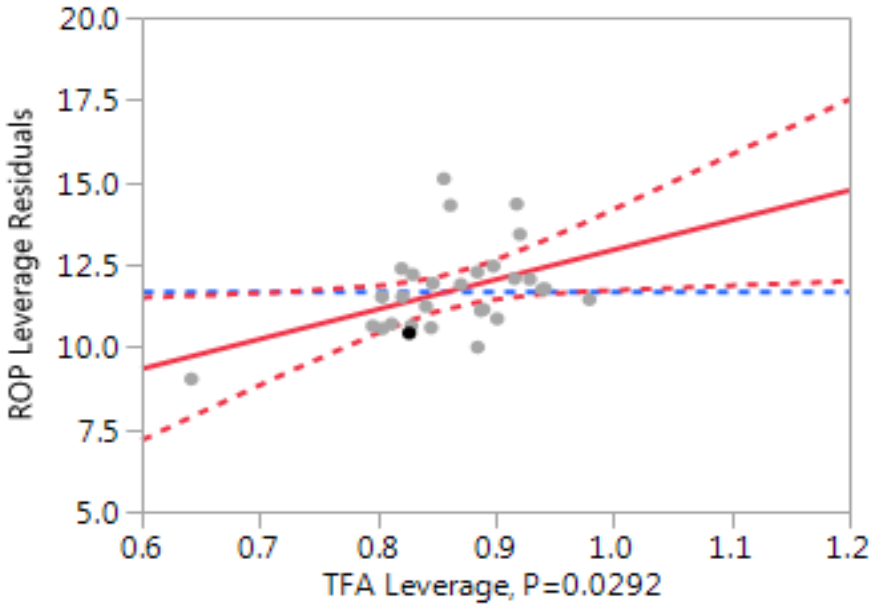

Figure.A.1 7. The total flow area effects on the ROP

Table A.1. 1Model sensitivity variables

Source	LogWorth	PValue
WOB	9.523	0.00000
MUD	1.822	0.01508
TFA	1.535	0.02916
FLOW RATE	1.403	0.03955
rpm	1.244	0.05696

Table A.1 2. Model statistical variables

Parameters	Value
RSquare	0.90608
RSquare Adj	0.885663
Root Mean Square Error	1.319109
Mean of Response	11.70172
Observations (or Sum Wgts)	29

REFERENCES

Aadnoy, B., & Hansen, A. (2005). Bounds on In-Situ Stress Magnitudes Improve Wellbore Stability Analyses. SPE Journal, 10(2), 2–4. http://doi.org/10.2118/87223-PA.

Aadnoy, B. S., & Chenevert, M. E. (1987). Stability of Highly Inclined Boreholes (includes associated papers 18596 and 18736). SPE Drilling Engineering, 2(4). http://doi.org/10.2118/16052-PA.

Al-Ajmi, A., & Zimmerman, R. (2006). Stability analysis of deviated boreholes using the Mogi-Coulomb failure criterion, with applications to some oil and gas reservoirs. Proceedings of the IADC/SPE Asia Pacific Drilling.

Al-Ameri, T.K., A.J Al-Khafaji, J. Zumberge, 2009, Petroleum system analysis of the Mishrif reservoir in the Ratawi, Zubair, north and south Rumaila oil fields, southern Iraq: GeoArabia, Gulf PetroLink, Bahrain, v. 14, no. 4.

Al-Bayatee, k., Al-Mutury, W., Al-Muhammad,R., (2010). Tectonostratigraphy of Lower Cretaceous in Southern Iraq. Iraqi National Journal of Earth Sciences.Res.10:29-44.

Al-Bazali, T. M., Al-Mudh'hi, S., & Chenevert, M. E. (2009). An Experimental Investigation of the Impact of Diffusion Osmosis and Chemical Osmosis on the Stability of Shales. Petroleum Science and Technology, 29(January 2015), 312–323. http://doi.org/10.1080/10916460903393989.

Alberty, M. W., Mclean, M. R., & Exploration, B. P. (2004). SPE 90493 A Physical Model for Stress Cages.

Almutury, W.Gh. and Al Asadi M., 2008 . Tectonic history of Mesopotamian passive Margin during Mesozoic. And Cenozoic, South Iraq. Journal of Kirkuk University - Scientific Studies,Res.03:31-49.

Al-Marsoumi and Abdul Wahab 2005.Hydrogeochemistry of Yamama Reservoir Formation Water-West Qurna oil Field-southern Iraq. Basrah Journal of Science.Res.23:10-20.

Al-Qahtani and Haq B.U., 2005, Phanerozoic cycles of sea-level change on the Arabian Platform: GeoArabia, v. 10/2, p. 127-160.

Alsharhan, A. S, &Nairn, A. E. M., (1997). Sedimentary Basins and Petroleum Geology of the Middle East. Elsevier Science.

Amin, F, and Al-Bahadily, A, 2014, Gravity and Magnatic Surveys to Delineate Subsurface Strctures In HOR-ALHiwazah Area, south Iraq. Iraqi Bulletin of Geology and mine.Res.10:59-85.

Anderson, E. M. (1951). The Dynamics of Faulting and Dyke Formation with Applications to Britain. Edinburgh, Oliver and Boyd.

Aquitaine. Maury. Sauzay.Elf. (1987). Borehole Instability: Case Histories, Rock Mechanics Approach, and Results.

Araujo, E., Pastor, J., & Fontoura, S. (2006). Incorporating Thermochemoporoelastic Effects in Wellbore Stability Design in Shales.

Armenta, M., Ept-wt, S., Rop, A. B., Wob, D. B., & Rop, D. B. (2008). SPE 116667 Identifying Inefficient Drilling Conditions Using Drilling-Specific Energy, (September), 21–24.

Asef, M., & Farrokhrouz, M. (2013). Shale Engineering: Mechanics and Mechanisms. Taylor & Francis.

Asuelimen, L. O., & Adetona, O. O. (2014). Stability Analysis in Shale using the Mohr Coulomb Failure Criterion, 4(4), 196–205.

Azar, J. J., & Samuel, G. R. (2007). Drilling Engineering. PennWell Corporation.

Azian, I., Azree, N., Waguih, A., Rojas, F., Fey, S., Subroto, B., … Conference, U. O. (2013). Integrating FPWD Measurements With Managed-Pressure Drilling, (April), 120–123.

Bailey, Louise,Tim Jones,Belaskie,Jim,Sheppard,Mike,Houwen, O. (1991). causes,Detection and prevention. SLP.

Barton, C. A., Zoback, M. D., & Burns, K. L. (1988). In-situ stress orientation and magnitude at the Fenton Geothermal Site, New Mexico, determined from wellbore breakouts. Geophysical Research Letters, 15(5), 467–470. http://doi.org/10.1029/GL015i005p00467.

Bell, J. S. (2003). Practical methods for estimating in situ stresses for borehole stability applications in sedimentary basins. Journal of Petroleum Science and Engineering, 38(3), 111-119.

Bible, M. J., Hedayati, Z., & Choo, D. K. (1991, January 1). State-of-the-Art Trip Monitor. Society of Petroleum Engineers. doi:10.2118/21965-MS.

Blanco, Y., & Turner, M. (2011). Application & Evolution of Formation Pressure While Drilling Technology (FPWD) Applied To The Gulf of Mexico. Proceedings of SPE Annual Technical Conference and Exhibition. http://doi.org/10.2118/147556-MS.

Blanton, T. L., & Teufel, L. W. (1985, January 1). In-Situ Stress Determination From Wellbore Elongation Measurements. Society of Petroleum Engineers. doi:10.2118/13877-MS.

Bourdon, J., Cooper, G. A., Curry, D. A., Mccann, D., & Peltier, B. (1989). Comparison of Field and Laboratory-Simulated Drill-Off Tests, (December), 329–334.

Bourgoyne & Young. (1974). A Multiple Regression Approach to Optimal Drilling and Abnormal Pressure Detection, 4.

Bourgoyne, A. T. (1986). Applied Drilling Engineering. Society of Petroleum Engineers. Retrieved from https://books.google.com/books?id=7VlQAQAAIAAJ.

Bradley,W. B. (1979). “Failure of Inclined Boreholes.” J. Energy Res. Tech., Trans. ASME, 102, 232.

Breckels, I. M., & van Eekelen, H. a. M. (1982). Relationship Between Horizontal Stress and Depth in Sedimentary Basins. Journal of Petroleum Technology, 34(September), 2191–2199. http://doi.org/10.2118/10336-PA.

Burnett, T., Freeman, J., Jones, D., Paske, W., & Zannoni, S. (1993). DENSITY MEASUREMENT WHILE DRILLING.

Castagna, J. P. (1985). Relationships between compressional-wave and shear-wave velocities in clastic silicate rocks. Geophysics, 50(4), 571. http://doi.org/10.1190/1.1441933.

Chang, C., Zoback, M. D., & Khaksar, A. (2006). Empirical relations between rock strength and physical properties in sedimentary rocks. Journal of Petroleum Science and Engineering, 51(3-4), 223–237. http://doi.org/10.1016/j.petrol.2006.01.003.

Chen M., Chenevert M.E., S. M. M. (2001). Chemical and Thermal effect on wellbore stability of shale formations. Society of Petroleum Engineers, (February), 2002.

Chen X., Tan, C. P., & Haberfield, C. M. (1998). A Comprehensive Practical Approach For Wellbore Instability Management, (December). http://doi.org/10.2118/48898-MS.

Chen, G., Chenevert, M. ., & Sharma, M. M. (2001). Poroelastic chemical, and thermal effects on wellbore stability in shales. The University of Texas at Austin.

Chen, G., Chenevert, M. E., Sharma, M. M., & Yu, M. (2003). A study of wellbore stability in shales including poroelastic, chemical, and thermal effects. Journal of Petroleum Science and Engineering, 38(3-4), 167–176. http://doi.org/10.1016/S0920-4105(03)00030-5.

Chen, X., Tan, C. P., Petroleum, C., & Haberfield, C. M. (2002). A Comprehensive , Practical Approach For Wellbore Instability Management, (December).

Chenevert, M., & Pernot, V. (1998). Control of Shale Swelling Pressures Using Inhibitive Water-Base Muds. Proceedings of SPE Annual Technical Conference and Exhibition, 793–803. http://doi.org/10.2523/49263-MS.

Chenevert, M.E., and Strassner, J.E. (1975): “Temperature Effects on Water Activities of Argillaceous Shale and Oil Mud Systems” fifteenth Oil and Gas Conference, Balatonfured, Hungary, September 14-19 Cunningham, L. W. (2012). Working Out of a Tight Spot, 16–23.

Devereux. (2015). Devereux, Steve. Drilling Technology in Nontechnical Language (2nd Edition). Tulsa, OK, USA: PennWell, 2012. ProQuest ebrary. Web. 28 December 2015. Copyright © 2012. PennWell. All rights reserved., (December).

Duffadar, R. D., Upstream, E., & Dupriest, F. E. (2013). SPE / IADC 163481 Practical Guide to Lost Returns Treatment Selection Based on a Holistic Model of the State of the Near Wellbore Stresses.

Dupriest, F. E., Koederitz, W. L., Totco, M. D., & Company, V. (2005). SPE / IADC 92194 Maximizing Drill Rates with Real-Time Surveillance of Mechanical Specific Energy.

Eaton, B. A. (1969). Fracture Gradient Prediction and Its Application in Oilfield Operations. Journal of Petroleum Technology, 21(10), 1353–1360. http://doi.org/10.2118/2163-PA.

Elahifar, B., Esmaeili, A., Fruhwirth, R. K., & Data, T. D. E. T. (2012). Determining the Accuracy of Ultrasonic Caliper Measurements for Real Time Drilling Application.

Escobar, R. G., & Santander. (2014). New Approach For Estimating Cavings Volume To Avoid Wellbore Instabilities.

Fairhurst, H. and. (1967). Initiation and Extension of Hydraulic Fractures in Rocks. Society of Petroleum Engineers.

Fakcharoenphol, P., Hu, L., & Wu, Y. S. (2012, January). Fully-implicit flow and geomechanics model: application for enhanced geothermal reservoir simulations. In Proceedings of 37th Workshop on Geothermal Reservoir Engineering, Stanford.

Fjaer. (2008). Petroleum Related Rock Mechanics. Marine Environmental Research (2nd ed.). http://doi.org/10.1016/0148-9062(93)92632-Z.

Fjar, E., Holt, R. M., Raaen, A. M., Risnes, R., & Horsrud, P. (2008a). Petroleum Related Rock Mechanics: 2nd Edition. Elsevier Science.

Fjar, E., Holt, R. M., Raaen, A. M., Risnes, R., & Horsrud, P. (2008b). Petroleum Related Rock Mechanics: 2nd Edition. Elsevier Science.

Freij-Ayoub, R., Tan, C. P., & Choi, S. K. (2003). SPE/IADC 85344 Simulation of Time-Dependent Wellbore Stability in Shales Using A Coupled Mechanical-Thermal-Physico-Chemical Model. SPE/IADC Middle East Drilling Technology Conference & Exhibition.

Freitas, D. (2009). Borehole Failure Related to Bedding Plane. Rock Mechanics.

Fuh, G., Morita, N., Boyd, P. A., & Mcgoffin, S. J. (1992). A New Approach to Preventing Lost Circulation While Drilling.

Fung, L. S. K., Wan, R. G., Rodriguez, H., Silva Bellorin, R., & Zerpa, L. (1999, December 1). An Advanced Elasto-plastic Model For Borehole Stability Analysis of Horizontal Wells In Unconsolidated Formation. Petroleum Society of Canada. doi:10.2118/99-12-01.

Kadyrov, T., & Tutuncu, A. N. (2012, November 4). Influence of Anisotropic Stress and Formation Property Use in Wellbore Stability Analysis and Field Development Plans: A Case Study for West Kazakhstan Field. Society of Exploration Geophysicists.

Karsakov, V. A. (2014, October 14). Decision for Optimum Number of Well Pads During Phase of Field Development Design. Society of Petroleum Engineers. doi:10.2118/171299-MS.

Kelly, T. E. 1968. Ground-water basic data, Grand Forks County, North Dakota. North Dakota Geological Survey Bulletin, Issue 53, Part II, Bismarck.

Gala, D. M., York, P., International, W., Pritchard, D., Energy, S., & Utama, B. (2010). SPE 129030 Drilling Hazard Mitigation Technologies Key in Eliminating Non-Productive Time in Challenging Wells. Complexity.

Ghalib, H. A. and Alsinawi, S.A., (1974). On The Seismotectonics Of The Arabian Peninsula- A Global Tectonic Approach. Bull. Coll. Sci. Vol. 15, pp151-169.

Gholami, R., Moradzadeh, A., Rasouli, V., & Hanachi, J. (2014). Practical application of failure criteria in determining safe mud weight windows in drilling operations. Journal of Rock Mechanics and Geotechnical Engineering, 6(1), 13–25. http://doi.org/10.1016/j.jrmge.2013.11.002.

Hale, A.H. and Mody, F.K. 1992. Experimental Investigation of the Influence of Chemical Potential on Wellbore Stability. Presented at the SPE/IADC Drilling Conference in New Orleans. Louisiana: IADC/SPE Paper 23885.

Hale, A. H., Mody, F. K., & Salisbury, D. P. (1993). The influence of chemical potential on wellbore stability. SPE Drilling & Completion, 8(3), 207–216. Retrieved from http://www.onepetro.org/mslib/servlet/onepetropreview?id=00023885

Hareland, G, W. YAN, R. NYGAARD, J. L. W., & J. L. WISE. (2007). Cutting Efficiency of a Single PDC Cutter on Hard Rock, 1–11.

Hareland, G. (2007). Cutting Efficiency of a Single PDC Cutter on, 1–11.

Hareland, G., & Nygaard, R. (n.d.). Calculating unconfined rock strength from drilling data.

Hareland, G., & Rampersad, P. R. (1994). Drag - Bit Model Including Wear, 657–667.

Horsrud, P. (2001). Estimating Mechanical Properties of Shale From Empirical Correlations. SPE Drilling & Completion, 16(02), 68–73. http://doi.org/10.2118/56017-PA

Holbrook, P.W., Maggiori, D. A. et al. (1993). Real-time pore pressure and fracture gradient evaluation in all sedimentary lithologies, SPE 26791.Offshore European Conference, Aberdeen, Scotland, Society of Petroleum Engineers.

Hubbert, M., & Willis, D. (1972). Mechanics of hydraulic fracturing. Underground Waste Management and Environmental Implications, 210, 239–257. http://doi.org/10.1016/S0376-7361(07)53011-6.

Jassim, S. Z., & Goff, J. C. (2006). Geology of Iraq. Printing, Mosul, Iraq.

Falconer,J.P. Belaskie, F. Variava. (1989). Applications of a Real Time Wellbore Friction Analysis. SPE/IADC Drilling Conference.

J.J. Orban, M.S. Dennison, . Jorion, and J.e. Mayes. (1991). New Ultrasonic Caliper for MWD Operations. SPE/IADC Drilling Conference.

John Jaeger, N. G. Cook, R. Z. (2007). Fundamentals of Rock Mechanics. http://doi.org/10.1007/s13398-014-0173-7.2.

Jasim, N,2010. SEISMICITY EVALUATION OF CENTRAL AND SOUTHERN IRAQ.M.SC.Thesis,University of Baghdad, published in Web; http://www.iasj.net/.

Jr, J. C. (1984). Wellbore stability. Journal of Petroleum Technology, (June), 889–896. http://doi.org/10.2118/13340-PA.

Kadyrov, T. (2013). Integrated Wellbore Stability Analysis for Well Trajectory.

Lacy, L. L. (1997). Dynamic Rock Mechanics Testing for Optimized Fracture Designs. SPE Annual Technical Conference and Exhibition. http://doi.org/10.2118/38716-MS

Lal, M., & Amoco, B. P. (1999). SPE 54356 Shale Stability : Drilling Fluid Interaction and Shale Strength.

Last, N., & McLean, M. (1996). Assessing the impact of trajectory on wells drilled in an overthrust region. Journal of Petroleum Technology, (July), 620–626. http://doi.org/10.2118/30465-MS.

Lee, D., Bratton, T., & Birchwood, R. (2004). Leak-Off Test Interpretation And Modeling With Application To Geomechanics. Gulf Rocks 2004 the 6th North.

Li, S., George, J., & Purdy, C. (2012). Pore-Pressure and Wellbore-Stability Prediction To Increase Drilling Efficiency. Journal of Petroleum Technology, 64(2), 98–101. http://doi.org/10.2118/144717-MS

Ljunggren, C., Chang, Y., Janson, T., & Christiansson, R. (2003). An overview of rock stress measurement methods. International Journal of Rock Mechanics and Mining Sciences, 40(7-8), 975–989. http://doi.org/10.1016/j.ijrmms.2003.07.003.

Matthews,W. R. and Kelly, J. (1967). “How to predict formation pressure and fracture gradient.” Oil and Gas Journal, February, 92–106.

Maury V., & Guenot, A. (1995). Practical Advantages Of Mud Cooling Systems For Drilling, (March), 42–48.

McLamore, Roy T., 1966, Strength-Deformation Characteristics of Anisotropic Sedimentary Rocks. Ph.D. thesis,Unversity of Taxas,Austin

McLellan, P. J., & Cormier, K. (2013). Borehole Instability in Fissile, Dipping Shales, Northeastern British Columbia. SPE Gas Technology Symposium. http://doi.org/10.2118/35634-MS.

Meng, F., Fuh, G., & Company, C. P. (2013). IPTC 16567 Wellbore Stability Evaluation Guideline For Reducing Non-Productive Time, (March), 26–28.

Mitchell, R. F. (1988). Dynamic Surge/Swab Pressure Predictions, (September), 325–333.

Mkpoikana, R., Dosunmu, A., Eme, C., & Harcourt, P. (2015). Prevention of Shale Instability by Optimizing Drilling Fluid Performance, (August), 4–6.

Mody, F. K., & Hale, A. H. (1993). Borehole-Stability Model to Couple the Mechanics and Chemistry of Drilling-Fluid Shale Interactions. Journal of Petroleum Technology, 45(11), 1093–1101. http://doi.org/10.2118/25728-PA.

Monitor, S. T., Bible, M. J., Hedayati, Z., Choo, D. K., & Schlumberger, A. (1991). State-of-the-Art Trip Monitor.

Montgomery, D. C. (2013). Applied Statistics and Probability for Engineers, 6th Edition: John Wiley & Sons.

Nguyen, D. A., Miska, S. Z., Yu, M., & Saasen, A. (2010, January 1). Modeling Thermal Effects on Wellbore Stability. Society of Petroleum Engineers. doi:10.2118/133428-MS.

Nygaard, R., & Hareland, G. (2007, January 1). How to select PDC bit for optimal drilling performance. Society of Petroleum Engineers. doi:10.2118/107530-MS.

Nygaard, R., Hareland, G., D., Budiningsih, Y., Terjesen, H. E., and Stene, F. (2002). Eight Years Experience with a Drilling Optimization Simulator in the North Sea. presented at SPE/IADC Aaian Conference, Jakarta, Indonesia, 9-11 September. SPE-77247.

Nygård, R., & Clay, K. B. (2002). Undrained Shear Behaviour of Some UK Mudrocks Explained by Petrology TABLE 1 : Index properties of Kimmeridge Westbury, 41(12), 37–46.

Numan, N.M.S., 1997. (A Plate Tectonic Scenario for the Phanerozoic Succession in Iraq). Jour.Geol.Soc.Iraq, Vol.30, PP.85-110.

Numan, N.M.S.,(2000): Major Cretaceous Tectonic Events in Iraq. Raf.Jour.Sci., Vol.11, pp.32-52 .

Ogoke, V., Schauerte, L., Bouchard, G., & Inglehart, S. c. (2014, October 27). Simultaneous Operations in Multi-Well Pad: a Cost Effective way of Drilling Multi Wells Pad and Deliver 8 Fracs a Day. Society of Petroleum Engineers. doi:10.2118/170744-MS.

Økland, D., & Cook, J. M. (1998). Bedding-Related Borehole Instability in High-Angle Wells. Proceedings of SPE/ISRM Rock Mechanics in Petroleum Engineering, 10. http://doi.org/10.2118/47285-MS

Pašić, B., Gaurina-međimurec, N., & Matanović, D. (2007). Wellbore Instability : Causes and Consequences Nestabilnost Kanala Bušotine : Uzroci I Posljedice, 19.

Pessier, R. C., & Fear, M. J. (1992). Quantifying Common Drilling Problems With Mechanical Specific Energy and a Bit-Specific Coefficient of Sliding Friction. SPE Annual Technical Conference and Exhibition, (SPE 24584), 373–388. http://doi.org/10.2118/24584-MS

Pritchard, D. (2011). Mitigating Drilling Hazards with Technologies (Part 3 of DHM Series) Table of Contents, (January).

Pritchard, D. M. (2011). Drilling Hazards Management – Excellence in Drilling Performance Begins with Planning (Part 1 of DHM Series) Table of Contents, (January).

Rabia, H. (2010). Well Engineering & Construction, 248.

Rahimi, R., & Nygaard, R. (2014). What Difference Does Selection of Failure Criteria Make in Wellbore Stability Analysis? 48th U.S. Rock Mechanics/Geomechanics Symposium. Retrieved from https://www.onepetro.org/conference-paper/ARMA-2014-7146

Rashidi, B., Hareland, G., & Nygaard, R. (2008). SPE 117109 Real-Time Drill Bit Wear Prediction by Combining Rock Energy and Drilling Strength Concepts.

Rastegar, M., Directorate, N. E., Hareland, G., & Nygaard, R. (n.d.). Optimization of Multiple Bit Runs Based on ROP Models and Cost Equation : A New Methodology Applied for One of the Persian Gulf Carbonate Fields.

Robinson, L. H., & Ramsey, M. S. (2001). Are You Drilling Optimized or Spinning Your Wheels? AADE 2001 National Drilling Conference, "Drilling Technology - The Next 100 Years'', (AADE 01-NC-HO-31), 1–11.

Rosenberg, S. M., & Gala, D. M. (2011). SPE 146158 Liner Drilling Technology as a Tool to Reduce NPT - Gulf of Mexico Experiences, (November).

Salehi, S., & Nygaard, R. (2012). SPE 135155 Numerical Modeling of Induced Fracture Propagation : A Novel Approach for Lost Circulation Materials (LCM) Design in Borehole Strengthening Applications of Deep Offshore Drilling, (Lcm), 1–12.

Shaw, D. B., & Weaver, C. E. (1965). The mineralogical composition of shales, 35(1), 213–222.

Shamsuzzoha, M. (2015). INFLUENCING FACTORS OF BOREHOLE FAILURE IN BEDDING PLANE OF A RESERVOIR. Journal of Mechanical Engineering, 45(1), 41-47.

Sharland, P.R., R. Archer, D.M. Casey, R.B. Davies, S.H. Hall, A.P. Heward, A.D. Horbury and M.D. Simmons 2001. Arabian Plate sequence stratigraphy. GeoArabia Special Publication 2, Gulf PetroLink, Bahrain, P 371.

Streit, J. E., & Hillis, R. R. (2002, January 1). Estimating Fluid Pressures That Can Induce Reservoir Failure During Hydrocarbon Depletion. Society of Petroleum Engineers. doi:10.2118/78226-MS.

Srivastav, R., Enfis, M., Crespo, F., Ahmed, R., & Saasen, A. (2012). SPE 152662 Surge and Swab Pressures in Horizontal and Inclined Wells.

Stern, R. J., & Johnson, P. (2010). Continental lithosphere of the Arabian Plate: A geologic, petrologic, and geophysical synthesis. Earth-Science Reviews, 101(1–2), 29–67.

Suping Peng, J. Z. (2007). Engineering Geology for UndergroundRocks. Springer-Verlag Berlin Heidelberg.

Tan, C. P., Richards, B. G., Rahman, S. S., & Andika, R. (1997). Effects of Swelling and Hydrational Stress in Shales on Wellbore Stability. http://doi.org/10.2118/38057-MS

Tan, C. P., Petroleum, A., Richards, B. G., & Rahman, S. S. (1996). Managing Physico-Chemical Mechanism Wellbore Instability in Shales with the Chemical Potential. http://doi.org/http://dx.doi.org/10.2118/36971-MS

Tan, C. P., Petroleum, C., Rahman, S. S., New, U., Wales, S., Chen, X., … Petroleum, C. (1998). IADCISPE 47795 Wellbore Stability Analysis and Guidelines for Efficient Shale Instability Management.

Tang, L., & Luo, P. (1998). The Effect of the Thermal Stress on Wellbore Stability. SPE India Oil and Gas Conference and Exhibition, (C), 2005–2007.

Tao, Q., & Ghassemi, A. (2007). Porothermoelastic analysis of wellbore failure and determination of in situ stress and rock strength, (1979), 1657–1664.

Tare, U. A., Mody, F. K., & E, S. I. (2002). AADE-02-DFWM-HO-31 Managing Borehole Stability Problems : On the Learning , Unlearning and Relearning Curve. Managing.

Teale, R. (1965). THE CONCEPT OF SPECIFIC ENERGY IN ROCK DRILLING, 2(July 1964), 57–73.

Teklu, T. W., Graves, R. M., Tutuncu, A. N., Kazemi, H., Alameri, W., & AlSumaiti, A. M. (2012). Geomechanics considerations in enhanced oil recovery. Society of Petroleum Engineers - SPE Canadian Unconventional Resources Conference 2012, CURC 2012, 2, 931–942. http://doi.org/10.2118/162701-MS

Tgtdcl, S., Nazrul, K., & Avenue, I. (2015). INFLUENCING FACTORS OF BOREHOLE FAILURE IN BEDDING PLANE, M(1), 41–47.

Terzaghi, K. (1943). Theoretical soil mechanics. J. Wiley and Sons, inc.

Warren, J. E. (1940, January 1). Causes, Preventions, and Recovery of Stuck Drill Pipe. American Petroleum Institute.

William C. Lyons, P. D. P. E., Carter, T., & Lapeyrouse, N. J. (2015). Formulas and Calculations for Drilling, Production, and Workover: All the Formulas You Need to Solve Drilling and Production Problems. Elsevier Science.

Woodland, D., & Bell, J. (1989). In situ stress magnitudes from mini-frac records in Western Canada. Journal of Canadian Petroleum Technology, 28(5), 22–31. http://doi.org/10.2118/89-05-01

Wu, B., & Tan, C. P. (2010). Effect of Shale Bedding Plane Failure on Wellbore Stability – Example from Analyzing Stuck-Pipe Wells, 10–11.

Yan, C., Deng, J., & Yu, B. (2013). Wellbore stability in oil and gas drilling with chemical-mechanical coupling. The Scientific World Journal, 2013(1993). http://doi.org/10.1155/2013/720271.

Yew, C. H., & Liu, G. (1992, January 1). Pore Fluid and Wellbore Stabilities. Society of Petroleum Engineers. doi:10.2118/22381-MS.

Yew, C. H., & Wang, C. L. (1992). A theory on water activity between drill-fluid and shale. Rock Mechanics, (1968), 717–725.

York, P., Int, W., Pritchard, D., Practices, S. E., Dodson, J. K., Company, J. K. D., … Utama, B. (2009). OTC 20220 Eliminating Non-Productive Time Associated W ith Drilling Trouble Zones.

Zhai, Z., & Corp, A. I. (2011). SPE 140946 Fully Coupled Chemical-Thermal-Poro-Mechanical Effect on Borehole Stability.

Zhang, J., Rojas, J. C., & Clark, D. E. (2008). Stressed-shale drilling strategy - Water-activity design improves drilling performance. SPE Drilling and Completion, 23(4), 385–393. http://doi.org/10.2118/102498-PA

Zhang, J., Standifird, W., & Keaney, G. (2006). Wellbore stability with consideration of pore pressure and drilling fluid interactions. Golden Rocks 2006, The 41st US …. Retrieved from http://www.onepetro.org/mslib/servlet/onepetropreview?id=ARMA-06-922

Zoback, M. D. (2007). Reservoir Geomehanics.

Zoback, M. D., Barton, C. A., Brudy, M., Castillo, D. A., Finkbeiner, T., Grollimund, B. R., … Wiprut, D. J. (2003). Determination of stress orientation and magnitude in deep wells. International Journal of Rock Mechanics and Mining Sciences, 40(7-8), 1049–1076. http://doi.org/10.1016/j.ijrmms.2003.07.001.

Zoback, M. D. and Healy, J. H. (1984). “Friction, faulting, and “in situ” stresses.” Annales Geophysicae, 2, 689–698.

Zoback, M. D., Mastin, L., & Barton, C. (1986). In-situ Stress Measurements in Deep Boreholes using Hydraulic Fracturing, Wellbore Breakouts & Stonely Wave Polarization. Proceedings of the International Symposium on Rock Stress & Rock Stress Measurements, 289–299.

VITA

Ahmed Ali shanshool Alsubaih grown up in Iraq. He borned in Fall, 1985. He graduated from Technical engineering collage in 2007. He worked in several postions in south oil company since 2008 but his job was mainly on drilling operations supervison. He was involved in drilling more than 70 devaited and vertical wells in southern iraq field. He got five years experience in drilling oil wells before he joined to gradute school of petroleum engineering in Missouri University of Science and Technology in Fall, 2014. He received his Master degree in Petroleum Engineering in July 2016.